Electron Beam Diagnosis for Weld Quality Assurance

A thesis submitted in partial fulfilment of the requirements for the degree of Doctor of Philosophy (PhD)

by

Aman P Kaur

The work detailed in this thesis has not been previously submitted for a degree in this University or at any other and unless otherwise referenced it is the author's own work.

Supervised by

Prof. Wamadeva Balachandran

Department of Electronic and Computer Engineering

College of Engineering, Design and Physical Sciences

Brunel University London
May 2016

Abstract

Electron beam welding is used for fabricating critical components for the aerospace and nuclear industries which demand high quality. The cost of materials and associated processes of fabrication is also very high. Therefore, manufacturing processes in these industries are highly controlled. However, it has been found that even minor changes in the electron beam gun itself can produce large variations in beam characteristics, leading to unpredictable welding performance. Hence, it is very important to ensure the beam quality prior to carrying out welds. This requires some kind of device and process to characterise the electron beam to indicate variations.

A detailed review of different technologies used to develop devices to characterise electron beams has been carried out. At this time, it is uncommon for beam measurement to be carried out on production EBW equipment. Research carried out for this thesis is focused on development of a novel approach to characterise the electron beams using a slit-probe to maintain the quality of the welds. The challenge lies in deriving relevant features from the acquired probe signal which can effectively differentiate between the beams of different quality. Wavelet transformation, with its advantages over other methods for simultaneous time and frequency localization of signals, has found its application to feature extraction in many pattern based classifications. This technique has been used to analyse probe signals considering that different quality beams will possess unique signal profiles in the form of their distribution of energies with respect to frequency and time.

To achieve the aim of the thesis, an experimental approach was used by carrying out melt runs on Ti-6Al-4V plates focusing on aerospace requirements, and varying beam properties and acquiring probe signals for all beam settings. Extracted features from the probe signals have been used in classification of the electron beams to ensure these will produce welds within the tolerance limits specified by aerospace standards for quality assurance. The features vector was compiled following statistical analysis to find the significant beam characteristics. By analysing the performance of classifier for different combination of parameters of the features vector, the optimum classification rate of 89.8% was achieved by using the parameters derived from wavelet coefficients for different decomposition levels. This work showed that the use of wavelet analysis and classification using features vectors enabled identification of beams that would produce welds out-of-tolerance.

Keywords: Electron beam welding, probe devices, electron beam characterisation, quality assurance, wavelet transform, features vector, linear discriminant classifier, weld profiles, weld defects.

Contents

List of Abbreviations

Abbreviation	Description
A	Approximation
AWS	American Welding Society
BSI	British Standard Institution
CCD	Charged Coupled Device
CNC	Computer Numerical Controller
CPLD	Complex Programmable Logic Device
CWT	Continuous-time Wavelet Transform
D	Detail
DoE	Design of Experiments
DWT	Discrete Wavelet Transform
EB	Electron Beam
EBW	Electron Beam Welding
EMFC	Enhanced Modified Faraday Cup
EWF	European Federation for Welding
FC	Faraday Cup
FCDA	Faraday Cup Detector Array
FWHM	Full Width Half Maximum
FWTM	Full Width Tenth Maximum
HPF	High Pass Filter
LPF	Low Pass Filter
MFC	Modified Faraday Cup
MSE	Mean Square Error
NASA	National Aeronautics and Space Administration
NOE	Number of Experiments
PI	Peak Intensity
PPD	Peak Power Density
PRD	Percent Root Difference
QA	Quality Assurance
RMSD	Root Mean Square Difference
SF	Sharp Focus
STFT	Short Time Fourier Transform
TWI	The Welding Institute
WT	Wavelet Transform

List of Nomenclature

Symbol	Description	Units
ψ	Mother wavelet	
A	Area	mm^2
a	Dilation	
B	Beam brightness	$mAmm^{-2}sr^{-1}$
b	Translation	
d	Decomposition	
D	Discriminant score	
E	Energy	J
f(t)	Signal	
FWe2	full width of the beam measured at $1/e^2$ of its peak power density	µs
I	Beam Current	mA
J	Emission current density at the cathode	$mAmm^{-2}$
j	Decomposition level	
n	Number of sample	
N_f	Number of Factors	
N_l	Number of levels	
Q	Beam Power	W
p	Percentage of energy	
r	Radius	mm
T	Temperature of the cathode	°K
t	Time	µs
tot	Total	
V	Beam Voltage	kV
v	Discriminant coefficient	
X	Predictor value	
σ	Standard deviation	
Ω	Solid angle	

List of Figures

List of Tables

Acknowledgements

Undertaking this PhD has been a very challenging experience for me and it would not have been possible to complete it without the support and guidance that I received from many people. First and foremost, I would like to thank Prof. W. Balachandran and Mike Nunn for providing me opportunity to carry out the present research and gratefully acknowledge the funding received towards my PhD from Brunel University and The Welding Institute (TWI).

I would like to convey my profound gratitude and deep regards to Prof W. Balachandran as my supervisor for his immense support not only through his extensive technical and academic knowledge but in all spheres. Without his moral support I could not have overcome the tough times I had during my PhD. His critical observations and discussions always guided me to move forward focusing in the direction of achieving the aims of the thesis. He has been a role model for me. I am equally grateful to my supervisor at TWI, Colin Ribton. This PhD would not have been accomplished without his continuous guidance and encouragement. Many of the ideas in this thesis originally came from my discussions with him. I feel fortunate to have both of them as my guides for this PhD and could not have imagined having better mentors. I would like to extend my gratitude to Dr. Maysam Abbod, my second supervisor at Brunel for his valuable feedback and suggestions during reviews. A sincere thanks to Andy Dack who introduced me to the world of electron beam and the probing systems.

In my attempted experimental work for this thesis, I thank Chris Punshon and Tim Mitchell for helpful discussions and their suggestions. Particularly, I am indebted to Vitalijs Jefimovs for his crucial role in carrying out the experiments and helping me in acquiring the test results. I also acknowledge the contribution of people from other departments such as admin, test house, library and IT for extending their support whenever required.

I believe it will be injustice to name a few because everyone in the EB department was encouraging and supportive. I thank them for their help and providing a conducive environment to carry out the research. I would also like extend my

thanks to Kathryn Beamish for always keep me motivating through her small chats.

I also appreciate the support of members of research office at Brunel for always being approachable and helpful. I cannot forget the graduate school for providing the resources and occasions of learning through trainings, workshops, annual conferences and various occasions to showcase the research. I also take this time to express my gratitude to the Brunel library members for their services. Their time to time help in arranging the required resources and guidance in finding the journals for publication cannot go without mention.

I am deeply thankful to my family for their blessings, love and constant encouragement without which I would have never thought of taken up this task and the courage to complete it. Special thanks to Ehimay for always being my source of inspiration in spite of all the odds faced during this time.

Above all, I owe the Almighty for giving me strength and wisdom to undertake this work and enabling me to complete it.

Chapter 1. Research Background

Research work for this thesis is aimed at using electron beam probing for quality assurance. The work is a collaborative project involving Brunel University London and TWI Ltd., Cambridge. The electron beam section of TWI is focused on development of electron beam welding and materials processing for a wide range of applications where beam profile, quality and repeatability are important. It has developed beam probing devices and some analysis technologies to use as quality assurance tools for production. This chapter covers the research background related to quality assurance of electron beam welding in the aerospace industry. First, a brief introduction to the electron beam welding process is given, followed by its importance in the aerospace industry. Further, a brief explanation of the need of quality assurance of electron beams is provided. The next part of the chapter includes the aims of the research, the thesis layout and the publications submitted to scientific journals and conferences.

1.1. Introduction

Welding and joining are an integral part of the manufacturing process of almost every product. The various welding technologies differ in their complexity, time to carry out and cost. However, with the exception of cold-pressure processes, all of the technologies are based upon the introduction of heat to soften or melt material to form a bond. Electron beams provide a precise and narrow heat source and they are widely used, for example in the manufacture of turbine engines.

1.2. Electron Beam Welding

As the name implies, in Electron Beam Welding (EBW) the heat is generated by a beam of electrons. As EWF (2007) mentions, electron beam welding is a fusion welding process where a narrow focused beam of electrons with high velocity is used to weld two pieces of metal. The work pieces melt as the kinetic energy of the electrons is transformed into heat upon impact. Various stages of the penetration in the EB process are shown in Figure 1.1. These stages happen almost instantaneously when the beam is placed on the work piece. When the focused electron beam initially strikes the material, the electrons penetrate to

some depth in the work piece. The transformed kinetic energy starts heating the surface layer. Due to the high power densities of the beams, the transfer of energy happens very quickly and melting of the material starts at the point of impingement without conducting much heat into the adjacent areas of the material. On further heating to a temperature that depends on the target material, the material starts vaporising and the vapour expands and is released upwards. Due to the reaction forces, the melt is pressed downwards and starts creating the keyhole (vapour surrounded by an envelope of the molten material) and moves in the direction of the welding as the beam is moved relative to the work piece. Depending on the energy of the beam, this keyhole can penetrate to several centimetres in the work piece. The welding is often carried out in conditions of a vacuum. This avoids electron scatter by minimizing impacts with gas molecules, and provides an inert environment so that there is no chemical degradation of the metal that would otherwise occur at the high temperatures generated.

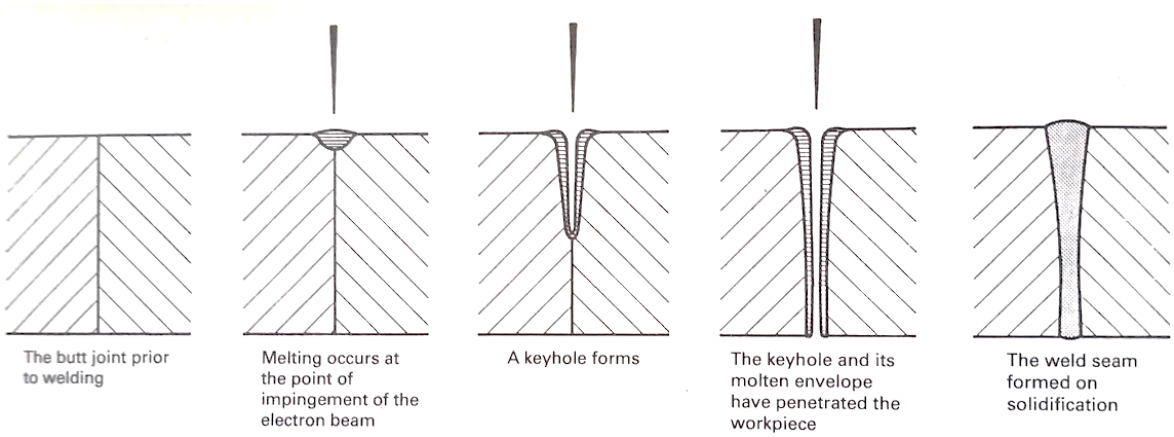

Figure 1.1 Different stages of welding using electron beam (Schultz, 1993) from melting of the metal to the joint formation.

Kenyon (1965) describes the origin of using the electron beams for heating applications back in 1907 with the design of furnace by von Pirani for melting tantalum and other refractory metals. However, the credit for using electron beams for welding for the first time goes to German physicist Karl-Heinz Steigerwald in 1958. Steigerwald had been conducting experiments on an electron microscope to increase the power of the scope and found, to his surprise, that the specimen which was being examined disappeared. On further experimentation, he determined that by regulating the power settings of the beam, the specimen could be melted and would re-solidify. From thereon, the

rapid developments in the field of EB welding began in the United States, Japan, Europe and Russia.

An electron beam gun, the essential part of the electron beam welding equipment, consists of mainly two components i.e. beam generation and beam manipulation as shown in Figure 1.2 (Ahmed, 2005). The beam generation further consists of a cathode operated at high voltage, the control electrode or grid that provides the first control of the electron beam, usually focusing it to a cross-over point, and the anode at ground potential. The electrons are accelerated from the cathode by applying a high-voltage between the cathode and an anode electrode. This potential difference between the cathode and anode determines the overall energy of the electron beam. The electrodes are shaped such that these accelerated electrons are allowed to pass through the anode through a hole in it's centre. After passing through the anode the electrons have near constant speed. A high voltage supply provides current to the cathode continuously.

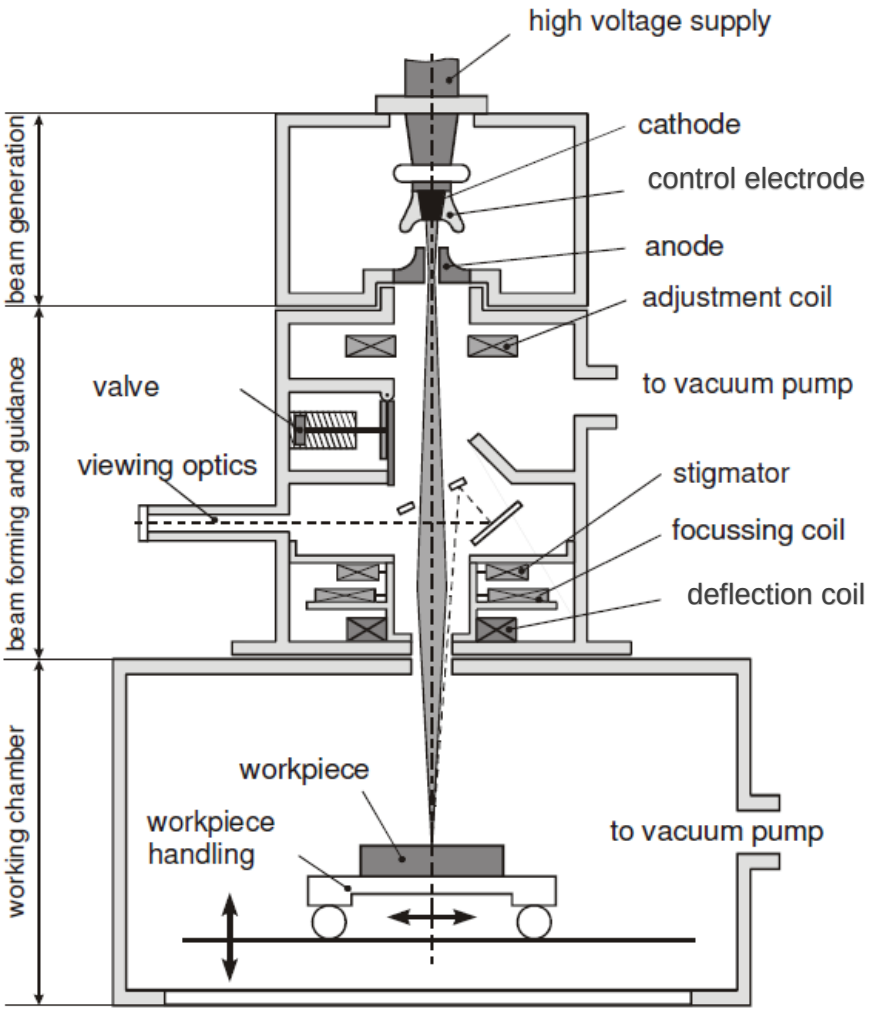

Figure 1.2 Schematic representation of an electron beam welding machine (Ahmed, 2005)

After the beam is generated it is passed through a set of coils which focus it on the work piece in the vacuum chamber. The first set of coils, are used to keep the electron beam in the centre of the lens axis. The stigmator coils are used to compensate for any aberrations of the lenses with the aim to compensate any out-of-roundness of the beam. Even after passing through the anode and achieving their final velocity, the diverging beam still needs to be focused on the work piece to achieve the required power density. For this purpose, one or more electromagnetic lenses i.e. the focussing coils are used to converge the electron trajectories on the work piece. In some cases, during welding, there is requirement of deflecting the electron beam on the work piece. The deflection coils are usually mounted at the end of the gun column. The focussed electron beam from the gun would diverge rapidly under atmospheric pressure due to scattering by gas molecules. Therefore, welding is usually carried out under vacuum, of the order of 10^{-3} mbar or lower.

1.1.1. Advantages of EBW

EB welding technology soon became very popular and was preferred over other technologies for specific applications because of distinct advantages. With electron beam guns, it is possible to generate very high power densities at the focus of the beam and thereby to minimise heat input. According to Gelles et al. (1996), the power density of the beam used for EB welding can reach the value of 10^{10} W/m^2. Very low heat input is required to weld because of high power densities and the process of welding occurs instantaneously. Thus, there is not enough time for significant heat to travel to the surrounding material. Birnie (1976) also mentions that since very low shrinkages are introduced by the EB welding process, materials that are considered unweldable (because of cracking during welding or thermal cycling) may also be welded.

As the beam is very intense and nearly parallel, very narrow welds can be achieved in thick sections of metal e.g. a 3 mm wide fusion zone penetrating a 100 mm thick joint. Also, very high welding speeds can be achieved with this technology even for thick sections that results in the possibility of very narrow heat affected zones e.g. 1200 mm per minute for 6mm thick titanium alloy for aero engine applications. It is possible to weld with very little contamination, as the welding process is typically autogenous i.e. no filler material is added and the

weldment is formed from melting of the parts to be joined along the joint plane. Moreover, the welding is done in the vacuum that ensures no contamination because of the surrounding atmosphere (Schultz, 1993).

By adjusting the beam parameters in the gun, the same machine can be used for welding very thin to thick sections of metals. Once the beam parameters are set, the quality of the welds produced by the EB should be highly repeatable and consistent.

When welding dissimilar metals, the problem of difference of thermal conductivity is faced when welding metals that have very different thermal conductivities. This can be alleviated with EB process as it involves very little heating of the surrounding material, has the ability to precisely locate the weld and permits good control over the relative amounts of the two metals in the weld (Metzger and Lison, 1976). Some metal combinations form brittle intermetallic compounds leading at best to poor mechanical properties for welds produced conventionally or are more likely to lead to weld cracks. However, with electron beam welding as there is such a small amount of intermetallic compound formed and without the need of a filler metal, it does offer an advantage for joining many dissimilar metal combinations (Kah et al., 2013) over other welding techniques.

1.1.2. Limitations of EBW

As mentioned earlier, EB welding is usually carried out in vacuum. The size of vacuum chambers becomes a limitation of the size of the component that can be welded in an EB machine. Also, pump down times are associated with any vacuum chamber.

In the early 1950s, the EBW in non-vacuum was developed and was patented by AEG (Bohm, 2014). This was generally applied to thinner section material of up to 12 mm thickness. Sanderson (2005) has also reported the development of a 150 kW non-vacuum EB gun.

In recent years, the possibilities of EB welding with local vacuum chambers have been explored (Punshon, 2013). In this technology, thick sections (up to 250 mm) of materials can be welded out of the chamber using mobile vacuum units which are much smaller in size as compared to the welding chambers. This facility allows welding of structures too large to fit into a work chamber, and is specifically

aimed at welding of marine foundations for the growing deployment of offshore wind turbines, power plant and nuclear containment vessels.

A further disadvantage of using EB is generation of X-rays during welding that are produced by Bremsstrahlung process as the electrons are decelerated by impact with the work piece (Schultz, 1993). At 60 kV accelerating potential, a steel chamber wall thickness is generally sufficient to provide shielding of X-rays. However, at higher accelerating potentials, where the X-rays produced are more penetrating, the emission of X-rays can be controlled by using shielding around the chambers; this can be lead, steel or concrete.

As EB welding can be done in very narrow regions, the accurate positioning of the welding parts is essential in order to avoid missed joint type defects. Ferrous parts with residual magnetism can deflect the electron beam so that it is not aligned with the joint line. When joining dissimilar metals, even non-ferrous materials, the beam might be deflected from its required path because of magnetic fields created by the dissimilar metals due to thermoelectric currents. This can make the alignment of electron beams with the joint line problematic.

1.3. Motivation for Electron Beam Welding in Aerospace Applications

The aerospace industry is ever demanding in terms of safety, reliability, higher speeds, higher strengths, operating conditions and lower costs. For the aerospace industry, designing aircraft with capabilities of flying higher and faster has been always an aim. This in turn demands the use of materials with higher strengths and lighter weight. Hence, the strength to weight ratio has been one of the prime drivers for choosing a material for both the engine and the aircraft. There are more than 120,000 material options available for manufacturing the airframe and engine (Mouritz, 2012). However, the main groups of the materials used in structural components are aluminium alloys, titanium alloys, steels and composites. Titanium and titanium alloys are the favoured choice in the manufacturing of many critical components in aerospace applications due to their high strength to weight ratio, excellent heat and corrosion resistance over the competing materials like steels, aluminium or super-alloys. As compared to steel, the density of titanium is only about 60% (Donachie, 2000). The Lockheed's SR-

71 Blackbird, the supersonic aircraft design, used almost 85% of the material as Titanium (NASA, 2014). Ti–6Al–4V, one of the α-β titanium alloys is being used in almost 60% of the total titanium production. This alloy possesses a good combination of the strength and manufacturability (Boyer, 1996). The 6% of aluminium provides α stabilization and 4% of vanadium provides β stabilization. They have more strength than its α-alloys and better welding capabilities than β-alloys. It also maintains good mechanical properties at high temperatures up to 400°C.

The aerospace industry faces challenges due to the complexity of manufacture of critical components such as spiral bevel gears, bearing housings, stub shafts, casings and compressor rotors that rotate at very high speeds under high loads. These components require a high order of dimensional accuracy and high reliability. These complex components in some cases can be manufactured either by machining these in one piece from solid or more typically by making individual less complex parts and then joining them together. The latter method is less costly and easier to manufacture if appropriate reliable and high integrity joining technology is used.

In addition to this, the operating capabilities at very high and sub-zero temperature levels, fatigue and crack development, mechanical load and working in stringent environments also play a significant role in selecting materials, their manufacturing technology and maintenance.

Welding is one of the major manufacturing processes used to join the metals to fabricate the components. The aerospace industry, because of its application area, demands high quality standards. Even a minor defect in the components can result in human life loss or huge structural damage. Although the nature of welding in the aerospace industry is characterized by low unit production, it is associated with high unit cost, extreme reliability and severe service conditions. Also, because of the specialized materials that are used for the components, the industry demands specialised welding techniques. The welding processes and the final products in the aerospace industry have to adhere to the qualification standards set by American Welding Society (AWS), British Standards (BS) or the standards set by the individual organizations such as NASA, which has its own standards for weld qualification.

Over the past 100 years, various welding techniques have been developed and used in the aerospace industry. However, for complex and critical components, the requirements are very stringent, as mentioned earlier, and distortion free welding with high dimensional accuracy is an essential requirement (Schultz, 1993). Therefore, EBW is preferred over other technologies as it is capable of achieving high dimensional accuracy and results in distortion free components. Also, it is capable of welding a wide variety of materials which are otherwise not possible or very difficult to weld with other technologies but are very important materials for aerospace industry.

1.4. Need of Quality Assurance of Electron Beams

Like any other process, the process of EBW can be described as a set of input, output and control variables as shown in Figure 1.3.

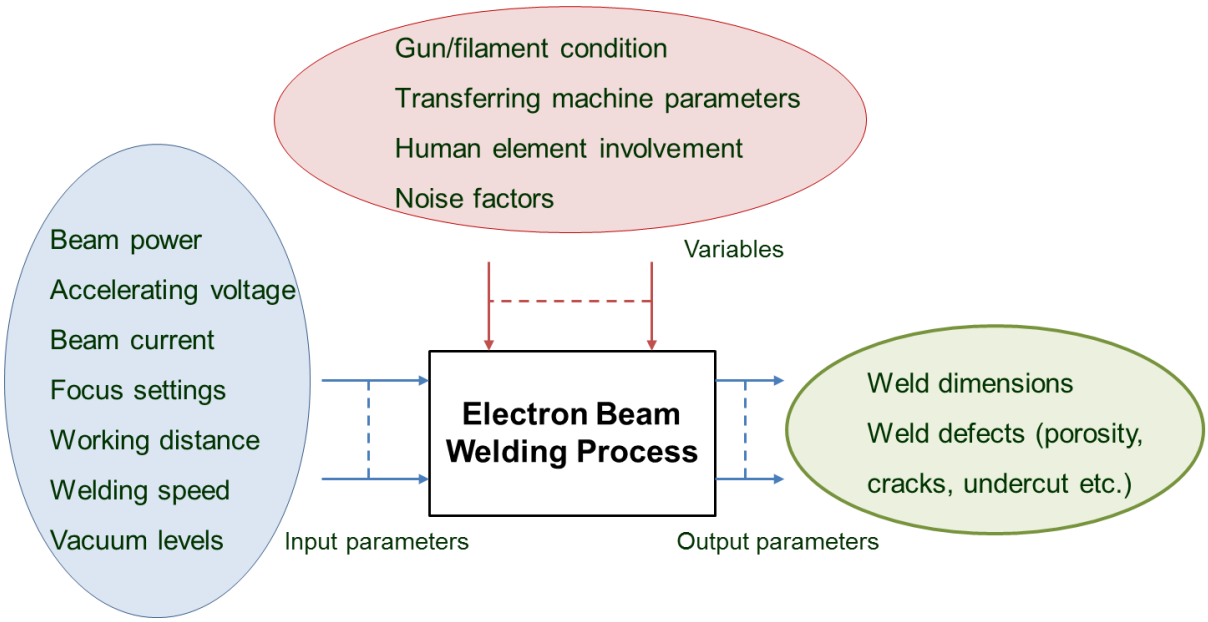

Figure 1.3 Process diagram of electron beam welding explaining different factors contributing to the process.

The output parameters of the EBW are the welds with penetration dimensions and the levels of weld defects. Like any other welding technique, weld defects

can occur with EBW in the form of porosity, cracks, undercut and many more. For the welds to be passed the qualification tests, these should be within the limits set by the standards. To meet the stringent aerospace standards, the input parameters should be tightly controlled.

The input parameters of accelerating voltage and beam current determine the power density of the beam. In most of the EB machines, the accelerating voltage is kept constant and the required power density is achieved by varying the beam current (Schultz, 1993). Welding speed is the speed at which the work piece is moved in the direction of the welding, relative to the beam. The speed determines the heating and cooling rates and also affects the penetration depth. The vacuum levels are mostly kept constant at about 10^{-3} mbar or better. The focus current is the input to the magnetic lens that determines the focus distance that can be a sharp focus, over focussed i.e. below the surface of the work piece or under focussed i.e. above the surface of the work piece.

For a particular weld, the beam parameters are controlled during the process and are generally defined electrically or within computer control systems. However, due to the noise elements or other variables, there can be variations in the characteristics of the beam produced (e.g. change in intensity) that can cause changes in the penetration dimensions as well as defect formation. Another parameter is the human element involved in the process, particularly determining the sharp focus setting. As the beam itself is invisible, the sharp focus is usually set by the operator observing the brightness of the heated spot on the work piece when a low current beam is positioned on it. The consistency of setting the sharp focus is a big question as the response of different operators may be different, there may be changes in viewing the brightness because of settling of metal dust on the optics. Consequently, although welding parameters may be consistently set, variables in machine set up and operation may lead to variation in welding performance.

To avoid this problem, probing systems came into existence. The purpose of probing systems is to characterise the electron beam prior to executing welds to ensure the quality of the beam and in turn the quality of the welds. They are of particular importance when the work piece is of high value, where rework or scrappage costs would be uneconomic.

Various probing systems based on different techniques are available. The Welding Institute (TWI) has also developed probing systems based on slit method. A lot of research work has been carried out on how to make use of these probing systems to provide assurance of the weld quality.

In usual practice, for a particular weld, the input parameters are fixed and controlled. In the case of the probing systems used, the beam characteristics are measured from the probe signals. However, it is very important to determine the variations in these measurements to detect the point where weld qualities start to get out of the boundaries for qualification. In the present research, a parameter box based on probe signal parameters has been created for using the titanium alloy Ti-6Al-4V. The research has been focussed on this alloy, as this alloy is one of the most commonly used in the aerospace industry.

1.5. Aim and Specific Objectives

The main aim of this thesis is investigate the use of analysis of electron beam measurements to detect variation in beam quality that precedes weld quality falling below the required threshold. This in turn needs to create a boundary using a set of the probe signal parameters to identify the edge of the limits to ensure the weld quality. A part of this task is to find significant parameters or develop a features vector that describe the probe signals in relation with the weld quality parameters.

The specific objectives of this research are outlined as follows:

1. To review the existing methods and devices for electron beam characterisation.
2. To develop or implement signal processing methods that will allow discrimination between electron beam measurements.
3. To verify, through practical trials representative of aerospace manufacture that beam characteristics can be detected where they would lead to welds below the required quality threshold.
4. To assess and improve the consistent acquisition of signals from the two-slit probe.
5. To assess the effectiveness of the developed method through practical trials.

1.6. Summary of the Methodology

The methodology for this thesis work involves review of published literature on the probing techniques, a review of different probe designs used for welding application and the type of beam measurements these can produce. The research work on the problem of characterisation of probe signals in relation with the weld quality is approached with an emphasis on the actual signals and welds obtained through experimentation. Hence, the methodology adopted involves experimentation to carry out the weldments and the acquisition of probe signals. The pre-trials are conducted to narrow the experimental matrix and the design of an experimental trial. As the target application is the aerospace industry the weld profile, material and quality acceptance standards have been chosen to be consistent with this application. The weldments carried out during the experimental trial are examined for their quality parameters and the probe signals are processed by applying signal processing techniques that is followed by developing the relationship model between the two. The limits of the probe signal parameters are identified based on the thresholds on the weld quality parameters.

1.7. Thesis Layout

This thesis is organized in five chapters and appendices following this introductory chapter. Layout of the thesis with reference to the objectives mentioned in section 1.2 is illustrated in Figure 1.4.

Chapter 2 includes the literature review of the probing techniques, the existing probing systems for welding applications, the previous work on correlation of the beam measurements with the beam quality using these systems, details of the slit based probing systems and the signal processing techniques.

Chapter 3 provides details about the methodology used, the pre-trials and using the results of weld parameters to narrow down and design the experimental trials.

Chapter 4 presents the measurements of the electron beam using slit probe and development of signal processing technique for generating features vector using the measurements.

Chapter 5 is focussed on experimental trails to develop the relationship model between the weld parameters and the features vector to differentiate between the beams that can give welds within or out of specifications.

Chapter 6 is finally concluding the research work and discusses about the future opportunities in this area.

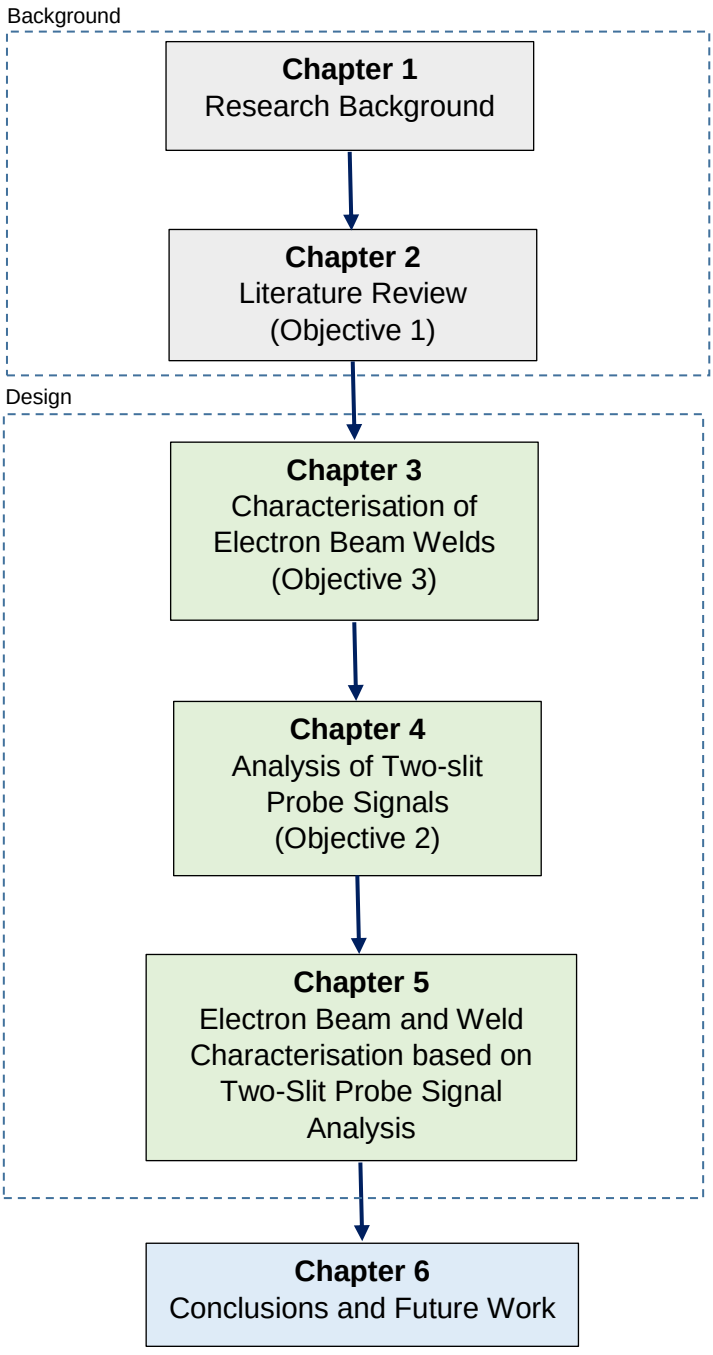

Figure 1.4 Thesis layout.

1.8. Contribution to Knowledge

As can be expected form the thesis layout above, Chapters 2-5 present the main research work to attack the problem of quality assurance of the welds in EBW using the two-slit probe method. The novelties arisen from this work on chapter-by-chapter basis are briefly outlined here.

Chapter-2: Through a detailed literature review, the developments in the field of beam probing in welding are brought out. Various techniques developed over the years are compared for their relative features. The features of slit probes have been critically analysed against other probing techniques being used in the welding industry.

Chapter-3: Different beam characterising devices being used in the industry are based on different concepts and hence provide different features sets to ensure the beam quality. To the best of the author's knowledge, the research in this field has been focussed on broadly differentiating the signals' features for sharply focused, over focused and under focused beams. In most of the research it is observed that the analysis or the relationship of the probing signals with the welds was limited to two or three parameters e.g. peak beam current intensity or the beam diameters at different intensity levels. However, to achieve the aims of this thesis it is felt that there was a need to examine more parameters to narrow down the operating limits where it is essential to determine the deviating point for the weld quality measures. In the present work, the emphasis was on developing a features set which could define a boundary of the probe signal characteristics to ensure the weld quality and indicate whenever it is approaching the weld quality limits. To achieve the aim, an experimental approach was used. The initial two pre-trials of melt runs helped in selecting the variables to use for the experimental work, finalising the experimental set-up and methods of assessing the welds for quality parameters.

Chapter-4: the probe signals were acquired for the pre-trials to establish the signal processing technique. This work has applied wavelet analysis to beam measurement signals for multi-resolution analysis by decomposing the signal into different decomposition levels. From the wavelet coefficients, distribution of

energy in these decomposition levels was assessed and it has been seen that it was able to differentiate between the beams with different characteristics.

Chapter-5: Earlier developments in this field were mainly focused on deriving the relationships between the weld dimensions and the peak intensity or the beam diameters. This research work is an effort in developing the relationship of the features vector with weld dimensions and the additional parameters such as weld defects in terms of porosity, cracks and undercuts that define the weld quality and are very important in aerospace industry. The results of the experimental work carried out for the present thesis has proven that the features vector generated from the wavelet analysis can contribute significantly to provide the fine differentiation of the beam quality necessary to detect variation before crossing weld defect thresholds. This has been proven by applying the classifier model based on the categories of the weld qualities derived from the aerospace specifications. The wavelet transform based features vector classified the experimental data accurately to 89.8% of the experimental samples.

1.9. Publications

Publications arisen from this research work and presented in scientific journals and conferences are listed in Table 1.1 with connection to the thesis chapters.

Table 1.1 Details of publications and related thesis chapters

Publication	Relevant thesis chapters
A. Kaur, C. Ribton, W. Balachandran. “Electron beam characterisation methods and devices for welding equipment”, Journal of materials processing technology, volume 221, pp. 225-232, (2015).	Chapter - 2
A. Kaur, C. Ribton, W. Balachandran. “Characterization of high power electron beams using a two-slit probe and wavelet transforms”, 2nd IET International Conference on Intelligent Signal Processing (ISP) (2015).	Chapter - 3 & 4

A. Kaur, C. Ribton, W. Balachandaran. “Development of a novel device and analysis method for characterising electron beams for welding applications”, Journal of Electrotechnica & Electronica, (2016).	Chapter – 4 & 5
A. Kaur, C. Ribton, W. Balachandaran. “Development of a novel approach for characterising electron beams and quality assurance of welds”, Accepted for publication in Journal of manufacturing processes.	Chapter – 3, 4 & 5

1.10. Summary

The chapter has covered a brief background and summary of the thesis. To obtain better understanding of the research problem, an in-depth literature review is presented in the next chapter covering developments of methods and systems for electron beam characterisation.

Chapter 2. Literature Review

This chapter presents introductory information about probing systems, their progressive development over time, various techniques and devices being used for welding applications, the work carried out using these devices to correlate beam measurements with weld parameters and details about the two-slit probing system and its comparison with other contemporary devices and systems. A brief literature review about probing techniques and their progression over time has also been published in a research paper (Kaur et al., 2015).

2.1. EB Probing

A very important feature of EBW is that the process can be automated entirely by controlling the electrical parameters. A computer numerical controller (CNC) machine programme can be set for a particular weld and reused to reproduce welding for the same type of component. However, in addition to the controlled process parameters, it is also essential that all the variables in the electron beam machine are within specified tolerances. Even very small changes in the gun or machine parameters can lead to large changes in the beam characteristics that can lead to erroneous welding performance.

An electron beam typically consists of a high intensity core accompanied by a low intensity fringe as shown in Figure 2.1. However, beams of the same diameter can have a different intensity distribution. Excessive beam power in the fringe may cause overheating of the work piece without having sufficient power for effective processing. It may also produce a weld fusion zone that has a wider than normal ‘nailhead’ shape, asymmetric feature or undercut when viewed in cross section. Each EB machine and gun combination will result in a different beam profile.

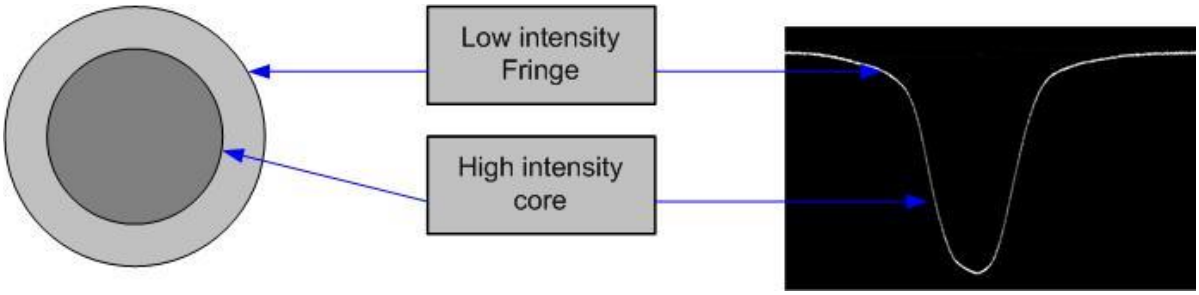

Figure 2.1 Schematic showing a cross section through an electron beam and its associated slit probe measurement.

In Chapter-1 the process diagram of EBW was described as a set of input, output and controlled variables. Once all the input parameters are set for a particular weld, variations can occur due to the gun/filament condition deterioration over time, differences in machine performance when transferring parameters from one machine to another, operator intervention in the process or any other noise factors.

Within the gun, the cathode (typically a heated tungsten filament) is an important component that is responsible for the generation of electrons. Cathodes are typically operated at the upper end of their temperature range to give high electron emissivity and correspondingly highly intense beams. These cathodes have a certain lifetime due to the evaporation that occurs at high temperatures (Pradeep, 2012). Also, during their lifetime the characteristics may change over time and can cause the changes in the beam shape.

Often there is a requirement to transfer the input parameters from one machine to another. Once the optimum welding parameters are set on one machine, the transfer of the parameters to another machine may not be straight forward and there may need to be some adjustments due to several reasons such as there may be differences in the electron guns on the two machines, the chamber size may be different that can cause changes in the placement of the workpiece or differences in the performance of the two machines due to age or maintenance (Palmer et al., 2007).

For EB welding, it is very important to set the required beam focus position usually just below the work piece surface. In this case, the beam diameter will be minimum and the current density will be at its maximum to get a maximum weld

depth. The sharp focus is usually set by the operators based on their experience; and they manually adjust this to find the focus coil current giving the maximum brightness of the beam (AWS, 2004). However, this method is very subjective and can vary from operator to operator causing inconsistencies in the focus settings that in turn change the beam power density (Elmer, 2009). Giedt and Tallerico (1988) carried out welding on different welding machines and with different operators with same beam power. Their results showed that there may be ±20% to ±40% variations in the weld depth just due to manual focus adjustment by different operators. Also, the focus settings will vary at different levels of beam current as the focus settings are also changed with the change in the control electrode voltage of the gun (Schiller et al., 1982). The control electrode voltage is used to vary the beam current. Hence, there is need to refocus the beam for different beam currents. The focus of the electron beam is relatively difficult to observe at higher beam currents (Lawrence, 1975).

Other than the above, there may be variations in the parameters due to noise or electrical parameter shift which may change the beam shape and its characteristics. However, to ensure the weld quality, it is essential to maintain and check the beam quality.

Various methods exist that guarantee the beam quality. One of the classical methods is empirical tests on the test-pieces (Mcnabb, 1969). It is a satisfactory method in many applications as it provides a near-binary test output i.e. ‘pass’ or ‘fail’. It is often used where the parts to be welded are very expensive especially in aerospace industry. However, it does not assess the state of the machine in terms of relative tolerance of the process. If the test fails, the reason is not clear and thus there is no indication for changing the process parameters or machine set up. It is a very time consuming method. Hence, this method is not ideal for production environments.

Beam probing techniques potentially offer both an assurance of beam quality and the reproducibility electrical beam parameters. Beam probing allows the user to inspect the electron beam directly rather than just monitoring the control parameters. There are a number of ways that this may be applied very effectively. For example, probing could be carried out at regular periods to monitor beam quality changes over time; the beam could be probed to ensure consistency prior to welding a high value component, or a batch of components. Probing could be

used as a tool to understand why weld quality has varied or is poor, following weld execution.

2.2. Electron Beam Characteristics

Electron beam probing can characterise electron beams in terms of various parameters as follows:

Beam Energy: According to Houldcroft (1977) the beam energy is the kinetic energy of the electrons and is defined as the overall potential difference that accelerates the electrons as they travel from the cathode source to the final aperture of the gun (measured as eV or keV). As the electrons are thermally emitted from the cathode, with a distribution of initial energies, they will not exit with exactly the same energy and there will be a small energy spread that is less than half an eV typically.

Beam current: Beam current is a measure of the quantity of charge that flows per unit time in an electron beam and is expressed in units of mA (Schultz, 1993). According to British Standards Institution BS EN ISO 14744-3:2001 (2001), the beam current is measured at the working distance. The beam current might be different from the emission current i.e. the total current that leaves from the cathode, as in the process of traveling down the gun and being focused some of the electrons may land on various gun elements. For the welding applications, the beam current together with the accelerating voltage affects the resulting weld (Schultz, 1993).

Beam power: Beam power is the beam energy being delivered per unit time and is equal to the product of the beam acceleration potential and the beam current (Schultz, 1993). It can be expressed as

$$Q = V \times I \tag{2.1}$$

Q = Beam Power, Watts (W)

V = Beam Voltage, kilovolts (kV)

I = Beam Current, milli-amperes (mA)

Beam-width or spot size: Beam-width is the beam diameter produced in the plane where the beam impinges on the surface of the work piece. It will either be equal to or larger than the minimum focal spot achievable in that plane from the focusing lens. The beam width will vary with the working distance.

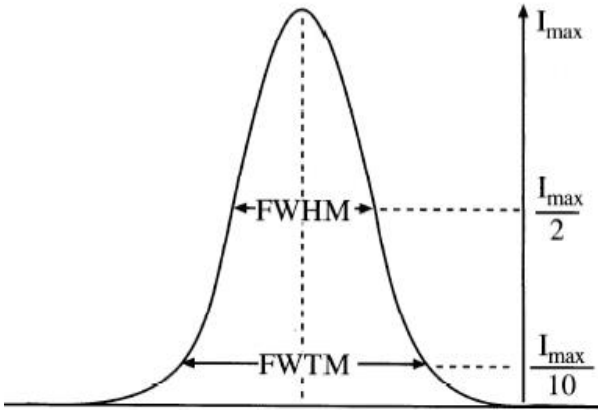

Figure 2.2 Diameter of a Gaussian beam at 10% and 50% of the peak current intensity (Williams and Carter, 2009).

With the assumption of beam being Gaussian distribution (Williams and Carter, 2009), the beam width is defined at Full Width Half Maximum (FWHM) i.e. the width at half of the total current as shown in Figure 2.2. In terms of Gaussian beam standard deviation σ, it should be 1.67σ (Hawkes, 2011). Sometimes, the beam width is also measured at Full Width Tenth Maximum (FWTM) and is 4.29σ for a Gaussian beam (Keast and Williams, 2000). According to Liao (2007), the actual beam width can be different from the calculated one as the misalignments of the electron beam and aberrations in the lenses prevent the formation of real Gaussian intensity distribution.

Beam Brightness: For welding applications, other than the welding parameters like accelerating voltage, beam current and beam focus diameter, the shape of the beam is equally important. The ideal beam would originate from a very small source diameter and diverge very little. For this desirable quality, the term "brightness" of the beam is used. The brightness dictates the beam angle and intensity of the image spot which will be formed on the target sample.

As Worster (1969) mentioned, the brightness (or directional beam intensity) of an electron beam at a given point in a given direction is defined as the current per unit area normal to the given direction, per unit solid angle.

$$B = I/A\Omega \qquad (2.2)$$

where I : total current of the beam

A : Area

Ω : Solid angle

As 'I', the total current of the beam is an important parameter, it is equally important to be able to collimate and focus the beam. The focus of an electron beam is similar to an optical beam as shown in Figure 2.3.

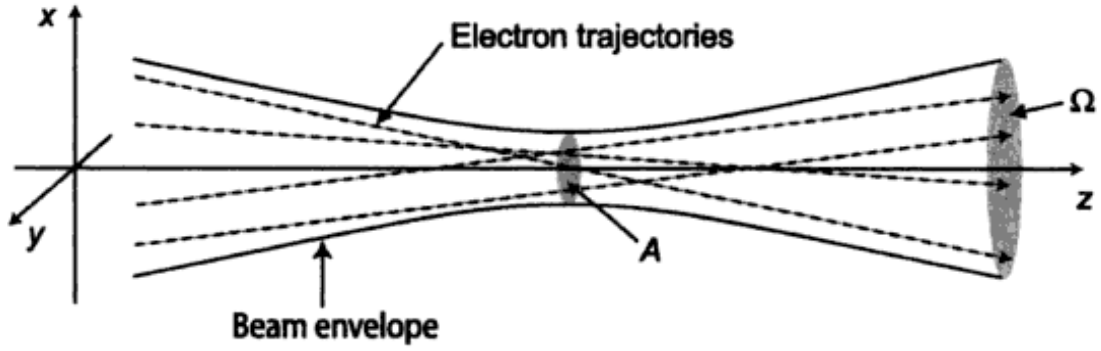

Figure 2.3 Electron beam at the focus.

According to Langmuir law, the maximum beam brightness from an electron gun with a thermionic emitter is limited by the thermal velocity spread of the electrons and this can be given as

$$\frac{B}{J} = eV/\pi kT \qquad (2.3)$$

where J : the emission current density at the cathode

T: the temperature of the cathode

Beam Current Density: Beam current density can be defined as the beam current per unit area of the target (Williams and Carter, 2009). The variation of beam current density at different positions in the spot is called the beam current distribution. In most guns, this distribution is similar to a Gaussian curve i.e. the

spot is brightest in the central area and fades off at the edges as shown in Figure 2.4.

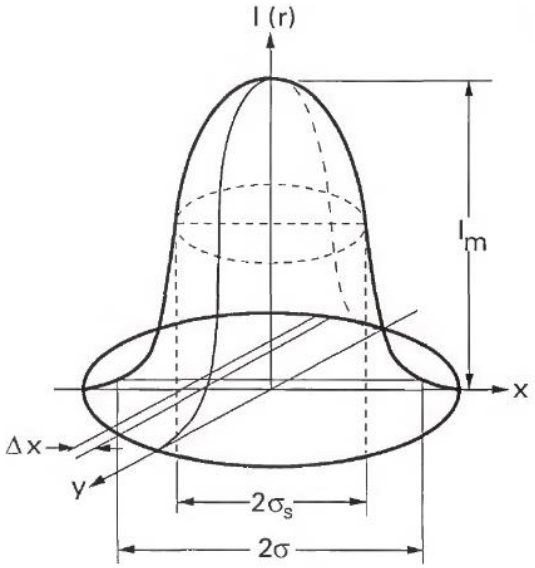

Figure 2.4 Gaussian distribution function (Hicken et al., 1991).

Hicken et al. (1991) have defined the beam current density distribution function as

$$I(r) = \left(\frac{I}{2\pi\sigma_s^2}\right) \exp(-r^2/2\sigma_s^2) \qquad (2.4)$$

where I(r) is the current per unit area at a radius r,

I is the total beam current,

σ_s is the standard deviation

Bocharov et al. (2006) emphasized on the significant effects of current density distribution on the weld penetration, weld width and the quality of electron beam welds. They worked on the identification and classification of the current density distributions on the basis of the number of the maxima of the density curves with the aim to calculate the geometrical characteristics of the of the penetration zone more accurately.

2.3. Beam Probing Techniques

Sanderson and Adams (1970) found that for welding purposes, the beam diameter at focus, beam energy density distribution and the rate of convergence of the electron beam are the most important beam parameters. Beam probing is

generally carried out by measuring the current carried by the beam - either the full beam current or part of the beam. This can be measured in various ways.

The basic device used to measure the current of the charged particle is a metallic conducting cup that collects the electrons of the beam, named a ‘Faraday Cup’ (FC) after Michael Faraday who first theorized ions around 1830. In its simplest form, a FC consists of a conducting metallic cup that collects electrons in a vacuum and the current can be detected by simply measuring the voltage produced across a resistor connected between the cup and ground. Other than a FC, a metallic wire can also be used to measure part of the beam current by passing the beam over the wire. The absorbed current by the wire can be detected in terms of voltage produced across a resistor connected between the wire and ground. There are many variations of FCs and wired systems used for the beam current measurements in the literature covered in the following paragraphs.

As Wojcicki and Mladenov (2000) mentioned, the major problem of measuring the current in this way, especially for high power electron beams, is that the beam current is concentrated in a very small area. If it is focused on a measuring device, it can damage it in a very short time. To overcome this problem, Sandstrom et al. (1970) have suggested that the measuring device should sample the electron beam with a very short duty cycle or it should be constructed in a way to dissipate the high power density. The British Standards Institution (2001) standard no. BS-EN-ISO 14744-3 also suggests keeping short measurement times with long cooling intervals or using the water cooled Faraday cups to avoid the measurement errors caused due to charged ion dissipation over large fusion area of Faraday cups while measuring high beam currents. Hence, most of the methods available are based on the short duty cycle sampling of the beam. The methods used also depend on whether the sensor is used to measure the full beam current or part of the beam current to characterize the beam features like beam width, current density distribution etc. These methods comprise the arrangements either to deflect the beam over the sensing element or move the sensor over the beam at high speeds to capture the current it contains. These are the slit, pin-hole or rotary wire methods.

2.3.1. Slit-probe method

In the slit probing method, the beam is deflected over one or more narrow slits with very high speed. The slit probe consists of a refractory metal plate through which a small portion of the beam current passes as it is deflected over the slit (Nello, 2001). This current is collected by the FC under the slits. A slit-probing system is shown in Figure 2.5.

The beam deflection can be achieved by manipulating the electrical current through a set of magnetic coils at the end of the gun column as part of a dedicated probing system. In certain cases, the deflection coils can be attached to the end of the gun column as part of a dedicated probing system. By adjusting the deflection speed and magnitude the beam path can be adapted to pass over the probe sensor.

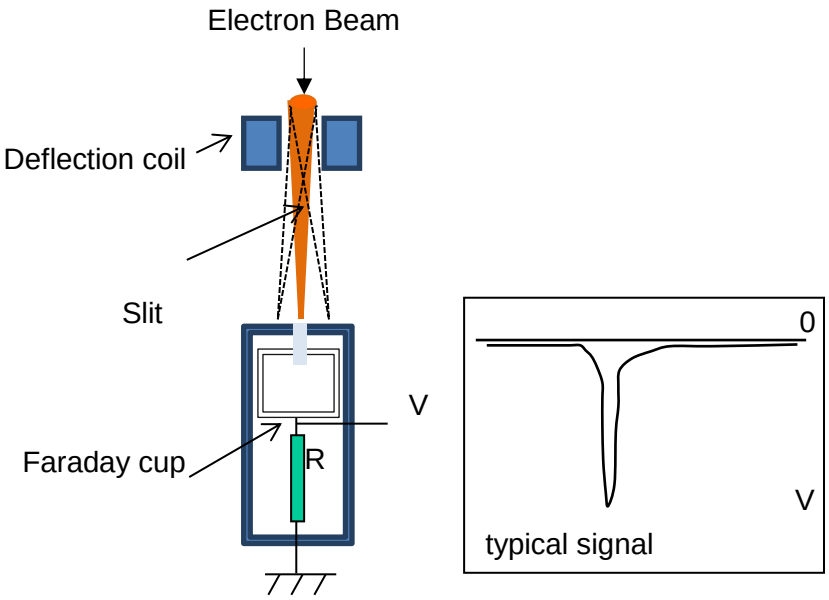

Figure 2.5 Schematic of a slit-probing system showing the beam deflected over the slit and captured through the slit using Faraday cup.

This method of beam probing can be achieved using potentially simple and compact hardware. This method is also immune to electrical noise and signal degradation due to back scattering as the sensor is enclosed and is only subjected to small part of the beam.

2.3.2. Pin hole probing method

The pin hole probing method is a similar technique to the slit probe. However, instead of the slit, there is a small diameter pinhole. The size of the pinhole is very small compared to the smallest beam diameter and to capture the beam characteristics, the beam is raster scanned over the hole. A typical pinhole probing system is shown in Figure 2.6. Since the pinhole size is a small fraction of the minimum beam diameter in order to have a useful resolution, this means that raster sweeps of high accuracy and precision are required over the pinhole.

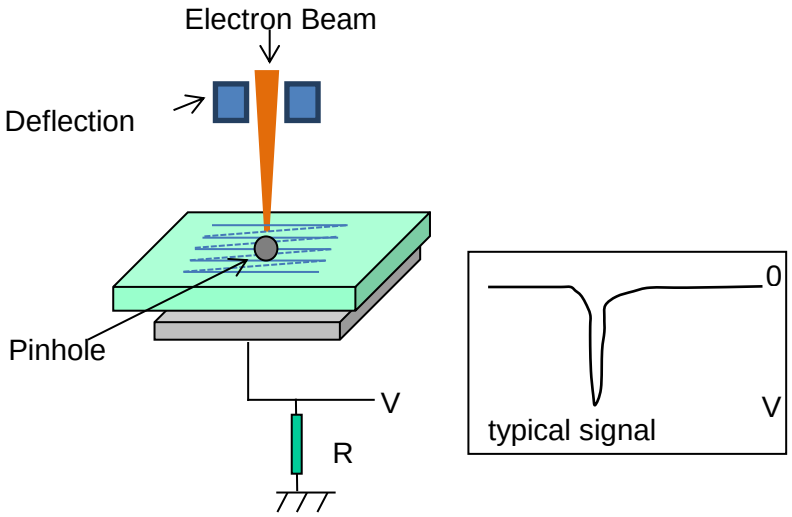

Figure 2.6 Pinhole-probe system using the raster scan over the pinhole.

Because of the small hole size and the typical current density in processing beams, the voltage signal is very small and hence the amplification of the signals is usually required. Also, there is a possibility of the hole becoming fully or partially blocked by debris, and this would result in a loss of signal and variation in measured current or melting of the hole edges by the beam, leading to a decreased resolution (Nello, 2001).

2.3.3. Rotary wire probing method

The rotary wire probing method utilises one or more refractory metal wires that are mounted on an arm which is rotated at high speed through the electron beam.

The current signal picked up by the wires gives qualitative information regarding current distribution of the beam, but can be used to quantify the beam width. The limiting factors for beams of high power intensity are the wire diameter, the wire sweep speed, and the thermal duty cycle applied to the wires. In a vacuum, relatively high wire sweep speeds are possible without a high power drive motor. However, the wires see a high thermal duty cycle even with a relatively long arm, and typical welding beams begin to damage and then sever the wires at powers of 30 kW or less. With smaller, more intense beams, damage may occur using focused beams of relatively lower power. A rotary probe schematic is pictured in Figure 2.7. A rotary wire system was designed by Sanderson and Adams (1970).

The primary advantage of this technique lies in its simplicity and versatility; almost any EB machine can be studied using this type of device since high speed beam deflection is not required. But on the other hand, multiple wires have to be taken out of the chamber, i.e. for the signal and the motor drive, which might not be possible or convenient for all machines.

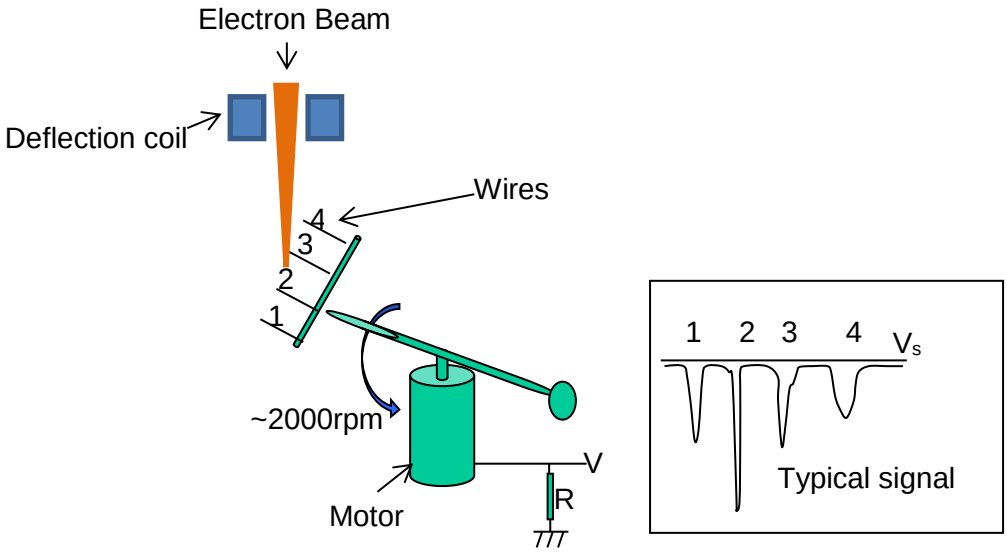

Figure 2.7 Rotary wire probing system.

A disadvantage of this technique is that the probe is relatively large, so this may prohibit routine probing immediately prior to welding or other processing, especially in small chambers. An additional issue is that prior to significant wire damage, some positive ions may be released, giving a potentially misleading signal from more intense beams. In addition, a significant proportion of the

electrons incident on the probe wires is lost by back scattering reducing the pulse amplitude. Therefore, the device cannot be used in a quantitative manner regarding current levels. Nevertheless, it remains a very useful tool.

2.4. Related Work

The above mentioned beam probing methods can be used in combinations or with different modifications to the basic designs. Prudnikov et al. (1973) discussed the design features and characteristics of a device based on scanning the beam with a thin metal probe to determine the beam profile and position of charged particles. The wire probing system was also used by Ragheb and Zakhary (2000) to study the variations of beam current, beam perveance, beam profile and beam emittance with the extracting voltage. Dilthey et al. (1997) presented the DIABEAM system that uses a pin hole diaphragm for estimating the beam power density distribution along with two parallel slits to evaluate the deflection speed. Dilthey et al. (2001), in their new version of DIABEAM system, a rotating probe has also been included as a part of the system to take into account effects on measurement of power density distribution due to the metal ions. However, a disadvantage of using slits or the rotating wire methods is that they carry out the measurements only in one axis.

Berte and Legrand (1981) used a matrix or array of m x n conducting elements to measure the current density of beam of charged particles. The conducting elements of cylindrical shape were used to collect the charged particles. With this design of the probe, it was possible to display the current density of the beam at different points of its cross-section simultaneously. Darling et al. (2005) also developed a FC Detector Array (FCDA) by utilizing the advanced micro-fabrication techniques used in mass spectrometers. Their design was based on the requirements that the FCDA must have a fine pitch of less than a mm from cup-to-cup, have a high fill factor, the connections between cups and electronic circuitry must have low leakage paths, and the cups must exhibit a high aspect ratio i.e. being much deeper than wider to reduce the emission of reflected or secondary electrons.

In the case of a circular beam that is parallel to the leading edge of the FCDA, a standard FC design can give good results. However, for shapes other than the circular e.g. strip shaped beams, the beam parameters cannot be measured

accurately. Also, Hayafuji (1986) found that when the beams scanned over the FC are not parallel to the leading edge or if the size of the strip cross section is bigger than the opening of the FC, the results obtained were not accurate. He developed a device that consisted of a number of cups spaced along the length of the cross section of the beam to measure the current distribution in that direction.

Hicken et al. (1991), developed a narrow-slit FC using two tungsten plates mounted on top of a copper body. The beam was deflected over the plate and the variation of current flow through the slit was measured as a measure of the current density distribution in the beam. This method was quite useful for circular beams. For measuring the beam profiles of irregular shaped beams, Elmer et al. (1996), used the FC with slit, naming it the Modified Faraday Cup (MFC). The beam was moved across the slit several times and the collected current recorded using an oscilloscope. Then, the cup was moved to other locations using the stepper motors and same procedure repeated to get the information of beam current at different locations. These measurements were then used to reconstruct the beam current distribution using computerized tomographic technique to produce the surface plots of the power density distribution of the electron beam. Elmer et al. (1993) have also compared the performance of ribbon shaped and hairpin shaped filaments with regard to their peak power density and power density distributions.

Giedt and Campiotti (1996), developed an electron beam focusing system using a 4-slit beam trap over the FC for measuring the diameter of the beam. The beam was swept over the detector and a minimum of two slits data were required to determine the profile of the beam current. The beam trap also had a hole in the centre of a size bigger than the size of the beam to measure the peak current. The focusing system included a digital storage oscilloscope to digitize and store the data that was used to calculate the beam profile. This information was used to control the focus coil currents automatically. Elmer and Teruya (1998) developed a fast method for measuring the power density distribution of electron beam using a refractory metal disc based on the above concepts. The disc had 17 radial slits evenly spaced. Instead of moving the cup to different locations, the beam was deflected over the disc in circular pattern to get the current information. This method of beam profiling was able to be used in real-time focusing.

Elmer and Teruya (2001) presented an improved design of MFC to overcome the sources of error in their previous design and named it the Enhanced Modified Faraday Cup (EMFC). They observed the incomplete electron capture and signal degradation with repeated use of MFC. Several modifications were made to the previous design like adding another slit disk of copper over the internal FC, a beam trap inside the FC, a graphite ring below the copper slit disk and a graphite disk below the beam trap to reduce the number of backscattered electrons, and improvement of the grounding between the tungsten slit disk and the outer copper body. They also changed the method of detecting the orientation of beam by replacing the double width with one wide-spaced set of slits to eliminate the errors introduced by using the double width slit. Similar systems have been used for characterising high power beams by introducing slight modifications to this design e.g. by providing a heat sink in close proximity to the FC components and active cooling system using water to keep the system from over-heating (Elmer et al 2008).

Peng et al. (2011) developed a quality test system comprising a control module, sensor module, driver module and analysis software based on high speed Complex Programmable Logic Device (CPLD). The developed system was based on a pin hole with a FC. They called it a four-dimensional system where the fourth dimension basically includes the variations of the power density distributions over different working distances. There is also evidence of using an imaging system with the slit method used by Yang et al. (2011) for the determination of electron beam density. The images were captured by a Charged Coupled Device (CCD) camera placed below the slit that was sensitive to both X-rays and longer wavelength photons up to visible.

Other than the beam parameters mentioned earlier, beam emittance is also considered as an important parameter which represents the angular distribution of the beam electrons. A review of the emittance measurement methods and devices has been presented by Koleva et al. (2014) along with an extension of the tomographic technique used with the EMFC to measure emittance.

2.5. Development of Two-Slit Electron Beam Probe

The two-slit probe has been designed comprising of two slit probing fingers perpendicular to each other, and has been designed to overcome the limitations of other types of beam probing systems. The rotary probe needs too many electrical feed-through connections to make it versatile for multi machine activities. Moreover, it is very delicate and needs motors to rotate it at very high speeds. The pinhole probing system demands for very precise scanning of the beam over the pin hole in X & Y directions. Palmer et al. (2011) also suggested that the pinhole based systems inherently suffers from low signal-to-noise ratio. In addition to this, though pin-hole systems provide a comprehensive analysis of the beam characteristics, it is harder to interpret the pinhole data. The limitation of the EMFC with multiple slits is that it is restricted to beams of power up to approximately 10 kW. A standard single slit probe provides data in one direction at a time and needs to be re-orientated to acquire data in both the X & Y directions.

The two slit probe consists of refractory metal covers with slits through which a small portion of the beam current passes as the beam is deflected over it. As the beam crosses over the slits, the electrons passing through the slits are captured underneath by a Faraday cup and converted into a corresponding voltage signal as the current flows to earth through a resistor. In this design, the detector element i.e. the Faraday cup is fully enclosed and only receives a small portion of the beam power. This results in less signal degradation due to electrical noise pickup, ion emission, secondary electron emission and electron backscatter because it is very effectively shielded. Typical slit widths that have been used are 0.1 mm. Depending on the requirements, smaller slit widths can also be used. For the data analysis, the earlier units were based on oscilloscopes but more recently PC based data capture systems have been used with sophisticated analysis software. This facilitates representation of the data in various forms that can be customised depending on users' needs. The new probe also includes a Faraday cup to measure the full beam current. The construction of the two-slit probe is as shown in Figure 2.8.

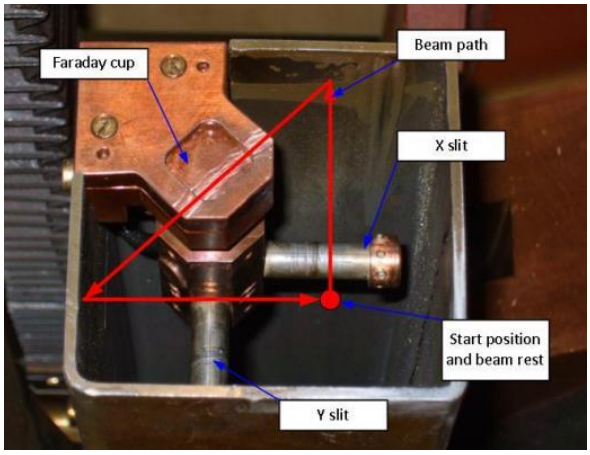

Figure 2.8 Construction of the two slit probe and its scanning pattern (Dack and Nunn, 2013).

The beam is deflected over the X probe, Faraday cup and Y probe to acquire the data related to the electron beam. The probe finger is isolated from the ground. The generated voltage is clamped with a diode to generate the speed calibration signal. A typical signal received as the beam passes over one slit probe finger is as shown in Figure 2.9.

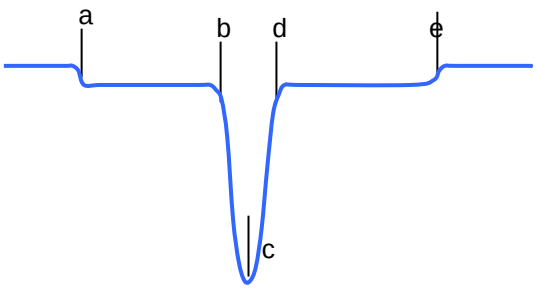

Figure 2.9 A typical signal from the slit finger.

The signal represents the sequence as follows:

a) Beam's first contact with the probe finger;
b) Beam's first contact with the slit. The first part of beam shape signal is generated;
c) Most intense part of beam is over the slit. The peak of the probe signal is generated;
d) Beam's last contacts with the slit. Last part of probe signal is generated;
e) Beam's last contact with the probe finger.

As the finger width is constant, from the time information between points ‘a’ and ‘e’, the speed of the beam scan signal can be verified. This signal is further analysed in the software and the extracted information can be represented in various forms. The software is capable of providing the sharp focus point, beam profile, beam asymmetry, the beam diameter and the full beam current. By running a focus sweep over a range and acquiring the X & Y probe signal data, the beam envelop can be measured (Figure 2.10). The complete traces of X or Y over focus sweep can be seen in a single window for comparison or observing trends (Figure 2.11). Also, by measuring the beam profiles at focus at different working distances the brightness of the beam can also be determined.

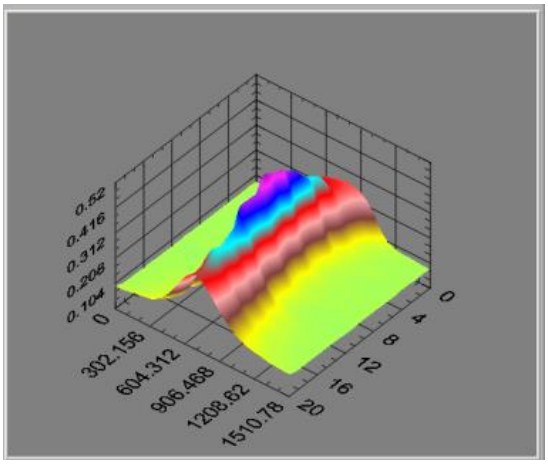

Figure 2.10 Three-dimensional representation of focus sweep using the peak current intensity and beam width for different focus settings.

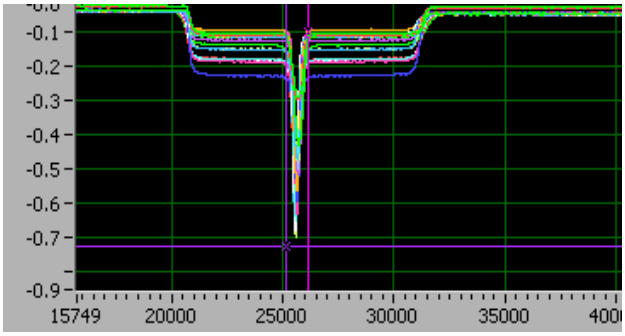

Figure 2.11 Two-dimensional representation of multiple traces over a focus sweep showing the relative difference in their peak amplitudes and widths.

The two slit probe has been used extensively for both research work and in production; one of the systems has been installed at an aerospace production facility and has been used as a QA tool in welding applications for more than two

years. Two versions of the probing system have been experimented on. One that uses the beam deflection of the EB machine, where with an electrical interface, the deflection can be controlled by the probing system, and the other is a standalone system that incorporates its own independent deflection system. The probing systems have been used for characterising electron beam guns, for transferring welding parameters from one machine to another and as a QA tool in the production environment for sharp focus settings and other diagnostics.

2.6. Inverted Double-Slit Probe

The two-slit probe described above does not need any regular maintenance or removal from the chamber once installed. However, the initial alignment of the probe fingers and fixing in the chamber requires effort and specialized skills. For better accuracy and consistency of the results, proper alignment of the fingers, positioning of the probe in the chamber and a way of verifying the same is essential. The inverted double slit probe was developed to overcome limitations of the earlier version of the probe. The construction of the inverted double-slit probe is shown in Figure 2.12. This probe consists of two fingers that are rectangular in shape facing towards each other having two slits on each. Two slits on each fingers of the probe are used for speed calibration by measuring the time taken by the beam to cover the distance between two slits. The inner slits on both the fingers are used for measurement of the signal as well as for verification of the alignment of probe. To measure the full beam current, a Faraday cup is placed between the two probes as shown in Figure 2.12.

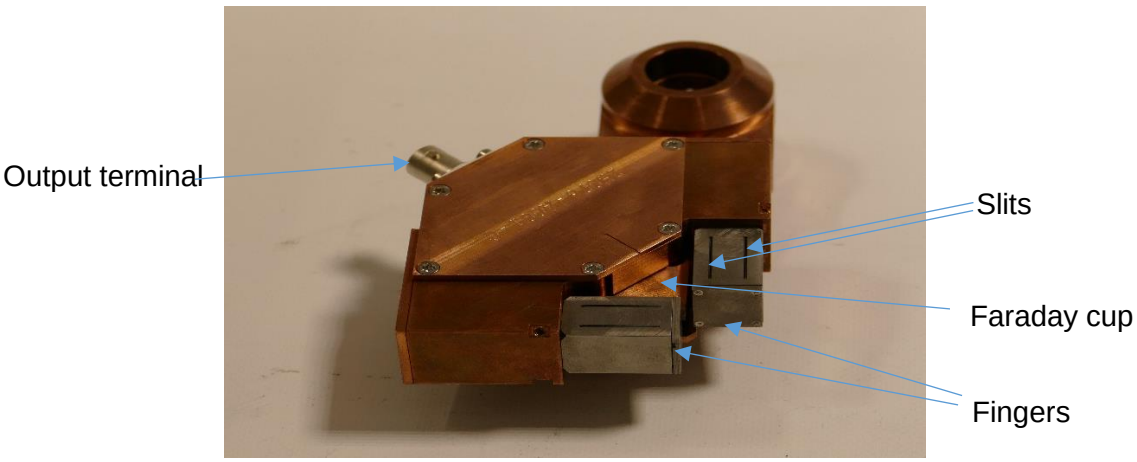

Figure 2.12 Construction of the inverted double-slit probe (Kaur et al., 2016).

As shown in Figure 2.13, beam is scanned over the probe in circular pattern as compared to the triangular pattern generated for earlier version. The circular pattern is generated by using a sine wave i.e. using a single frequency, whereas the triangular waves consist of multiple frequencies. Due to this, the deflection amplifiers perform better for sinusoidal inputs as compared to any other type of inputs. As shown in the Figure 2.13, the beam travels over the first finger, the Faraday cup and the second finger. Either the pattern is repeated in the same fashion over the slits or the beam is stopped in a parking position at 16:30 as shown.

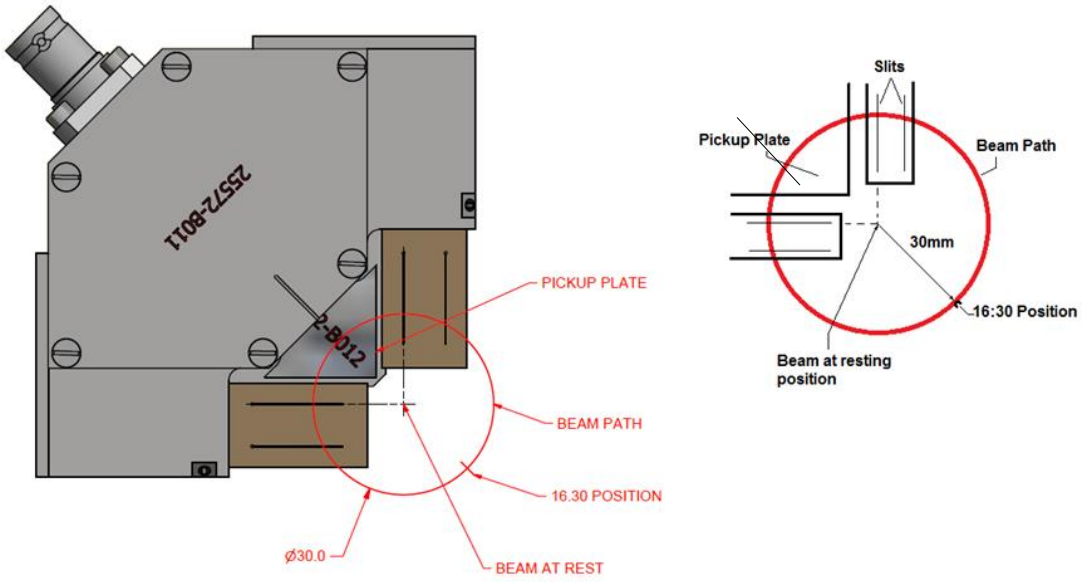

Figure 2.13 Scanning of the beam over probe.

In response to the deflected electron beam, a typical output signal of the probe is shown in Figure 2.14. The distance between points ‘a’ & ‘b’ or ‘d’ & ‘e’ can be used for speed calibration. When the probe is accurately aligned with the beam in the chamber, the time difference between points ‘b’ and ‘d’ should be 90°. In terms of microseconds, it will depend on the scanning frequency. For instance, for a scanning frequency of 5 kHz, these should be 50 µs apart, i.e. a quarter of the period.

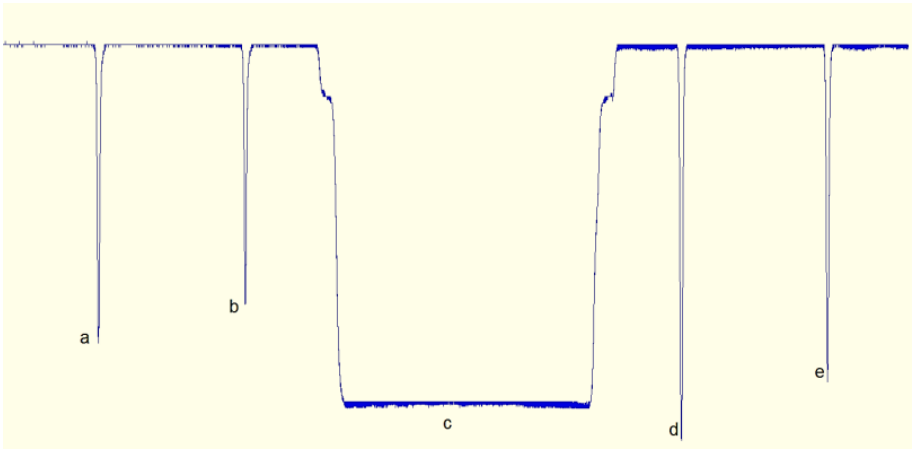

Figure 2.14 Typical output of the probe.

In case the time difference is not the same as above, the position can be adjusted to bring the probe to a position by moving it in ‘x’ and ‘y’ axis. The probe system has been tested in the laboratory and the above method proven very helpful in alignment of the probe reliably.

2.7. Industrial Electron Beam Diagnostics Systems for Welding

Other than the two-slit probe, there are two systems that are commercially available and are used for welding applications. These are a multi-slit probe also known as EMFC mentioned in earlier paragraphs and a pin-hole probe. As the name suggests these systems work on different probing techniques and have relative advantages and limitations. These systems have been briefly described in the following paragraphs.

EMFC a multi-slit probe sensor consists of Faraday cup beneath a disk having a series of radial slits. It collects part of the beam current when the electron beam is scanned over the radial slits. The multi-slit radial disk is shown in Figure 2.15.

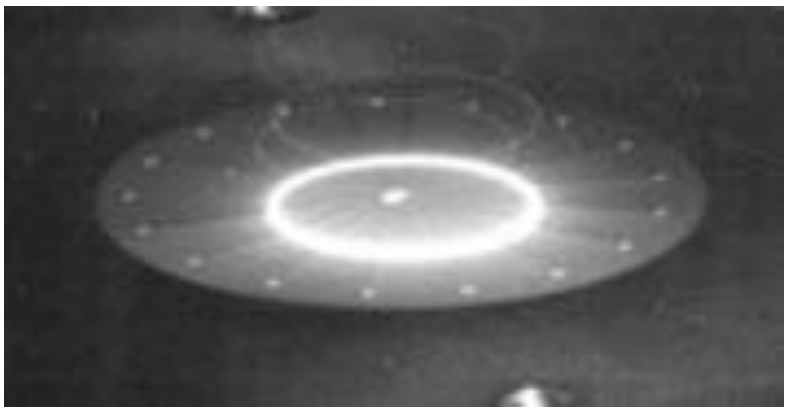

Figure 2.15 Multi-slit radial disk used in EMFC with electron beam being deflected over the disk (Palmer et al., 2007).

The beam current collected is converted into voltage signals across the resistor. After collecting the signals from all the slits as shown in Figure 2.16, the signals are processed using tomographic imaging to construct the power density distribution.

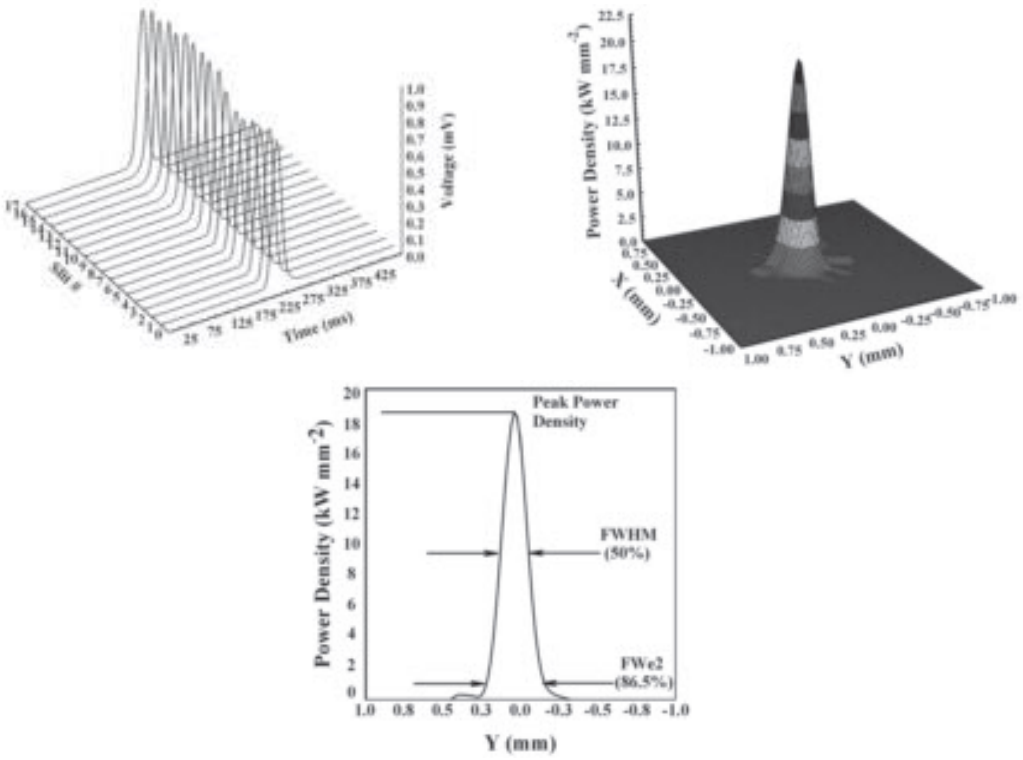

Figure 2.16 Beam measurements with EMFC (Palmer et al., 2007) showing signals from the 17 slits, 3-d power density distribution and different diameters.

From the power density distribution, the Peak Power Density (PPD) and two other distribution parameters i.e. the beam diameter at Full Width Half Maximum (FWHM) of the PPD and the full width of the beam at $1/e^2$ (FWe2) are measured. FWe2 represents the beam diameter at 86.5% of the PPD and according to Pierce and Burgardt (2014) FWe2 corresponds reasonably well to the width of the keyhole produced by the beam.

Another probing system is based on the pin-hole technique. This system also incorporates the slit measurement for fast focus setting determination. A map of the beam current density of the beam spot is captured by deflecting the beam over the pin-hole diaphragm on a line-by-line basis. The schematic of the beam deflection and the sensor plate is shown in Figure 2.17.

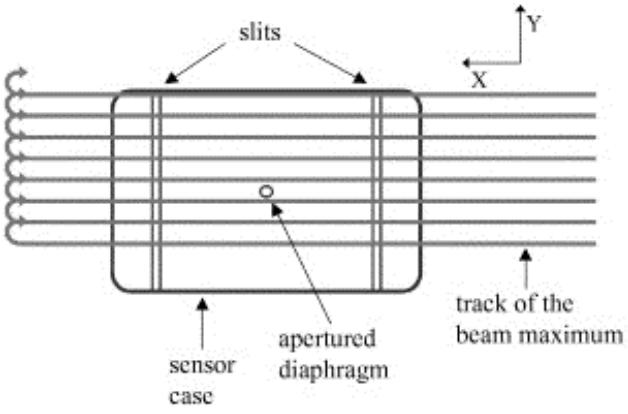

Figure 2.17 Beam deflection and measuring sensor of pin-hole diaphragm (Dilthey et al., 2001).

The signal obtained from the pin-hole is providing a 3-dimensional view of the power density distribution of the electron beam as shown in Figure 2.18. In addition to this, the beam shape is also defined in terms of five different beam diameters at 10%, 30%, 50%, 70% and 90% of the maximum signal amplitude.

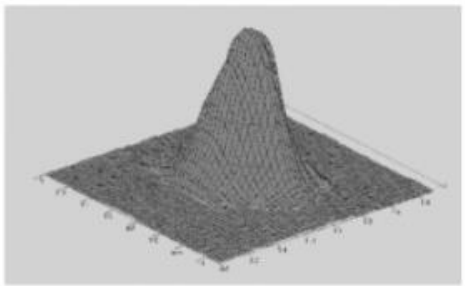

Figure 2.18 3-d power density distribution measurement (Dilthey et al., 2001).

The various devices described above for welding applications have relative merits and limitations. The comparison of three main devices available commercially has been carried out and results are shown in Table 2.1.

Table 2.1 Comparison of commercially available electron beam probing systems for welding.

Feature	**Multi-slit probe (Enhanced Modified Faraday Cup)**	**Pin-hole probe (DIABEAM)**	**Two-slit probe/Inverted double-slit probe**
Max. Power	10 kW [1]	30 kW [3]	40 kW [5]
Resolution	100 µm [2]	20 µm [4]	50 µm [6]
Scanning pattern	Circular	Raster	Triangular/Circular
Complexity	Simpler scan pattern that might not need any modifications to the gun deflection system	High frequency and precise scanning. Specialised scanning	Medium frequency scanning. Modifications in gun deflection system to generate the pattern may be required.
Measurement data information	Reconstruct the power density distribution map of the beam. Two beam diameters at FWHM & FWe2	Measures the power density distribution of the beam directly. Five beam diameters at 10%, 30%, 50%, 70% & 90%	Measures the beam profile for focus sweep, Speed of deflection, Beam diameter at FWHM.

Note: [1] (Elmer et al., 2008), [2] (Elmer and Teruya, 2001), [3] (Reisgen et al., 2014), [4] (Dilthey et al., 2001), [5,6] (Dack and Nunn, 2013)

The two slit probe provides beam profiling for focus sweep, whereas the pin-hole probe and multi-slit probe can also provide a current density distribution map of the beam spot. However, the information the two slit probe provides gives a good indication of the variations in the gun parameters required for the welding

application. The probe can detect if the beam shape is circular or elliptical with the exception being when the ellipse major axis is at 45° to the probe slits. At high power operation the two slit probe does not require a thermal management system or active cooling as compared to other systems. In two slit probes, most of the time the beam is placed on the beam dump and is deflected on the slits only during the very short periods of measurement and hence its heat input is minimal and does not damage the slit surfaces. This could be a very useful feature of the system to reduce maintenance costs, and in the case when it is to be used in hot cells in the nuclear industry where the disposal of spent probe components has high cost, due to their activity.

2.8. Research Work Carried out with the Above Systems for Beam Measurements

The devices mentioned in the above paragraphs have been tried in various beam measurements to be used in welding applications.

Palmer and Elmer (2007) have used the EMFC to characterise two different EB machines when operated with the same welding parameters at sharp focus settings. It was also used to determine the beam crossover locations in the gun by analysing the beam measurements at different working distances. The EMFC was used for transferring the welding parameters from one machine to another by correlating the beam distribution parameters on two machines that were achieved at different working distances on the two machines (Palmer et al., 2007). As a result, the welds were made with a variation of approximately 8% in the weld depths. The utilization of the EMFC in process control as a quality assurance tool was examined by Palmer and Elmer (2008) over a period of 18 months involving approximately 90 welds. Usually the focus is controlled by an experienced operator during the production runs to ensure the weld quality. This work aimed at finding out the differences between the variations in operator's set focuses and the ones readjusted with the EMFC. By using the EMFC, they were able to control the variations in peak power density, FWHM and FWe2 to 5.24%, 3.05% and 2.23% levels as against to 6.86%, 4.28% and 2.91% that were

achieved with operator's settings. In the above cases, the material used was stainless steel and the beam powers used were less than 1 kW.

A pin-hole probing system was used to investigate the beam parameters i.e. beam diameters and beam power density distribution on the weld shape and dimensions (Dilthey and Weiser, 1997). As compared to the earlier studies to analyse the influence of the machine parameters on the weld characteristics, they found that the beam parameters such as beam diameter and the power density distribution have a strong correlation with weld shape and must be included in the welding report to ensure the weld quality. Again in these experiments steel was used and beam powers of less than 10kW were employed for diagnostics and welding.

The two-slit probe has been installed in an industrial environment at one of the aerospace industry sites for nearly 4 years. It is being used for capturing beam characteristics in terms of beam diameter at the FWHM and the peak current intensity. During production, whenever there are maintenance events, variations in the captured data are observed (Dack and Nunn, 2013). The probe has also been used to study variations in the weldment dimensions against the focus sweep in a controlled industrial environment with the aim of establishing the ability of the probe to relate the probe measurements with physical weld profiles. The two-slit probe was also used by Huang (2012) for estimating the beam diameters at focus to validate its keyhole models for EB welding.

2.9. Summary

A detailed literature review on the devices used for characterising electron beams for welding applications have been presented in this chapter. The development of the two-slit probe and inverted two-slit probe have been described. The applications of these devices in industry have also been highlighted. The devices built with different concepts have been compared.

As described, the different devices have their respective pros and cons. Some devices are capable of providing a detailed image of the power density distribution but their operation has been found only at low powers in the published literature. Due to the complexity of the devices in construction, these also need

regular maintenance. There are devices that can be used at high power and need less maintenance, however, the evidence on the use of extracted information from the device is limited. Because of all these reasons, the use of such devices in uncommon in the industry. Through the research work in this thesis, the potential of the device capable of use at high power is explored further by using novel techniques of data processing. The next chapter introduces the experimental work carried out towards achieving the above said aim.

Chapter 3. Characterisation of Electron Beam Welds

As described in the previous chapter, the present work is focused on identifying the beam characteristics that can indicate the point when the weld quality starts deviating from the tolerance limits set by the qualification standards. As the application area is focused on the aerospace industry, aerospace standards for electron beam welding have been used to define the weld quality parameters. This chapter provides the details about the method of arriving at those beam characteristics that relate to the weld quality and can help to detect the variations before these go out of tolerance limits. There are different ways of achieving the objective stated. It could be a numerical or an analytical approach which would describe the process using a mathematical model. Alternatively, one could use an experimental approach to describe the processes and the effects of the process parameters by employing statistical techniques. Sometimes, a combination of both techniques is used. For the present research, an experimental approach was used by carrying out the welds and acquiring the probe traces for the corresponding parameter settings. The welds were examined to measure their profiles and to identify any defects. The acquired probe traces were also analysed to generate the characteristics of the electron beam.

3.1. Experimental Approach

To characterize the EB welds in a systematic way, the Design of Experiments (DoE) technique was used. Design of Experiments (DoE) is a statistical technique developed in early 1920s by R. A. Fisher (Roy, 2001). The technique was first used in agriculture field in understanding the effect of multiple variables on crop conditions. As compared to the classical method of experimentation i.e. changing one variable at a time, the DoE method requires fewer total experiments to be conducted and also the joint influence of all the variables can be assessed (Eriksson et al., 2008). DoE involves planning, designing and the analysis of experiments to draw the valid and objective conclusions efficiently.

In DoE, the process variables are known as control factors and the process outputs are known as responses. A block diagram of a process known as P-diagram is shown in Figure 3.1. The output y or the response can be described in terms of the input parameters.

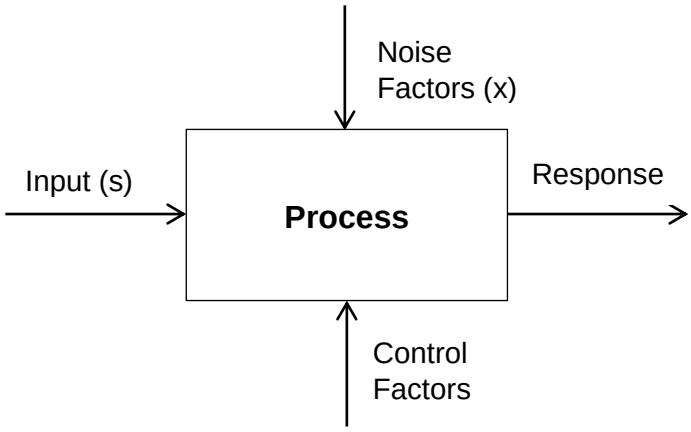

Figure 3.1 Block diagram of a process (Phadke, 1989).

The control factors are the factors which can be controlled in the production environment; these are also called the design parameters. To get the response 'y' i.e. the quality factor within the limits, it is essential to determine the optimized levels of the control factors. The noise factors are the factors which cause deviation in the quality responses from their nominal values and cannot be or are difficult to control in the production environment, but might be controllable in the experimental environment.

Several models for DoE have been developed over time including Full Factorial, Fractional Factorial and Taguchi approaches (Zohrevandi and Bashiri, 2014). The Full factorial designs use all the possible combinations of the control factors. Mostly, the industrial experiments involve a significant number of control factors, the full-factorial approach results in a large number of required experiments. Total number of experiments needed in full-factorial design is given by equation 3.1

$$NOE = (N_l)^{N_f} \quad (3.1)$$

where N_l = number of levels

N_f = number of factors

There are various DoE methods to reduce the number of experiments that selects the small set from all the possible combinations of experimental runs. Whatever method of DoE is used; these are implemented in the following procedure as shown in Figure 3.2.

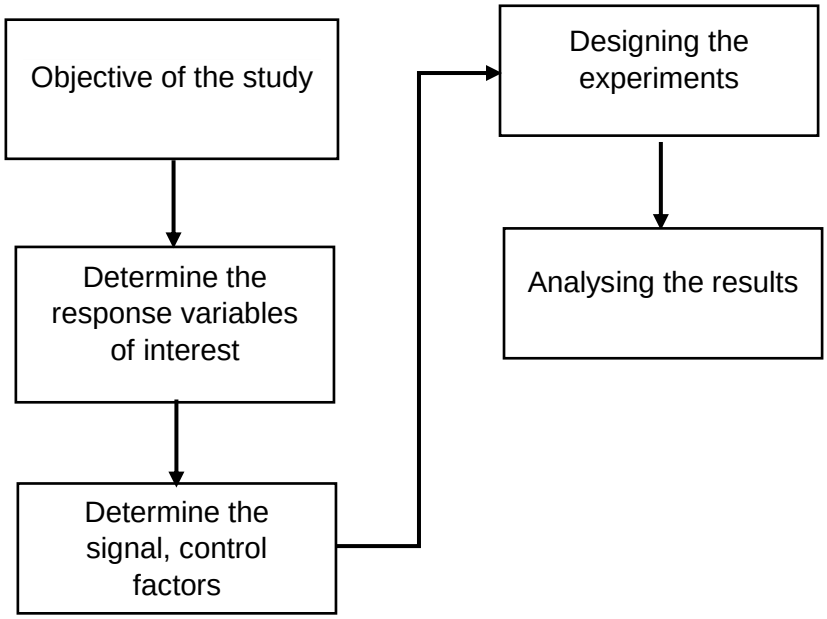

Figure 3.2 DoE implementation procedure.

3.1.1. Materials

As mentioned in Chapter-1, the titanium alloy Ti-6Al-4V is the workhorse of the aerospace industry. There are many titanium alloys that are categorized into four different groups i.e. unalloyed titanium, α-structure, β-structure and α-β structure. The α-structure is more ductile phase and the β-structure is stronger but less ductile. The α-β structure of the titanium exhibits the mechanical properties which are in between both. Ti-6Al-4V is a α-β structure alloy with 6% aluminium, 4% vanadium and trace amounts of iron. In addition to the high strength, this alloy also exhibits the property of super plasticity which enables it to be formed into very complex parts which are light weight. It is being used in aero-engine components and in most of the sections in the airframes. Hence, with the aim to focus on the industrial relevance, this material has been chosen for the present study. To carry out the experiments 8 mm thick Ti-6Al-4V plates are used for 4 mm partial penetration. As Antony (2014) has suggested, to use the quality

characteristics that can be measured precisely, accurately and with stability. Hence, the aim of choosing partial penetration was to get the fine measurements of the dimensions and any defects occurring which are more accurate to measure on partially penetrated welds as compared to the fully-penetrated welds. Also, the dimensions of the welds and the defects produced are more sensitive to the beam characteristics than for full penetration welds.

3.1.2. Equipment and experimental set-up

To carry out the melt runs, 150 kV EB machine was used. For each pump down, titanium plates of 110 mm length in the welding direction were mounted. The plates were 80 mm wide to carry out five melt runs on each.

To characterize the electron beam, a two-slit probing system described in section 2.2 was also installed in the chamber at the same working distance as that of the work pieces. The block diagram of the experimental set-up is shown in Figure 3.3. A high voltage power supply is connected to electron beam gun to provide required accelerating and control voltages. To deflect the beam over the two-slit probe for electron beam measurements, scanning pattern is generated by a pattern generator and fed to deflection amplifiers.

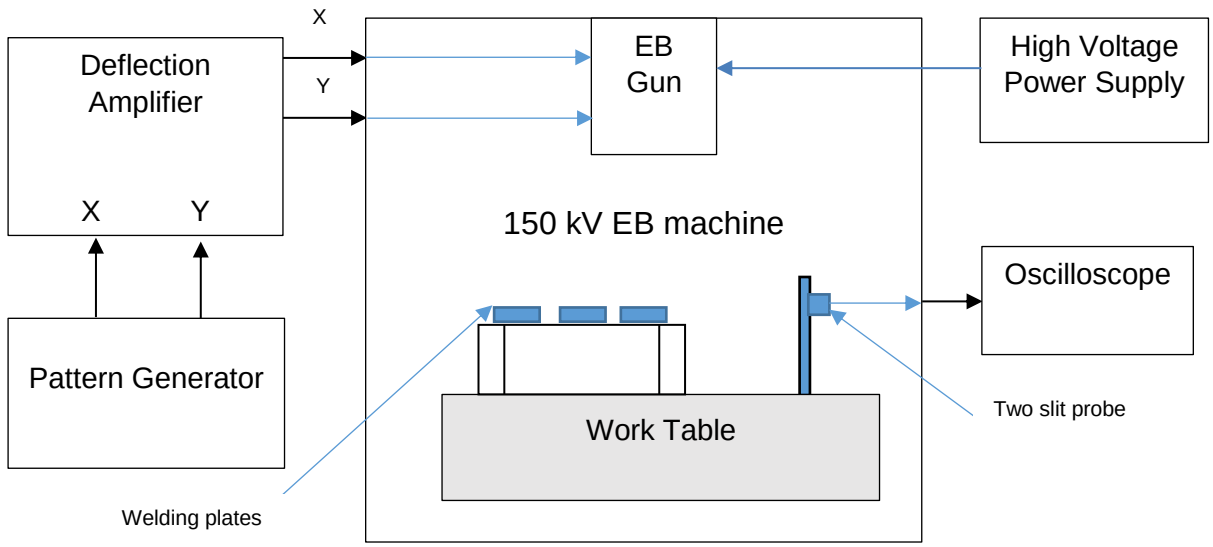

Figure 3.3 Block diagram of experimental set-up.

3.1.3. Response variables

Different weld characteristics were chosen for weld quality measurements that describe the weld shape and weld defects. Weld quality in terms of defects basically dictates the allowable size, spacing and amount of defects. For the present study, weld penetration depth, weld width at the surface and weld width at 50% of the depth are measured to estimate the weld shapes as shown in Figure 3.4.

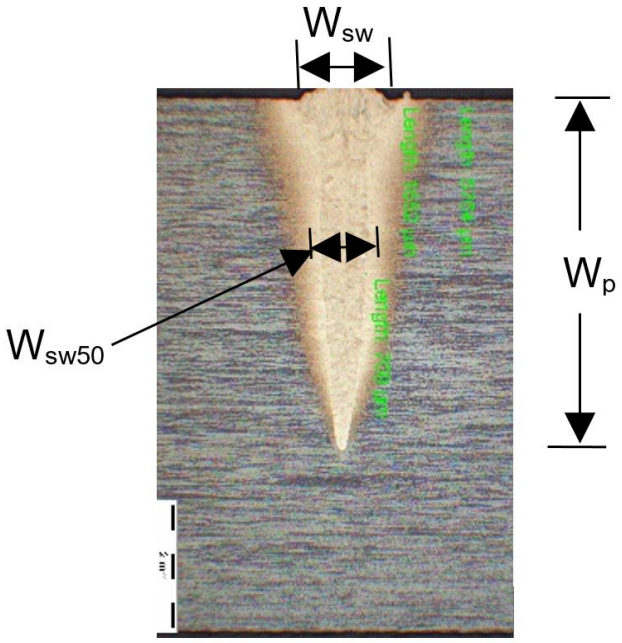

Figure 3.4 Micro-section of a weld with dimensions.

There are different types of defects that can occur during the welding process such as porosity, undercuts, cracks, root defects, incomplete penetration. These defects can occur due to the imperfections in the product design, the material properties, contamination or the welding process itself. Porosity is described as the voids or the gas holes within a weld. During the welding process, sometimes, gases are trapped in the molten keyhole and are not able to escape from the weld pool and create a hole when solidified. The size and distribution of the pores are of concern with regard to weld quality. This depends upon the location, size and distribution, whether uniformly over the weld length or more concentrated to specific areas (Jeffus, 2012). The allowable levels for these conditions are specified by the qualification standards. Cracks might also occur during the

welding process due to shrinkage. The cracks can either occur at elevated temperatures during welding or during the cooling process due to residual stresses. One of the reasons for the development of cracks is the rigidly clamped workpieces that are used to prevent shrinkages during the welding process. Undercut is formed on the surface because of the complex interaction of the surface tension in the weld pool, its movements and the solidification process (Schultz, 1993). The undercuts form a sharp notch on the surface and should be within limits. These defects have been chosen as the response variables as the beam parameters can affect the level of defects when all the other prevention methods have been taken care of. For example, Saresh et al. (2007) observed lack of fusion, root porosity and undercut in the top bead even with a marginal increase in the beam power.

For the present research, the aerospace standards have been considered to determine the tolerances for the weld dimensions and the levels of the allowable defects. There are several standards which define these parameters. The British Standards BS-EN-ISO-13919-1:1997 (1997), BS-EN-ISO-13919-2:2001 (2001) describes the quality levels for imperfections in electron beam welded joints for steel and aluminium and its weldable joints respectively. These standards have defined quality levels in three categories i.e. B, C, D where ‘B’ is the most stringent quality level, ‘C’ is the intermediate and ‘D’ defines the moderate level. The allowable limits for ‘B’ quality level for 4 mm thick weld are tabulated in Table 3.1.

Table 3.1 British standard (BS-EN-ISO-13919-1:1997) acceptance criterion

Weld quality parameter	**Type**	**Allowable level**
Penetration depth		±0.5 mm
Cracks		Not permitted
Porosity	Individual pore diameter	≤ 1.2 mm
	Distance between individual pores	≥ 2 mm
Undercut		≤ 0.2 mm
Root concavity		≤ 0.4 mm

Another standard related to aerospace industry is given by American Welding Society (AWS) i.e. D17.1:2010. This standard specifies the specifications for fusion welding for aerospace applications. Again, quality levels are defined for

three different categories named as Classes A, B and C. In this case, Class A is the most stringent and the quality level for the present work has been derived from this class as tabulated in Table 3.2.

Table 3.2 American welding society (D17.1:2010) acceptance criterion

Weld quality parameter	**Type**	**Allowable level**
Penetration depth		±0.5 mm
Cracks		Not permitted
Porosity	Individual pore diameter	≤ 1.32 mm
	Distance between individual pores	≥ 4 x larger adjacent pore
	Accumulated length in 75mm	5.32 mm
Undercut		≤ 0.28 mm
Root concavity		≤ 0.28 mm

Both the above standards are comparable. Cracks are not permitted in any of the standards. Porosity and undercut requirements are slightly more stringent in British standard whereas root concavity has lower limits in AWS standard. AWS provides an additional parameter for porosity measurement i.e. the accumulated length of the pores over 75 mm of weld length. For the present analysis, British standard has been used and the cumulative length measurement from the AWS standard has been used as additional porosity measure. No specific tolerances for weld width been mentioned by the above standards. However, the British Standards Institution mentions about the weld width measurements in its document BS-EN-4677-001:2012 (BSI, 2012). According to its specifications, for 4 mm weld, the weld face width can be between 1 mm to 3.4 mm.

3.1.4. Signal and control variable

As described in chapter-1 weld dimensions and weld quality depend on many factors. These are related to the electron beam itself i.e. accelerating voltage, beam current and focus current; the welding parameters i.e. working distance, welding speed, vacuum levels in the chamber; and the material properties. The present research aims at identifying the variation in beam parameters captured by the two-slit probe and relating these to the weld quality. As the vast majority of EB machines work on fixed accelerating voltage and beam power is varied by

varying the beam current, hence, the accelerating voltage was fixed at the optimum level of the machine i.e. 140 kV. To generate the variations in beam parameters, the beam current and focus current are chosen as the control variables. There are other ways also to generate variations in beam characteristics; for instance, generating different quality beams by changing the cathode configurations. However, it is not considered for the experimental work as it is difficult to quantify the beam quality in terms of cathode variations and difficult to repeat the same settings.

Other parameters such as welding speed, working distance and vacuum levels are selected based on the earlier experience and are defined in Table 3.3.

Table 3.3 Welding parameters

Signal/Fixed Factors	Level
Accelerating voltage	140 kV
Working distance	240 mm
Welding speed	1 m/minute
Vacuum	10^{-4} mbar

3.2. Design of Experiments

To characterize the electron beam welds, the experiments were carried out in two steps i.e. Melt runs -1 and Melt runs -2.

3.2.1. Melt runs – 1

In the first step, the welds were carried out with initially determined input and control variables for screening purpose. A single titanium plate of size 100 mm x 80 mm x 8 mm was used. The focus setting was fixed at the sharp focus at the plate surface adjusted by the operator at low beam current values. Once the sharp focus was set, the melt runs were carried out by using different values of the beam current beginning with 30 mA. The weld at 30 mA fully penetrated the plate and therefore, lower beam currents were tried out by changing the beam current to 25 mA, 15 mA, 10.5 mA and 8.5 mA.

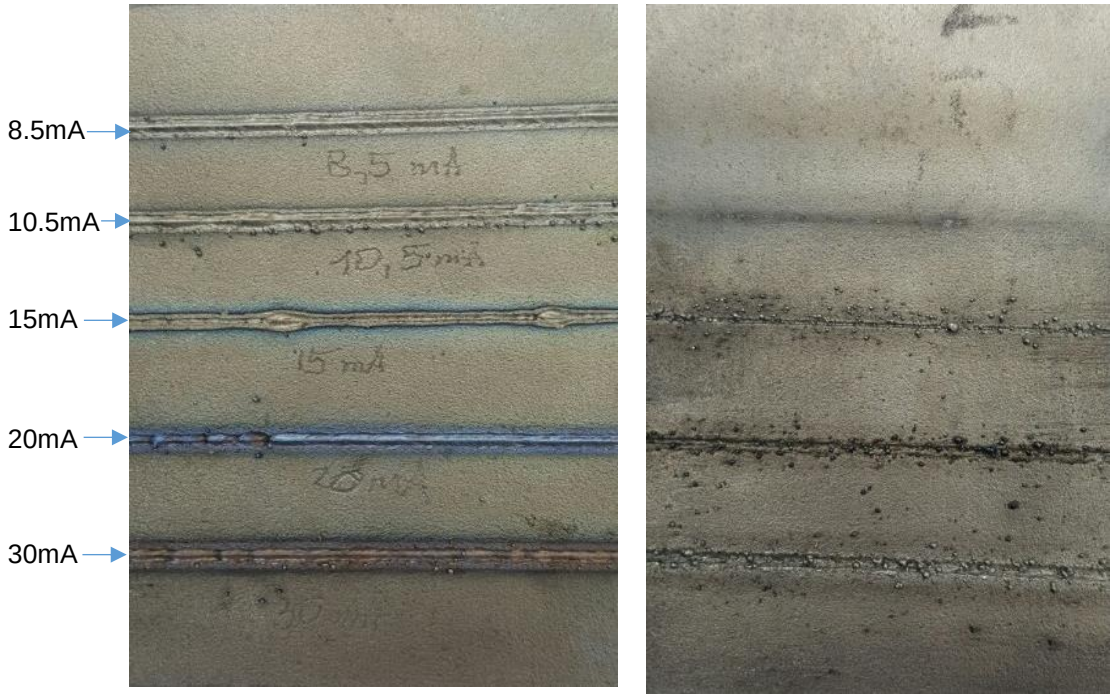

Figure 3.5 Top bead (a) and the underside (b) of the melt runs for different beam currents.

Figure 3.5 shows the top bead (a) and the underside (b) of the plate. It was clear from visual inspection and shown in Figure 3.5 (b) that a beam current of more than 10 mA is too high for the targeted weld penetration depth as it is already penetrating a 8 mm deep weld plate. Hence, for the Melt runs - 2 experiments, the range of beam current was selected to be from 7.5 mA to 10 mA.

3.2.2. Melt runs – 2

The aim of this set of experiments was to establish the experimental set-up and find out if any modification in terms of experimental set-up, measuring equipment and methods or selection of control and response variables was required. The experiments were also aimed at narrowing down the levels of control factors i.e. beam current and focus settings.

The range of beam current was selected from 7.5 mA to 10 mA based on the results of the Melt runs – 1. The five levels of focus settings were chosen including sharp focus. There were two under-focused levels and two over-focused levels at an interval of 10% denoted by U2, U1, SF, L1, L2 as shown in Table 3.4. The sharp focus (SF) was again adjusted by the operator and was at a machine setting of 2.54, arbitrary units.

Table 3.4 Beam current and focus settings

Focus Settings / *Beam Current (in mA)*	*U2* 2.49	*U1* 2.52	*SF* 2.54	*L1* 2.57	*L2* 2.59
7.5					
8.0					
8.5					
9.0					
9.5					
10.0					

During this set of melt runs the two-slit probe was also installed as shown in Figure 3.6 to capture the probe traces for all the combinations of the control factors. The sharp focus setting was verified by the probe signal as well i.e. at the highest intensity and the narrowest beam width.

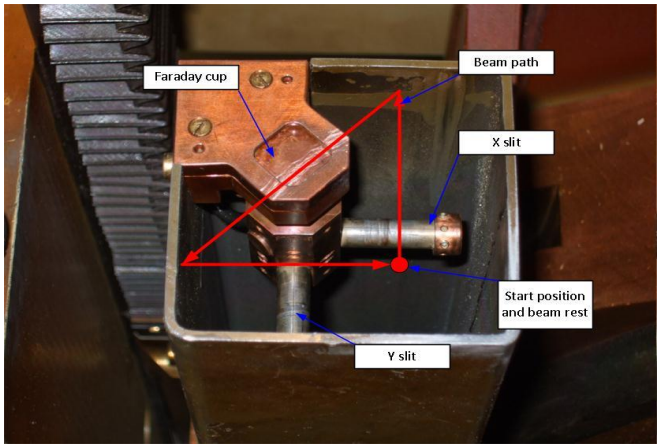

Figure 3.6 Two-slit probe installed in the vacuum chamber.

The DoE was designed as a general factorial (multiple level) experiment. All the possible combinations of the control factors were used without any replication. A total of 30 melt runs were carried out and corresponding probe traces for all the combinations before the welds were collected.

3.3. Examination of the Welds

Two tests on the welds were carried out. The first was radiographic examination to determine the porosity and other defects. The second was micro-sectioning of the welds to assess the weld profiles. In the radiographs the porosity was quantified. To accurately measure the sizes of the defects, the radiographs were

digitized using a high resolution camera to measure the porosity. The radiographic images of all the weld plates are shown in Figure 3.7 (a) to (e) for all five focus settings given in Table 3.4.

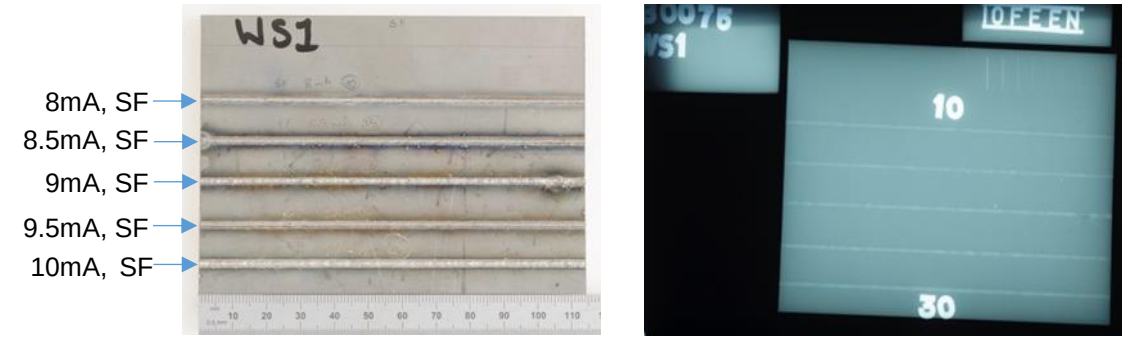

Figure 3.7(a) Weld and radiographed image at sharp focus

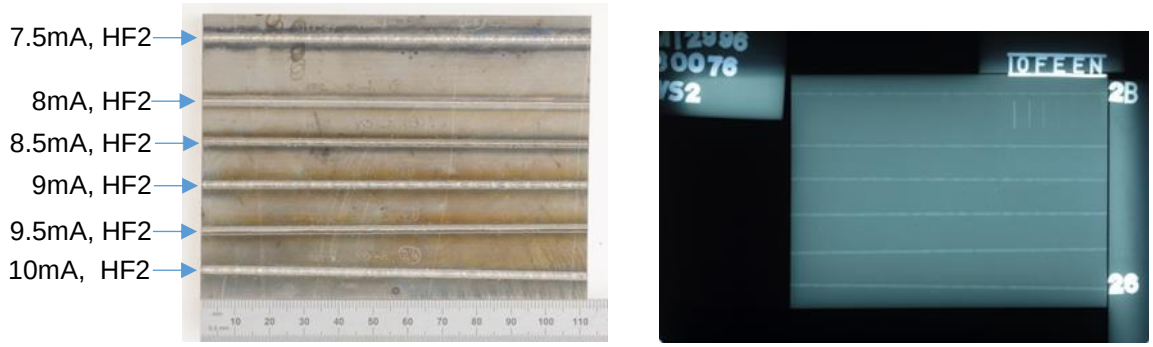

Figure 3.7(b) Weld and radiographed image at focus U2.

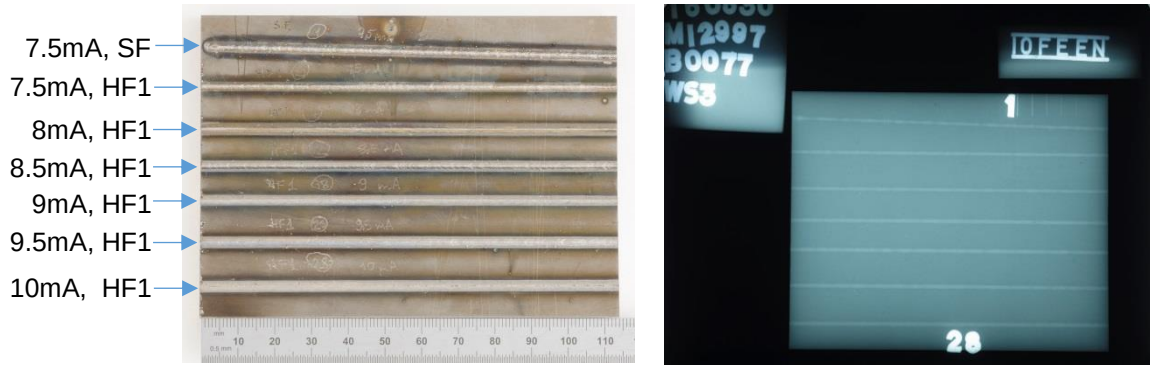

Figure 3.7(c) Weld and radiographed image at focus U1

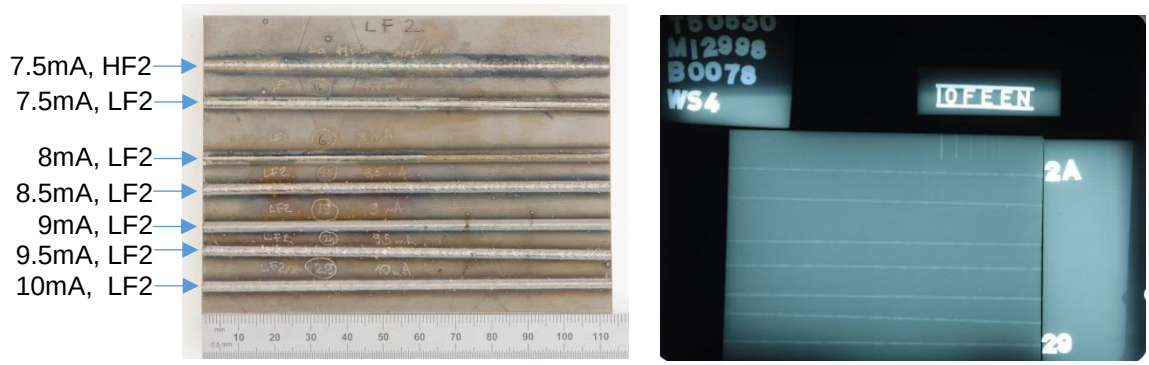

Figure 3.7(d) Weld and radiographed image at focus L2.

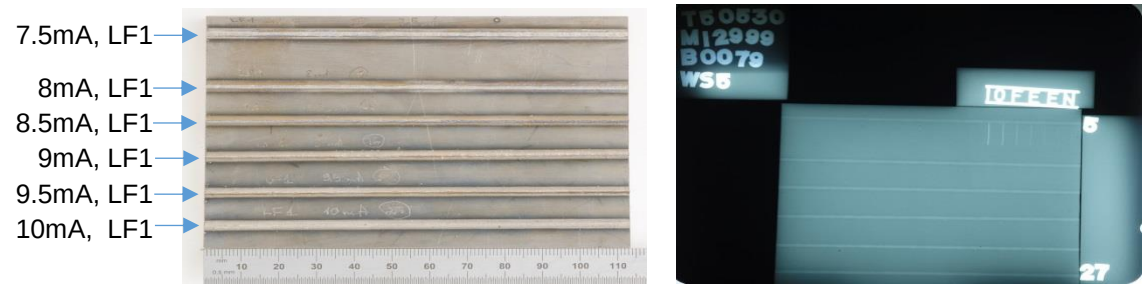

Figure 3.7(e) Weld and radiographed image at focus L1.

Figure 3.7 Weld and radiographed image at different beam current and focus levels.

The radiograph images were examined in the image software at pixel levels to measure the porosity. The linear porosity was observed in the welds and compared against the standard's specifications. At 8 mA beam current, the welds were very clear and no porosity was observed for all focus levels. At other beam current and focus levels, all pore sizes were within limits. Inter- pores proximity at 10mA was observed to be higher than the specifications. An undercut at 7.5 mA for over focused position L2 was observed but is within the specifications. No cracks in the welds were observed. The welds with undercut and the porosity are shown in Figure 3.8 (a) and (b) respectively.

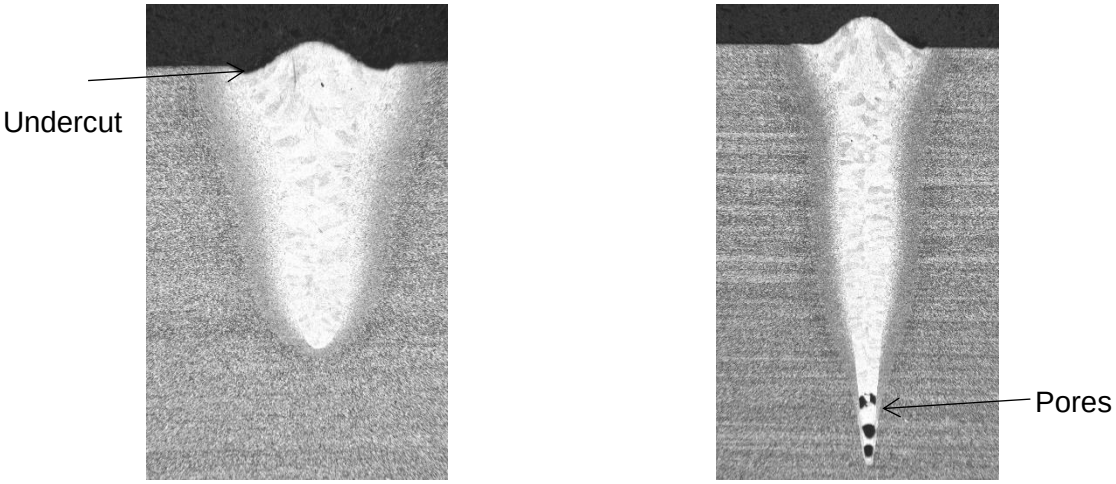

(a) Weld with undercut (b) Weld with root porosity

Figure 3.8 Welds with defects.

The Table 3.5, 3.6 and 3.7 summarise the results of the micro-sectioning i.e. the weld penetration depth, weld width at the top surface and weld width at 50% of the weld penetration respectively.

Table 3.5 Weld penetration depth measurements (Within acceptable limits have been highlighted)

Weld Depth	Focus Levels				
Beam Current	**U2**	**U1**	**SF**	**L1**	**L2**
7.5	5.608	6.204	4.983	3.71	3.242
8	3.846	4.434	4.178	4.132	3.208
8.5	5.676	6.953	6.859	5.459	4.132
9	6.399	8.033	7.748	5.906	4.557
9.5	5.778	7.250	7.621	7.182	5.676
10	5.821	8.187	7.889	7.344	6.046

Table 3.6 Weld top width measurements

Weld Width top	Focus Levels				
Beam Current	**U2**	**U1**	**SF**	**L1**	**L2**
7.5	1.991	1.932/1.808	2.251	2.153	2.379
8	2.008	1.421	1.821	1.702	2.574
8.5	2.127	1.642	1.915	2.055	2.498
9	2.183	1.528	1.898	2.153	2.464
9.5	2.383	1.821	2.021	2.008	2.162
10	2.349	1.728	1.936	1.889	2.43

Table 3.7 Weld width at 50% of depth measurements

Weld Width 50%	Focus Levels				
Beam Current	**U2**	**U1**	**SF**	**L1**	**L2**
7.5	0.919	1.085	1.259	0.945	1.366
8	1.285	1.132	1.225	1.294	1.651
8.5	0.885	0.774	0.94	0.957	1.204
9	0.894	0.745	0.817	0.979	1.064
9.5	0.987	0.732	0.868	0.919	1.17
10	0.979	0.74	1.17	0.928	1.119

The weld penetration depth was required to be more tightly controlled and was targeted to be between 3.5 mm to 4.5 mm according to the allowed tolerances for a nominal value of 4 mm deep welds. As can be seen from Table 3.5, there were few highlighted weld depths achieved within the specified range for a set of control factor values.

The above measurements of weld profiles and porosity helped in narrowing the set of beam current and focus settings for the further experimental work.

3.4. Analysis of Probe Traces

As mentioned earlier, during this trial of experiments, the probe traces were captured for all the settings prior to each weld. These were recorded using an oscilloscope. A typical acquired probe trace is shown in Figure 3.9.

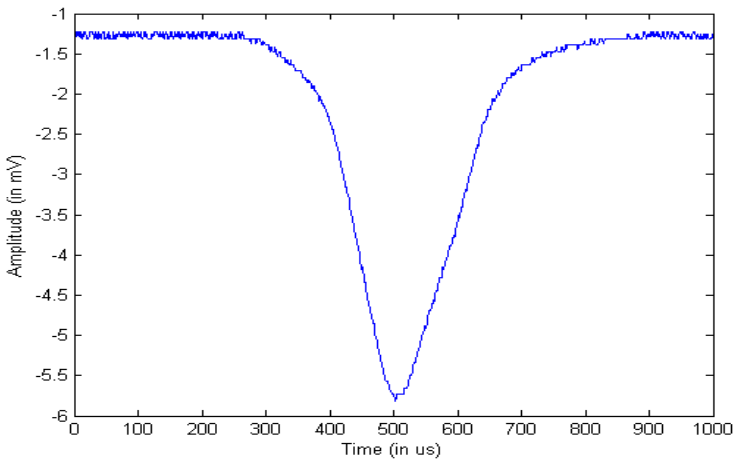

Figure 3.9 Acquired probe trace.

However, during the analysis of the probe traces, some problems were encountered. It is noticed that there was too much variation in the peak intensity and the beam width. These variations were random and were not correlating to the control factor settings used during the experimental runs. In this case, it was not possible to derive the probe trace parameters and correlate with the weld quality parameters.

On repeating the capture of probe traces, it was found that the traces were not stable and the peak amplitude and the widths were varying. It was expected that the variations could be due to high voltage power supply ripple. This problem was not observed in the weld profiles as the weld pool averages out the variations in the keyhole, and generally does not respond to the high frequency of the ripple. In the similar fashion, averaging of the probe traces was carried out using an option available on the oscilloscope. The stability in the probe traces was observed. It was decided at this point to recapture the probe traces using the averaging for all the combinations of the control factors.

Another problem was encountered during the recapturing of the probe traces. The filament had worn and was required to be changed. Following its maintenance, changes in the sharp focus settings were observed. At this stage it was decided to carry out the probe trace measurements with the changed setting of the sharp focus and adjusting the over focused and under focused levels accordingly. Because of these variations during the experiments, it was not justified to relate it to the weld quality parameters for the weldments carried out earlier. However, the analysis of the probe traces to generate the features vector was carried out using the method detailed in the next chapter.

3.5. Summary

As described, two sets of melt runs were carried out and the probe traces were acquired for the same settings. These experiments helped in identifying the machine settings for further experiments. Unfortunately, the probe traces could not be related with the welds because of the problems in capturing these first because of the ripple and second set because of changes in the machine settings. However, the acquired probe traces in the second set were analysed

separately to generate the features vector and to examine the possibility of using it to characterise electron beams. The next chapter is focused on the analysis of the probe traces to relate it to the beam characteristics.

Chapter 4. Analysis of Two-Slit Probe Signals

In the previous chapter the details about the experimental method of first and second set of melt run trials has been described and details given of the equipment and methodology for capturing the two-slit probe signals. These probe signals measure the beam width and give indications of the beam current intensity distribution, and it is proposed that these in turn give a sensitive representation of beam quality. However, for machine recognition and quantification of the signal it is often useful to define a set of parameters known as the features vector which in this case could be derived from the probe signals and which it is proposed can be related to weld quality characteristics. For an ideal Gaussian type of signal, the peak intensity amplitude and the beam width have been directly related with the weld profile (Kaur et al. 2015). However, there might be changes in the beam shape and the beam parameters due to variations in the electron beam gun parameters, welding parameters, cathode erosion or other machine variations. With this aim, a novel method has been applied to analyse the probe signals using the Wavelet Transforms which are detailed in this chapter. The results achieved through this work have also been published in (Kaur et al., 2015a).

4.1. Introduction to Signal Analysis

The two-slit probe can be used to capture measurements of the electron beam. A typical signal from the probe is a Gaussian type pulse signal. However, depending on settings in the gun and welding parameters, the variations in shape and other parameters of the beam captured by the probe can be observed. To derive a set of useful parameters to describe the probe signals, some signal analysis techniques are required. There are numerous techniques used in literature to characterise or differentiate between different pulse shapes. These are either based on time domain or frequency domain analysis.

Many examples in the time domain are found in the nuclear industry that relate to pulse shape discrimination to determine the alpha/beta/gamma rays (Yasuda et al., 2001). These techniques are based on measuring different parameters like

peak amplitudes, rise time, decay time, zero-crossings, integration of the signals, and combination of parameters or customized algorithms. Choice of the parameters and the technique used depends on the application requirements. Similar kinds of signal analyses are also found in partial discharge, electrocardiography, machine diagnostics, non-destructive testing and in many other applications. A detailed review of the wavelet industrial applications has been carried out by Truchetet and Laligant (2004).

In the frequency domain, the Fourier transforms have been used extensively for signal analysis. The Fourier transform decomposes the signal into its frequency components using a series of sine and cosine functions. It provides information about what frequency components are present in a signal. However, it does not provide any information about the time i.e. what frequency components are present at what time. To access the time information along with the frequency contents the Short Time Fourier Transform (STFT) was developed that is based on a windowing function. To effectively decompose the signal, the selection of an appropriate window size is necessary (Gao and Yan, 2010) which is not always possible if the signal characteristics are not known already. Also, multiple window sizes need to be used to extract the different signal features localized in time and frequency domains. Hence, if the signals contain different patterns of frequencies, the analysis using STFT is not suitable (Ganesan et al., 2004). In order to analyse these types of signals, wavelet transform has been developed.

4.2. Wavelet Transforms

In recent years, wavelet transforms have been widely used in the field of signal processing mainly because of their capability to analyse signals in both time and frequency domains. Although STFT also gives information localized in time and frequency, the window is a square wave that truncates the sine or cosine function to fit a particular size and also the window size is the same for all frequencies. In contrast, the wavelets have a window size that varies with the frequency scale and hence this is useful in analysis of signals that consists of both discontinuities and smooth components (Rioul and Vetterli, 1991). Because of this, wavelet transforms provide a variety of signal analysis outputs that are used in a wide area of industrial applications for denoising, multiresolution analysis, feature

extraction and many more. A review of applications of wavelet transforms have been carried out by Kobayashi (2001).

Just as a Fourier transform decomposes the signal into series of sine and cosine functions, the wavelet transform breaks a signal into its wavelets. Wavelets are short waves with limited duration, also called basis functions or mother wavelets that can be scaled and translated. Hence, the wavelet transform provides information in the time domain via translations (shifting) and in the frequency domain via scale stretching or dilations. Essentially, the wavelet transform is a measure of correlation between the signal being analysed and the mother wavelet (Gao and Yan, 2010). The wavelet transforms are of different types i.e. continuous-time wavelet transform (CWT) and discrete wavelet transforms (DWT).

CWT of a signal f(t) is defined as

$$CWT_f^{\psi}(a,b) = \int_{-\infty}^{\infty} f(t)\,\psi_{ab}(t)dt \tag{4.1}$$

where $\psi_{ab}(t) = \frac{1}{\sqrt{a}}\psi\left(\frac{t-b}{a}\right) \quad a,b \in \Re;\ a \neq 0$

Here, ψ is the mother wavelet with two continuously varying characteristic parameters i.e. dilation (*a*) and translation (*b*). The wavelet coefficients are given as the inner product of the function being transformed with each basis function. As represented in the above equations, the coefficients of CWT are computed from an integral and can have any resolution. For practical computations with digitally sampled signals, they possess limited resolution. The computation of CWT with computers also follows the same pattern i.e. the coefficients are obtained at discrete intervals by selecting a different number of samples.

Wavelet transforms can also be applied in a discrete version i.e. Discrete Wavelet Transforms (DWT). The DWT decomposes the discrete signal into components under different scales. DWT acts as a pair of complementary high pass and low pass filters and iteratively decompose the signal into multi-resolution subsets of detail (D) and approximate (A) coefficients (Merry and Steinbuch, 2005). For each decomposition level i, low pass and high pass filters are followed by down-sampling of the signal at that level which represents the reduction of a sampling

rate by a factor of 2. cA_i and cD_i are approximate and detailed coefficients for i^{th} decomposition level. The decomposition process of the DWT at different levels is shown in Figure 4.1. Each level is half the bandwidth of the level above it.

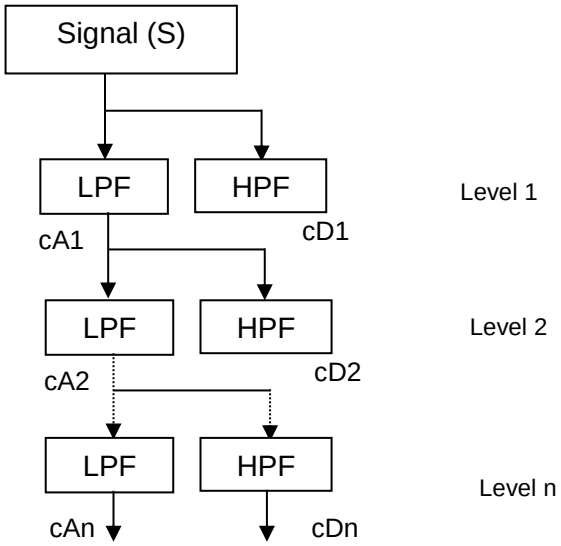

Figure 4.1 DWT decomposition at different scaling levels.

As compared to DWT, CWT provides better time and frequency resolution, however, it requires high processing time and memory usage. On the other hand, DWT is computationally efficient and provides sufficient information for analysis of the signal (Arafa et al, 2009). Hence, DWT is preferred for real-time applications.

Another advantage of wavelet transforms over other techniques is the availability of a variety of mother wavelet forms that have been developed over time. For specific applications, customised wavelets can also be designed and used. A number of wavelet families are available in literature such as Harr, Daubechies, coiflets, symlets, or bi-orthogonal wavelets (Misiti et al, 2007). The choice of a particular mother wavelet depends on the application. For instance, Harr wavelet is the simplest wavelet in the form of a step but is not suitable for representing signals that are smoother in nature due to its discontinuities, whereas the Daubechies wavelets are smoother in nature and better suited for representing the signals with smoother components (Ganesan et al., 2004). Various methods have been used for selecting the optimum mother wavelet. For denoising purposes, the calculations of Percent Root Difference (PRD), Root Mean Square Difference (RMSD), Mean Square Error (MSE) are used to select the optimum

mother wavelet (Umamaheswari and Sarathi, 2012), (Khanam and Ahmad, 2013). There are other methods which are based on energy and energy entropy used for selection of the mother wavelet (Katul and Vidakovic, 1995). Seo et al. (2015) proposed a method based on normalized correlative energy. For the present analysis, various mother wavelets were compared for the above parameters. The lowest value for PRD, RMSD and MSE were observed for dB3 and hence was chosen for the present analysis.

4.3. Wavelet based Feature Extraction

To characterise the probe traces, a set of features, also known as a features vector, have been extracted from the wavelet coefficients. As the wavelet transform decompose the signal into various frequency bands, a high dimensional feature vector can be generated from its coefficients. Depending on the application, a required band or scale can be identified with prominent features and thus reducing the dimensions of the features vector. Numerous applications are found in literature that use wavelets for feature extraction purpose and some examples are described below.

There has been intensive research carried out in different application areas such as medical, fault classification in power systems, acoustics, ultrasonics, image processing and finance to use wavelet transforms for feature extraction and classification (Gargoom et al., 2004, Sifuzzaman et al., 2009). To detect the defects in bearings, the magnitudes of the wavelet coefficients were used (Li and Ma, 1997). These were able to detect the localized defects under different operating conditions. Antonino-Daviu et al. (2006) have used DWT based differences in the energy levels in various decomposition levels to identify breakage in the rotor bars in induction machines for predictive maintenance of the electrical machinery used in the industry. Keswani (2008) has used the energy distribution among the decomposition levels in identifying the faults in the High Voltage Direct Current transmission systems.

The applications of wavelet transforms are also found in the field of EB welding. These applications are mainly concerned with detection of secondary current signals using X-rays or ion detectors. Yoon (2003) has analysed the signals of X-ray and ion detectors using Fourier analysis and also using a wavelet transform.

He could differentiate between partially penetrated, fully penetrated and over-penetrated conditions better with wavelets, compared to Fourier analysis. Wavelet analysis has been used to identify the frequency range of the maximum energy of the beam based on Root Mean Square (RMS) deviation of the Discrete Wavelet Transform (DWT) coefficients (Trushnikov, 2013).

4.4. Feature Extraction for Two-Slit Probe Signals

As mentioned earlier, penetration of the welds is related to the peak current intensity and the beam diameter (the Full Width Half Maximum (FWHM) pulse width), which were directly measured from the acquired probe traces of the two-slit probe. To acquire further parameters, wavelet transform techniques were performed on the acquired signals. From the analysis of the wavelet decompositions it was observed that the energy levels in different scales were able to represent the features that could differentiate between different beam traces obtained from the experimental work described in the previous chapter. To capture the beam traces, a sampling frequency of 25 MHz was used and eight decomposition levels were able to represent the signal of interest. Multi-signal analysis in 1-D has been carried out using proprietary software (Misti et al, 2009).

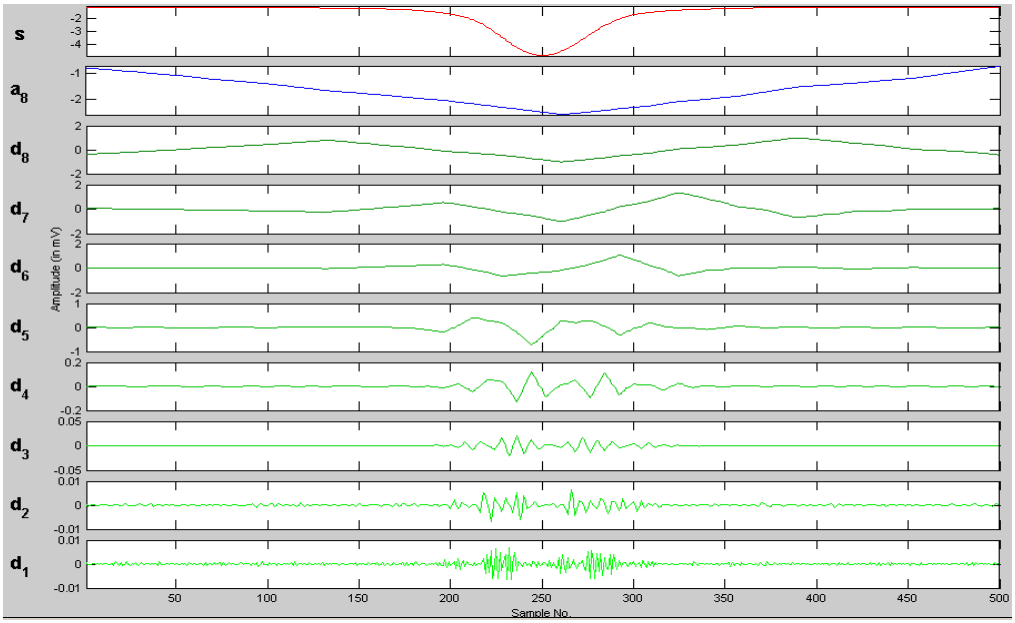

Figure 4.2 Decomposition levels of the acquired signal.

Figure 4.2 shows the decomposition levels of one of the probe signals. The x-axis represents the sample number and the amplitude of the signal is presented on y-axis. Signals d1 to d8 are the detail and a8 is the approximate signal after decomposing into 8 levels. The frequency band represented by each decomposition level is given in Table 4.1.

Table 4.1 Frequency ranges for decomposition levels

Decomposition level	*Frequency band (in MHz)*
d1	6.25 – 12.5
d2	3.12 – 6.25
d3	1.56 – 3.12
d4	0.78 – 1.56
d5	0.39 – 0.78
d6	0.19 – 0.39
d7	0.10 – 0.19
d8	0.05 – 0.10
a8	0 – 0.05

The feature extraction is based on the parameters derived from the wavelet coefficients at different decomposition levels. These include the total energy of the signal and the energy distribution among the detailed coefficients and the approximate level among the decomposition levels.

Energy for each decomposition level is calculated as given in equation (4.2).

$$E_j = \sum_n \left| d_j\,(n) \right|^2 \tag{4.2}$$

Where j is the decomposition level and n is the n^{th} sample of the acquired signal. Also the normalised wavelet energy or the percentage of energy at different decomposition levels is given by equation (4.3).

$$p_j = \frac{E_j}{E_{tot}} \times 100 \tag{4.3}$$

where E_{tot} is the total energy of the signal.

In the present analysis, the feature vector consists of both the total energy as well as the percentage of energy. The total energy is contributing to the weld pool dimensions and the percentage of energy to represent the beam characteristics.

The probe traces were captured for 20 signals at different beam current and focus settings mentioned in the previous chapter. Various features of the signals were captured to characterise the probe traces.

4.4.1. Features based on direct measurements of the signal

The peak intensity and FWHM were measured directly from the acquired signal and are tabulated in Table 4.2 and Table 4.3 respectively.

Table 4.2 Peak values of acquired signals

Focus Settings / *Beam Current (in mA)*	*U2*	*U1*	*FC*	*L1*	*L2*
7.5	3.5	4.85	5.9	5.77	4.08
8.0	3.76	4.97	6.09	5.88	4.44
8.5	3.73	5.13	6.01	6.31	5.14
9.0	4.01	5.45	6.37	6.55	4.88

Table 4.3 FWHM of acquired signals

Focus Settings / *Beam Current (in mA)*	*U2*	*U1*	*FC*	*L1*	*L2*
7.5	2.26	1.60	1.31	1.51	2.15
8.0	2.28	1.71	1.37	1.51	2.07
8.5	2.53	1.82	1.56	1.47	1.95
9.0	2.56	1.87	1.55	1.52	2.19

Figure 4.3 and Figure 4.4 represent the peak signal and FWHM respectively with respect to the different beam currents and the focus levels set around the sharp focus setting.

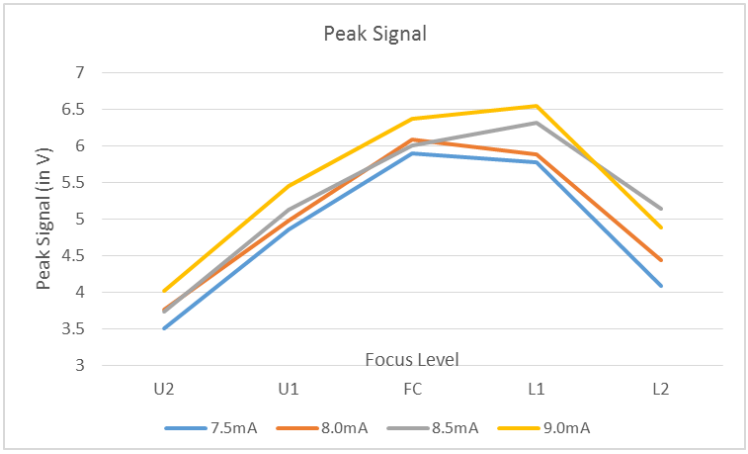

Figure 4.3 Peak signal for different beam currents and focus levels.

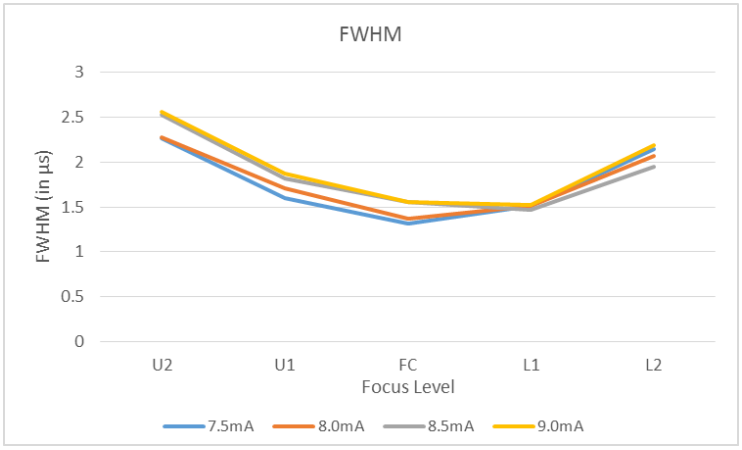

Figure 4.4 FWHM for different beam currents and focus levels.

4.4.2. Features based on wavelet transform of the signal

The acquired signals were processed using wavelet transformation. The signals were decomposed into 8 levels. The total energy of the signals and their distribution among different decomposition levels were interpreted as the features vector, as mentioned in the earlier paragraph. Figure 4.5 – 4.7 represents the total energy of the signals at different beam current and focus levels, the distribution of energy among different decomposition levels at 8mA beam current and distribution of energy at level d7 for all possible combinations of beam current and focus settings.

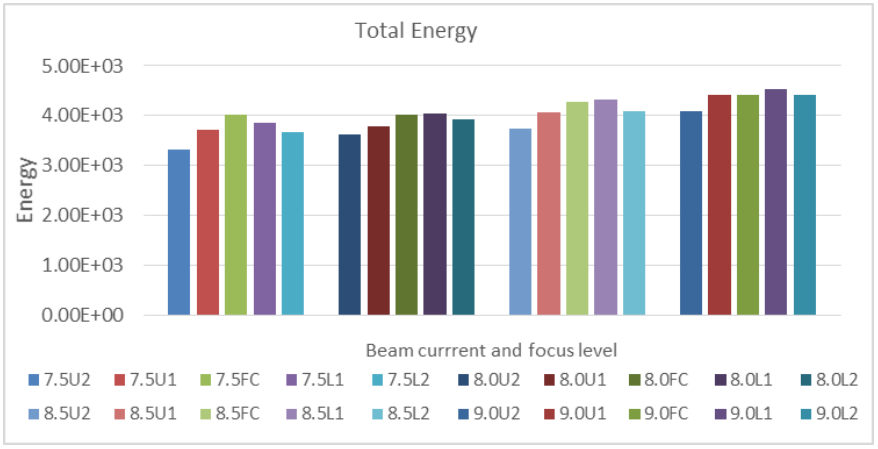

Figure 4.5 Total energy of the signals.

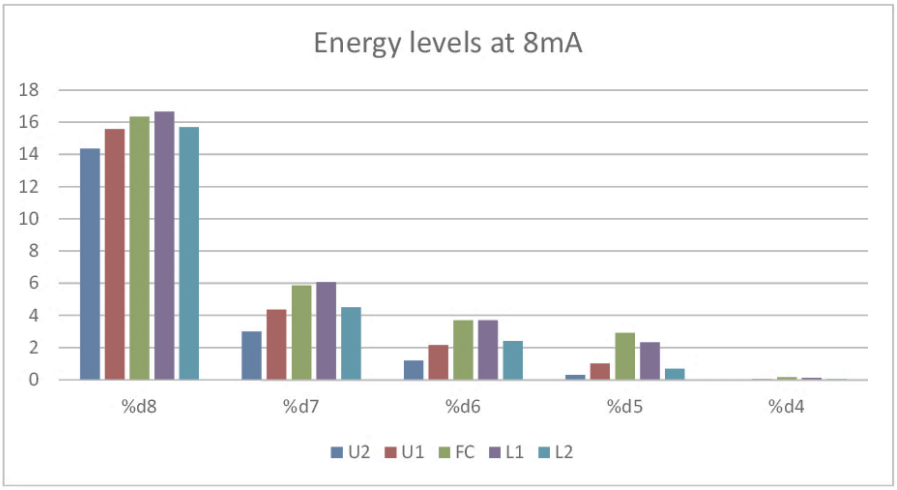

Figure 4.6 Energy distributions among decomposition levels at 8mA.

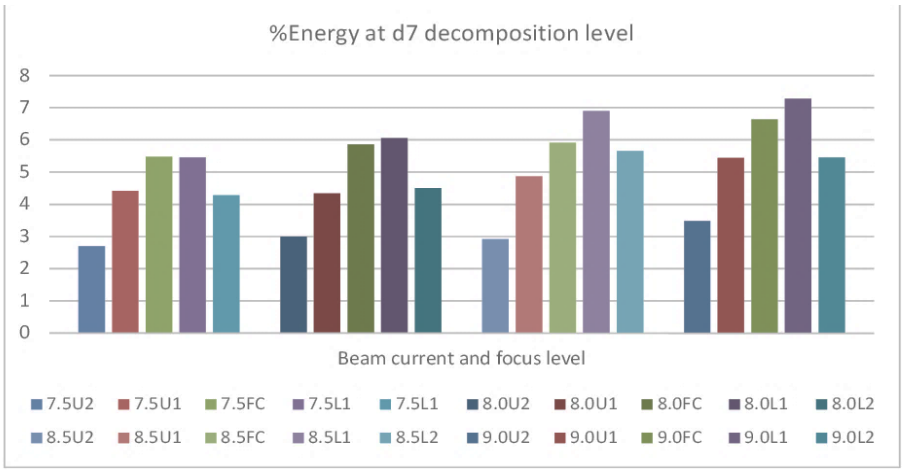

Figure 4.7 Energy distributions at d7 decomposition level for all combinations of beam current and focus settings.

4.4.3. Analysis of features vector

The features extracted in section 4.4.2 give a clear distinction of differing beam qualities at different input settings of beam current and focus levels. The peak signal values and FWHM indicated the trends as expected. At larger beam currents, the peak values were increasing and at sharp focus showing the maximum. Similarly, at sharp focus settings, the peak values were at maximum and decreasing either side i.e. at over-focused and under-focused levels. FWHM was narrowest at the sharp focus and becoming broader on either side. However, it was observed that the peak values at 8.5 mA and 9.0 mA were slightly shifted towards the lower focus levels i.e. L1. Also, the FWHM values representing the sharp focus were also shifted. From this, it appears that the sharp focus had shifted towards the lower focus level as the beam current was increased. This was in line with the explanation given in Schiller et al. (1982) i.e. the focus of the beam depends on the focus coil current as well as on the control-electrode voltage. Although the focus coil current for a typical setting is constant, however, the control electrode voltage changes with the beam current. Hence, the shift in the sharp focus at higher beam currents was observed.

The wavelet coefficients indicated that there were no high frequency components above about 400 kHz. In a few signals only a small portion of the energy about 0.02% was observed above this frequency. Other than the last approximation i.e. a8, the rest of the energy was distributed among detailed levels d8, d7 and d6. The maximum change in the energy level was found in d7 around 76% from minimum to maximum value. The distribution of the energy percentages in these levels showed similar trends as that of peak values and FWHM i.e. the energies at these levels were increasing as these were moving towards the sharp focus as well as the levels were increasing with the increase in beam current. The lower levels of energy towards the sharp focus in distribution at approximation level a7 also indicated that as the beam was more focused, the low frequency contents decreased and higher frequency contents increased (which is consistent with the pulse shape becoming sharper). Also, the energy distribution among the detailed levels d8, d7 and d6 might be due to the pulse width that varies between 4 – 12 µs and was represented by the frequency bands of these details levels.

The results of the analysis show that there are significant differences between the energy distributions among the decomposition levels. Even a 0.5 mA difference in the beam current gives sufficient difference in the energy levels distribution. This suggests that the features distinguishing between different beam quality traces may predominantly lie in the total energy of the signal and their distribution among different decomposition levels. Through this work, it has been demonstrated that wavelet transforms can potentially be used in characterising the probe traces to define features vector for the beam quality.

4.5. Summary

A novel method of analysis of probe data has been developed and applied to real data to characterise the electron beam. It has been observed that the developed method is able to detect the differences between beams with different characteristics. The limitation of the present analysis is the lack of weld data available at the same settings and conditions due to the problems faced capturing of the probe traces i.e. ripples, instability of the data and changes in the electron beam gun settings as mentioned in the previous chapter. Further work reported in the next chapter was carried out by doing the weldments and capturing the probe traces at the same time. The captured probe traces were analysed by the method of wavelet transformation and features vector developed in this chapter.

Chapter 5. Electron Beam and Weld Characterisation based on Double-Slit Probe Signal Analysis

In Chapter-3, a method for characterisation of the weldments using an experimental approach was discussed and Chapter-4 provided insights on the processing of the probe signals to develop a features vector to characterise the electron beam. However, due to the problems faced with the probe signals during the earlier experiments, the relationships between the features vector describing the electron beam and the weldment parameters could not be developed. Based on the outcomes of the earlier work, further experimental work was carried out. In this work, probe traces were captured for various beam settings along with melt runs with an aim to characterise the electron beam and to relate this with the weld profile parameters. This chapter provides details about the experimental work carried out, the results obtained from the welds, processing of the probe traces and their data analysis.

5.1. Introduction

In the process of electron beam welding, once the beam and welding parameters are set for a particular weld, the parameters are usually kept within tight tolerances. However, variations in the electron beam can occur over time, due to changes in the equipment or deterioration of components that can impair the quality of the welds in terms of their profile or the level of defects. To ensure the quality of the beam before carrying out the welds, the probing systems described in Chapter-2 were developed. The two-slit probe has been used in work reported in the previous chapter and it has been shown that the probe signals can be uniquely represented in terms of wavelet coefficients of different frequency bands. This provides distinguishing features to discriminate between signals from beams with different beam characteristics. These have been correlated with the weld qualities with the aim to define the beam characteristics and the associated tolerances to maintain the weld quality.

The problem of developing a features vector to characterise electron beam welding performance has been combined with the classification of the welds to determine the boundaries of the beam characteristics. The features vector provided a means of processing a set of beam characteristics so that they could be correlated with welding performance.

5.2. Methodology

To achieve the above said purpose, an experimental approach was adopted. The various stages of the methodology have been presented in Figure 5.1. The melt runs were carried out alongside the beam probing for various machine settings. The probe traces were processed to extract features using direct measurements and from a wavelet transform in proprietary software (MathWorks, 2012). The extracted features were analysed using the statistical technique using a statistical software package (IBM Corp, 2011) to classify the welds into pre-defined categories that can give an indication of whether it was within or outside tolerance limits. If the classifier results were not satisfactory, the extracted features or the classifier options were re-adjusted until the highest classification rate was achieved.

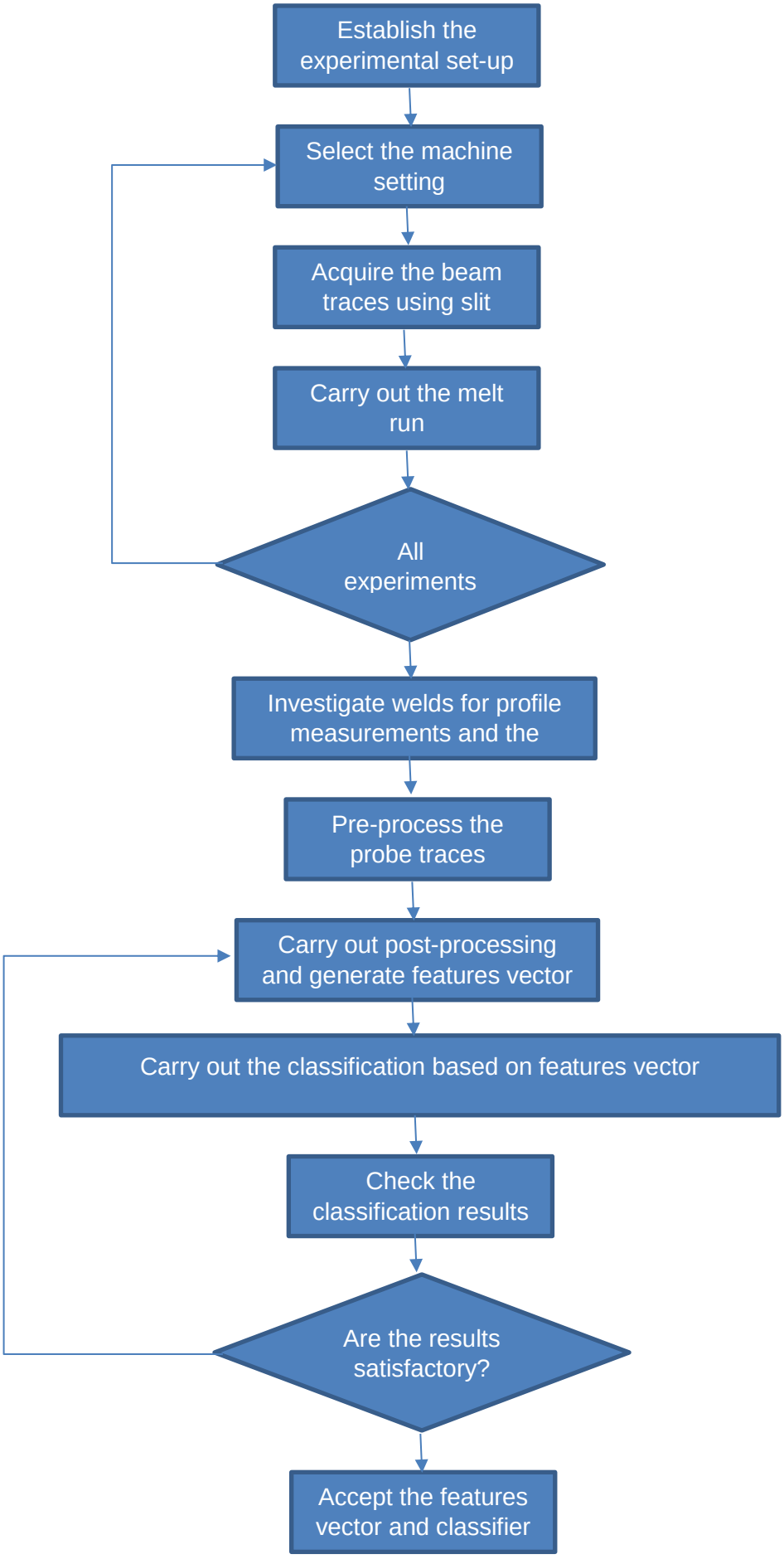

Figure 5.1 Flow chart used for experiments and data analysis.

5.2.1. Experiment design

To carry out the experiments a 6 kW, 150 kV EB machine was used. To overcome the problems of alignment of the probe with the beam that was faced with the earlier version of the two slit probe, the double-slit probe was used. The block diagram of the experimental set up is shown in Figure 5.2 and Figure 5.3, shows the probe installed in the chamber of the EB machine. The probe and the plates for the welds were installed in the chamber. To deflect the beam over the probe, a circular pattern was generated using an arbitrary function generator and this was used to drive the beam deflection coils via a current amplifier. Two cycles of the pattern in every 500 ms were generated in burst mode. The beam was positioned at 45º for parking during the time it was not being scanned. The output of the probe was connected to an oscilloscope to acquire the probe traces. After capturing the probe signal, the probe was moved away and the weld plates were moved into position to carry out the welds. This process was repeated for all the settings for 75 experiments, as detailed below.

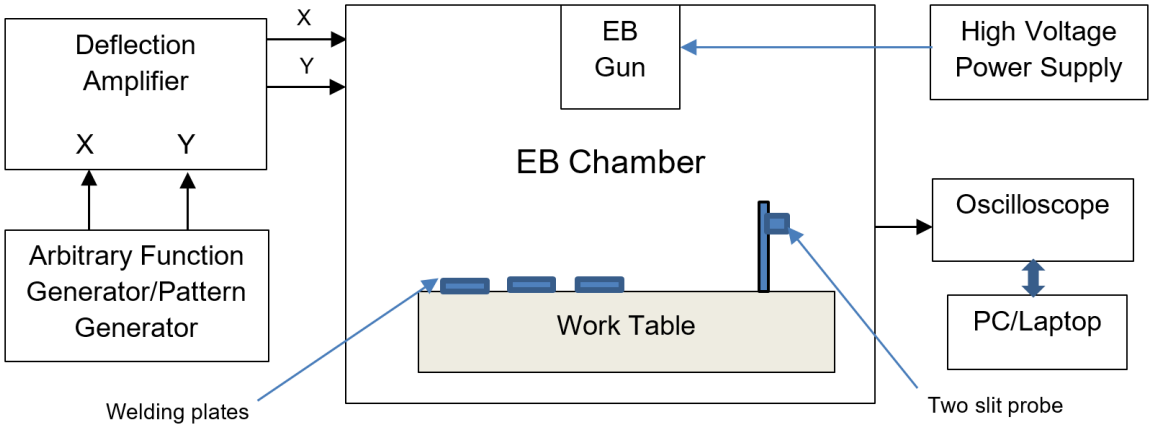

Figure 5.2 Experimental set-up.

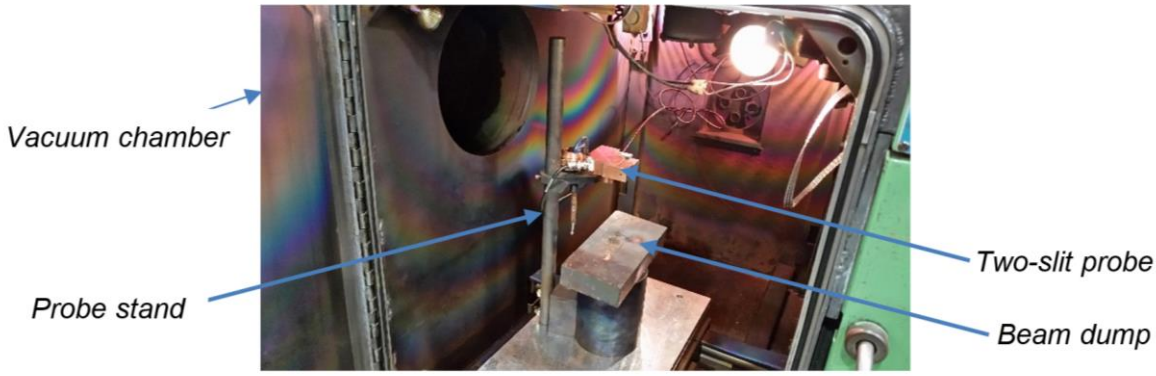

Figure 5.3 Probe installed in the chamber of EB machine.

Based on the results obtained in Chapter 3 and Chapter 4, it was decided to use beam current and focus settings as control variables as these were enough to give sufficient variations in the beam and the weld profiles. Five settings of beam current and focus settings were chosen based on the weld profile results of the earlier experiments. Beam currents chosen were 7.0 to 9.0 mA and focus settings same as in Table 5.1. Other fixed parameters on the machine were set as earlier in section 3.1.4.

A full-factorial approach was chosen with 2 replicates of each combination resulting in 75 experiments in total. Material was the same as before i.e. Ti-6Al-4V. The melt runs were carried out on 15 plates of size 110 x 80 x 10 mm with 5 melt runs made on each of them. Before starting the welds, the sharp focus was set by the operator at lower current and verified by the probe trace. The rest of the focus settings U1, U2, L2 and L1, i.e. two under-focused levels and two over-focused levels, were set at intervals of 10%. The welds on the plates were carried out with beam current and focus setting combinations in random order. Before carrying out each weld, the probe was brought back to the free fall position to acquire the electron beam at that particular setting. Each time the position of the probe was verified by observing the interval between points ‘b’ and ‘d’, see Figure 5.4.

5.2.2. Outcomes of the experiments

There were two types of outcomes from the experiments; first the weldments, second the probe signals as described in the following paragraphs.

Weld data

In addition to visually observing the weld quality, the welds were further inspected to assess their quality. First, radiographic examination was carried out to see types of defects such as porosity and cracks in the welds. Secondly, the welds were micro-sectioned to allow measurement of the transverse profile.

The radiograph images of the welds were digitized to measure the pores and cracks accurately. No cracks were observed in any of the welds. The pores were examined for maximum diameter of individual pore, the minimum distance between the adjacent pores and an accumulated size of the pores over a length of 75 mm as prescribed by the aerospace standard D17.1M:2010 (AWS, 2010). No gas pores were observed but linear porosity was observed over the length of the welds. However, it was within the tolerance limits of the standard specifications. The maximum pore size in the welds observed was 0.35 mm and maximum accumulated length of the pores was 3.8 mm.

Micro-sectioning of the welds was carried out to assess the welds for profile measurements. The profile measurements were taken for the weld penetration depth, the top surface width and the width at the 50% of the penetration depth. All the weld profile measurements have been tabulated in Table A1 in Appendix 'A'.

5.2.3. Processing of probe data

For each of the machine settings, the probe traces were acquired and stored. A sampling rate of 1 GHz was used to capture the signals. Before starting the measurements, the alignment of the probe was carried out by adjusting the time between points 'b' and 'd' as shown in Figure 5.4. As these parts of the signal are generated by slits that are positioned at 90^{o} from each other around the deflection circle, the time between them will be one quarter of a period of the deflection waveform when the probe and beam are correctly aligned. Before each weld the probe was positioned back to the free fall position and verified for its alignment.

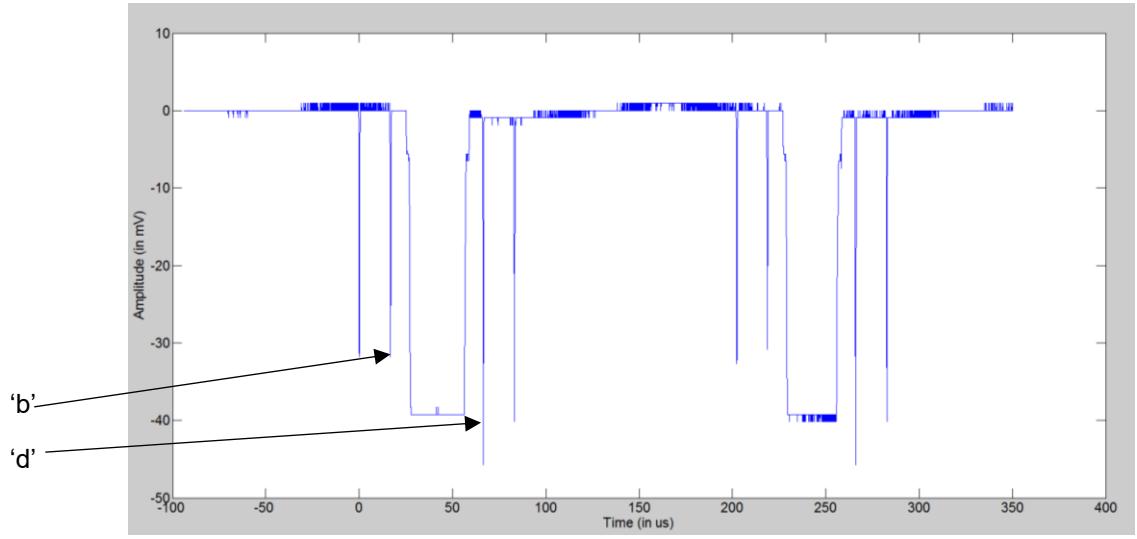

Figure 5.4 Probe trace for one of the signals.

Once all the traces were captured, the 'b' and 'd' waveform from the full signal were extracted representing the signal in the direction and across the weld respectively. This part of the signal was used for further processing and analysis. The peak intensity and FWHM measurements of all the signals are given in Table A2 of Appendix 'A'.

Based on the results achieved during the earlier probe analysis in Chapter 4, wavelet transforms were used for generating the features vector. All the signals were decomposed in different frequency bands and the total energy in each of the bands was utilised to characterise the electron beam along with the weld profiles. The signal was decomposed into 11 levels using 'db3' wavelet transform in a similar way as in Chapter 4.

Based on 1 GHz sampling frequency, the frequency bands for all the decomposition levels are listed in Table 5.1

Table 5.1 Frequency ranges for decomposition levels.

Decomposition level	*Frequency band (in MHz)*
d1	250 – 500
d2	125 – 250
d3	62.5 – 125
d4	31.25 – 62.5
d5	15.62 – 31.25
d6	7.81 – 15.62
d7	3.9 – 7.81
d8	1.95 – 3.9
d9	.977 – 1.95
d10	.488 – .977
d11	.244 – .488
a11	0 - .244

On decomposing the signals, it was observed that there was a very small percentage of the total energy present in the higher frequency bands i.e. in the decomposition levels d1-d7 whereas d8-d11 were the major energy components that was dictated by the beam widths. Hence, total energy, peak intensity, FWHM, the energy in detail decomposition levels d8-d11 and approximation level a11 were used to generate the features vector. After generating the data for all the signals, the classification model was developed using the statistical software as mentioned in section 5.2.

5.2.4. Development of classifier model

The process of development of a classifier model consists of feature extraction and feature selection & classification stages. The peak intensity, FWHM, from direct measurements and total energy, and energy in different decomposition levels from wavelet coefficients have been used as the features of the probe signals. The feature selection stage differed based upon the classification method used. There are two types of classification methods i.e. discrimination and clustering also known as supervised and unsupervised learning methods

respectively. In the unsupervised or the clustering technique there are no defined groups of the data i.e. it is essentially an unclassified data whereas in the supervised learning technique the data is already classified into groups (Landau and Everitt, 2004). In the present case, the output data was categorised based on the tolerance limits according to the qualification standards, hence, the data was already grouped into defined categories before the classification process. Therefore, the supervised learning method i.e. the discrimination analysis method was selected for classification.

There are also other methods of supervised learning in literature. Discriminant analysis is basically an extension of the multiple linear regression. In the multiple linear regression models, the relationship is between the quantitative dependent variable and the independent variables. However, in the case of discriminant analysis, the dependent variable is a qualitative or categorical variable. Another technique known as logistic regression requires the dependent variable to be dichotomous (Menard, 2001). The problem under investigation is essentially a multivariate problem. All the parameters in the features vector are independent variables also known as predictors in classification problem. For this work, the predictors were continuous metric in nature and the dependent variable was categorical with more than two categories. Hence, the discriminant analysis was used for classification process.

The discriminant analysis technique was developed by Fisher in 1936 (Tinsley and Brown, 2000) and is composed of descriptive and predictive discriminant analysis. Descriptive analysis describes characteristics of different groups specific to them, whereas predictive analysis classifies cases into pre-defined groups by examining the similarity between the case under test and other cases associated with the groups. Discriminant analysis derives a linear equation also known as a discriminant function based on the linear combination of the predictors (Burns and Burns, 2009). The output of the discriminant function is called the discriminant score, based on which it predicts which group or category the case belongs to. Discriminant analysis accomplishes this analysis by investigating differences among groups, discarding the variables that are not or relatively little related to the group distinction, classifies the cases into defined group categories and tests the discriminant functions by examining whether

cases are classified into groups according to the prediction. A discriminant function is described as

$$D = v_1X_1 + v_2X_2 + v_3X_3 + \ldots\ldots v_iX_i + a \qquad \ldots\ldots\ldots (5.1)$$

where D = discriminant score

v = discriminant coefficient

X = predictor value

a = constant

i = the number of the predictor variable

The weld parameters that were used for characterising the weld quality were weld penetration depth, weld width, porosity and other defect measurements. As mentioned earlier, the porosity parameters were within the tolerances defined by the standards. The weld penetration depth limits were derived from the tolerances mentioned in the standards i.e. for 5 mm depth, the tolerance limits were set between 4.5 to 5.5 mm.

The tolerances on the weld width are not specifically defined by the standards. Though, the British standard BS-EN-4677-001:2012 (BSI, 2012) mentions about the face widths to be and for 5mm thick weld, it should lie in the range of 1 mm to 3.4 mm. However, on discussing with the experienced members of the EB department at TWI, it was felt that few of the welds though were within the tolerance limit but were appearing too wide and hence, accepting the widths in the absolute terms was not sufficient. For the present work, these have been derived from the weld profiles of the welds within the penetration depth limits and have been detailed in the following paragraphs.

Like any classification process, discriminant analysis also consists of two phases i.e. the training phase and the test phase. The classifier model trains itself based on the pattern of the input data and its accuracy depends on the training data. Hence, the key component of designing the classifiers is the choice of inputs for training the model. The training data should be well distributed, sufficient and accurate. All the captured data are assumed to be normally distributed. For training the classifier, 60 cases were selected. There were 15 cases which were

within class 1 category, 11 cases in class 0 and remaining in class 2. Hence, the requirement of carrying out the discriminant analysis i.e. the minimum number of cases in the smallest group size should be more than the number of predictor variables was satisfied. To perform the discriminant analysis, the steps and assumptions suggested by (Tinsley and Brown, 2000) were adopted. The method is fairly robust to the violation of assumptions of linearity, normality, multi-linearity and equal variances but highly sensitive to outliers (Tabachnick and Fidell, 2013). Hence, one of the cases where the weld shape was not related to the probe trace parameters was excluded from the analysis resulting in 59 cases for training data.

Once all the required conditions on the data were checked and satisfied, the data was fed to the statistical analysis software. From the analysis function, classification using linear discriminant analysis was selected. The group parameters were selected and as the sample size in all the categories was different, it was decided to use the prior probabilities based on the relative sizes of the groups. The statistical outputs achieved from the above analysis, for different output variables have been explained in the following paragraphs.

Classifier for weld penetration depth

The data acquired through the probe traces was processed to extract the wavelet coefficients at different decomposition levels. For statistical analysis, peak intensity, FWHM, total energy, energy levels at decomposition levels d11, d10, d9, d8 and a11 were used as predictors. The output variable i.e. the weld penetration depth was classified into three categories. The cases which were within required tolerances were classified as class 1, below the tolerances as class 0 and above the tolerance limits as class 2.

To begin the analysis, the above mentioned predictor variables were selected based on the earlier experience gained from the work carried out in Kaur et al. (2015) and Chapter 4, but refined as the analysis progressed. After entering all the data into the statistical analysis software, the analysis was carried out. Table 5.2 presents the group statistics providing information about group means and variances. The means of the predictors in different classes showed differences, which means the selected features representing the beam characteristics were

useful in discriminating among different classes. The same has also been shown through the stacked histograms of predictor variables for all the three categories in Figure 5.5 (a) to (h). The graphs clearly showed the differences in range of values of predictor variables for all three categories. Another output from the analysis was the tests of equality of group means, given in Table 5.3. The parameter Wilks Lambda gives the ratio of within-groups sums of squares to the total sums of squares. The smaller value indicates that the variable is better at discriminating between groups. This indicates high F values giving a strong evidence of significant differences of means among the three categories. Hence, this shows potential for further analysis.

Table 5.2 Group Statistics

wpclass		Mean	Std. Deviation	Valid N (listwise)	
				Unweighted	Weighted
0	PI	-.195	.062	10	10.000
	FWHM	7.37E-7	2.91E-7	10	10.000
	energy	20.368	5.938	10	10.000
	d11	5.449	1.561	10	10.000
	d10	4.506	2.409	10	10.000
	d9	1.130	1.537	10	10.000
	d8	.0486	.066	10	10.000
	a11	9.223	1.190	10	10.000
1	PI	-.230	.042	15	15.000
	FWHM	6.42E-7	1.49E-7	15	15.000
	energy	27.097	4.965	15	15.000
	d11	7.094	1.353	15	15.000
	d10	6.556	2.624	15	15.000
	d9	.805	.981	15	15.000
	d8	.037	.074	15	15.000
	a11	12.583	1.827	15	15.000
2	PI	-.388	.080	34	34.000
	FWHM	3.84E-7	1.07E-7	34	34.000
	energy	45.551	10.266	34	34.000
	d11	9.766	1.832	34	34.000
	d10	13.486	3.847	34	34.000
	d9	7.930	4.585	34	34.000
	d8	.760	.762	34	34.000
	a11	13.585	2.495	34	34.000
Total	PI	-.315	.110	59	59.000
	FWHM	5.09E-7	2.18E-7	59	59.000
	energy	36.591	13.680	59	59.000
	d11	8.355	2.400	59	59.000
	d10	10.202	5.132	59	59.000
	d9	4.966	4.972	59	59.000
	d8	.455	.679	59	59.000
	a11	12.591	2.665	59	59.000

Table 5.3 Tests of equality of group means (indicate the measure of predictor variables' potential before the model is created).

	Wilks' Lambda	F	df1	df2	Sig.
PI	.388	44.097	2	56	.000
FWHM	.525	25.289	2	56	.000
energy	.381	45.396	2	56	.000
d11	.474	31.104	2	56	.000
d10	.417	39.145	2	56	.000
d9	.508	27.114	2	56	.000
d8	.722	10.776	2	56	.000
a11	.643	15.529	2	56	.000

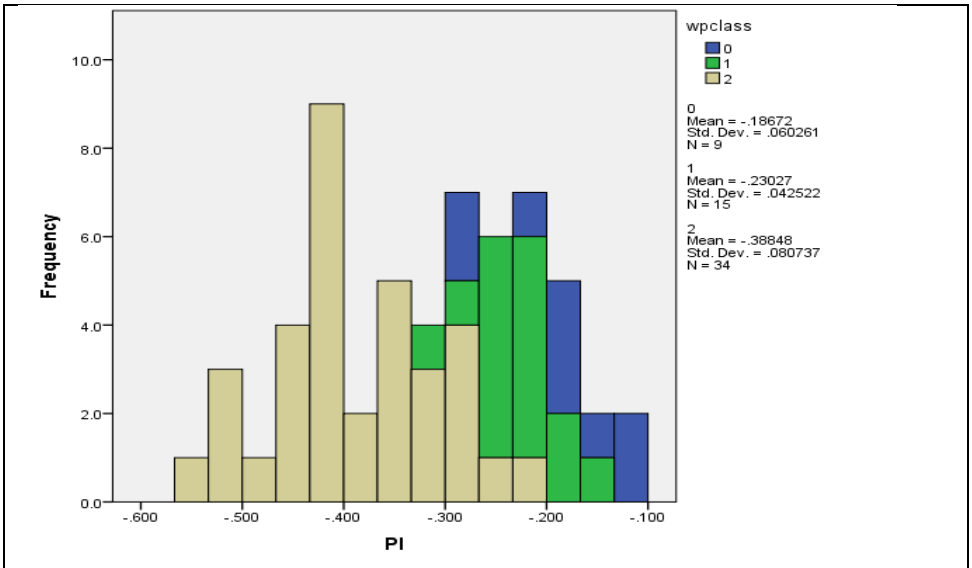

a.

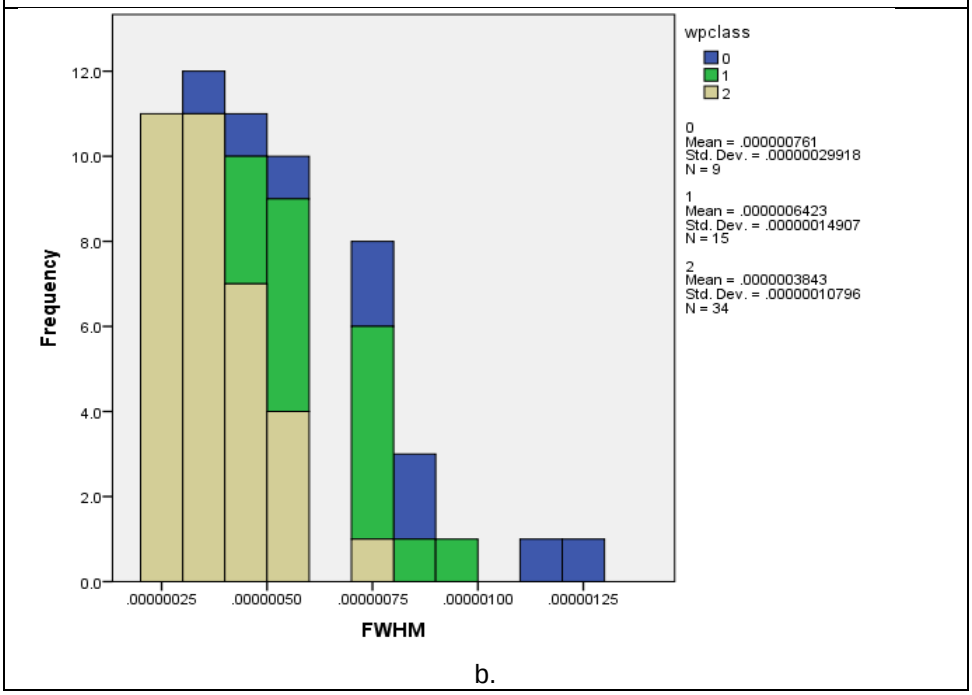

b.

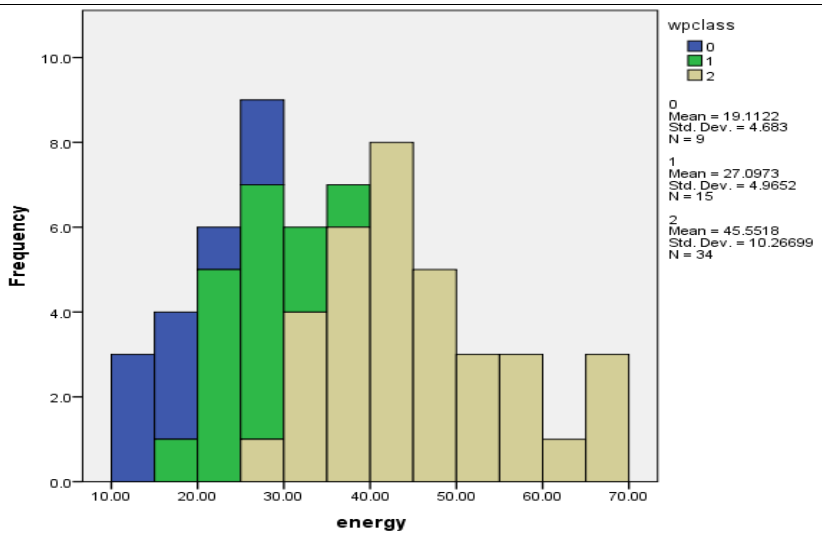
wpclass
0
1
2
0
Mean = 19.1122
Std. Dev. = 4.683
N = 9
1
Mean = 27.0973
Std. Dev. = 4.9652
N = 15
2
Mean = 45.5518
Std. Dev. = 10.26699
N = 34
Frequency
energy

c.

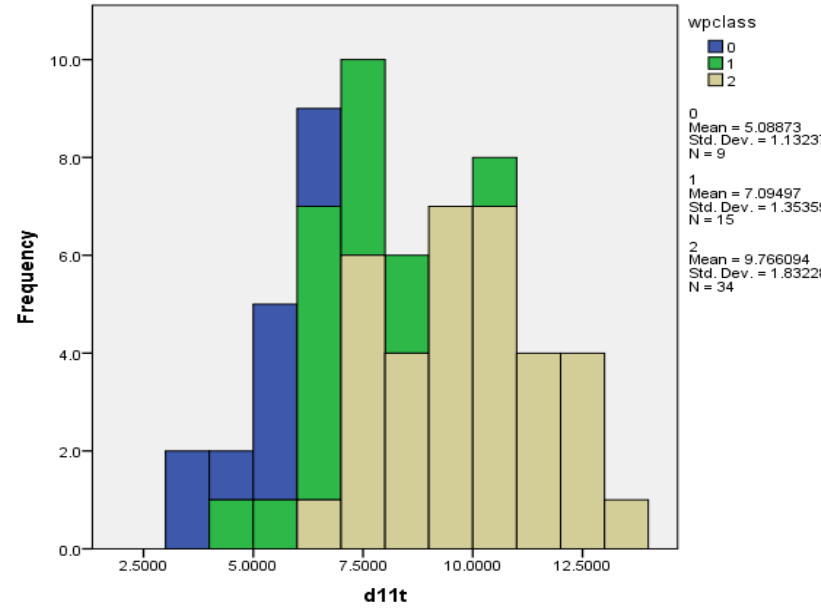
wpclass
0
1
2
0
Mean = 5.08873
Std. Dev. = 1.1323753
N = 9
1
Mean = 7.09497
Std. Dev. = 1.3535998
N = 15
2
Mean = 9.766094
Std. Dev. = 1.8322881
N = 34
Frequency
d11t

d.

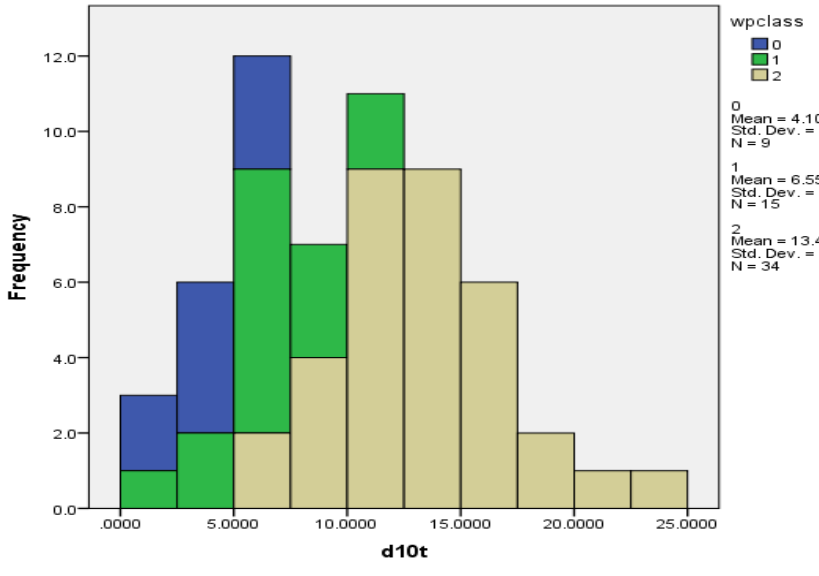
wpclass
0
1
2
0
Mean = 4.100347
Std. Dev. = 2.1631729
N = 9
1
Mean = 6.556408
Std. Dev. = 2.6244654
N = 15
2
Mean = 13.486785
Std. Dev. = 3.8470093
N = 34
Frequency
d10t

e.

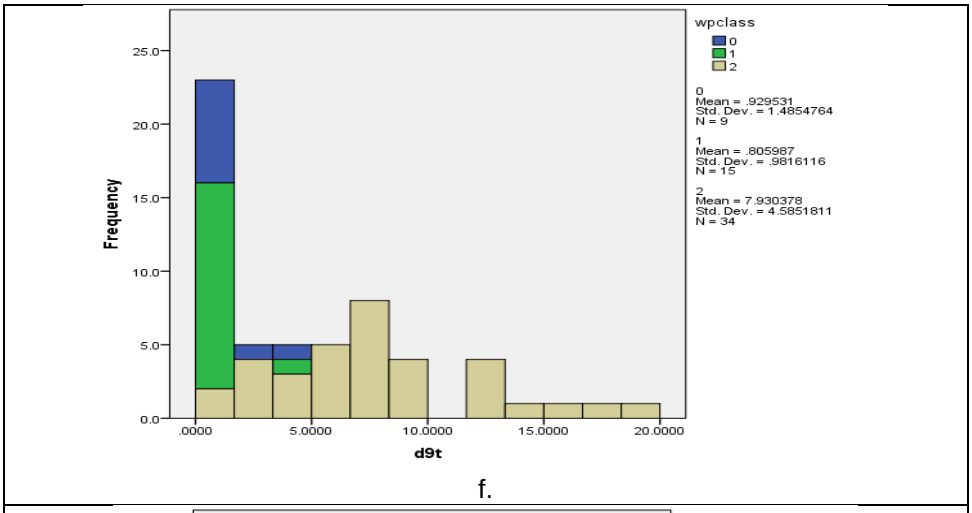

f.

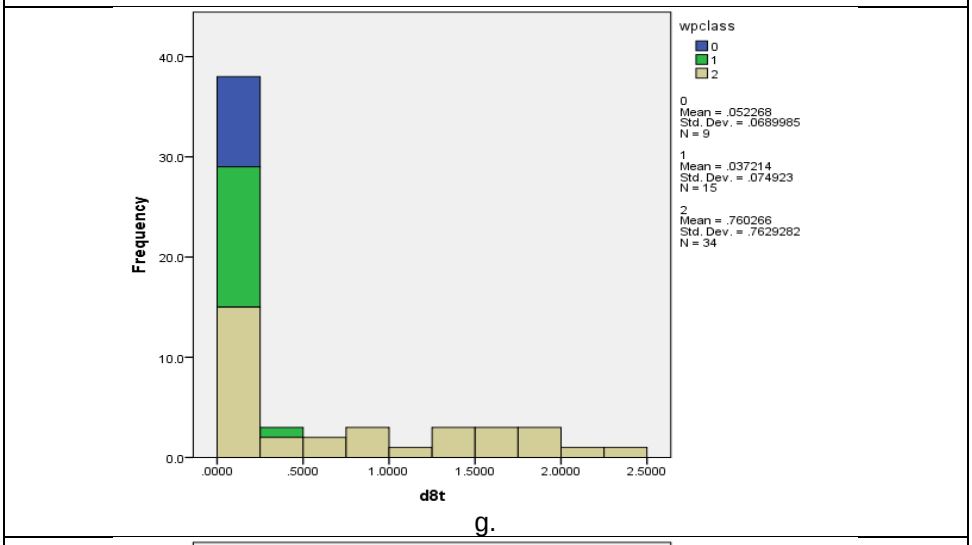

g.

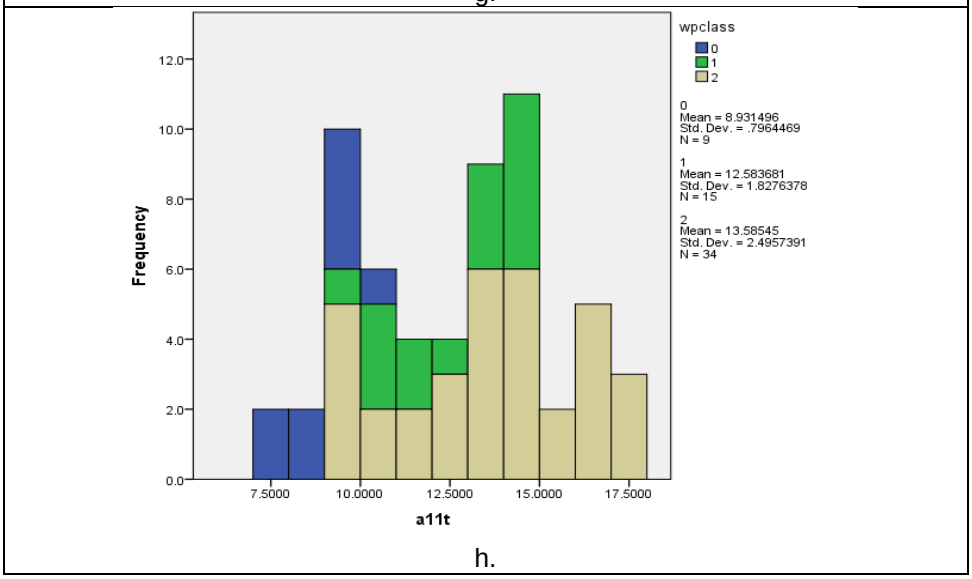

h.

Figure 5.5 Contributions of parameters to classification of weld penetration depth.

a. Peak intensity distribution
b. FWHM distribution
c. Total energy distribution
d. Energy at decomposition level d11 distribution
e. Energy at decomposition level d10 distribution
f. Energy at decomposition level d9 distribution
g. Energy at decomposition level d8 distribution
h. Energy at decomposition level a11 distribution

In response to the input data, two discriminant functions were generated. One function to distinguish between class 0 from the other two classes, and another between class 1 and class 2. Hence, the first function describes the most variation and the remaining variation is explained by the second function. This is supported by Eigen values and Wilks lambda in Tables 5.4 and 5.5 respectively. Eigen values indicate that 80.2% of variance is accounted by function 1 and 19.8% by function 2. The value of the Wilks Lambda is the proportion of the total variance in the discriminant scores not explained by differences among groups. A small lambda indicates that group means appear to differ. The significance parameter of Wilks lambda also shows that both the functions can help in discriminating among the groups.

Table 5.4 Eigen values

Function	Eigenvalue	% of Variance	Cumulative %	Canonical Correlation
1	2.036[a]	80.2	80.2	.819
2	.503[a]	19.8	100.0	.578

[a]. First 2 canonical discriminant functions were used in the analysis.

Table 5.5 Wilks' Lambda

(Sig. value indicates that both the functions contribute to the model for discrimination significantly).

Test of Function(s)	Wilks' Lambda	Chi-square	df	Sig.
1 through 2	.219	80.439	14	.000
2	.665	21.587	6	.001

Statistical analysis provides the standardised coefficients that represent the weights of each predictor variable in the features vector showing their relative importance based on its own scale of measurement. From Table 5.7, it is evident that PI stands out for function 1 whereas function 2 is dominated by total energy and energy at decomposition levels 9-11.

Table 5.6 Standardized Canonical Discriminant Function Coefficients

	Function	
	1	2
PI	2.213	-.407
FWHM	-.429	.911
energy	.714	-7.338
d11	-.649	2.731
d10	-.046	2.684
d9	.744	3.609
d8	.082	.386

In addition to the above, the unstandardised coefficients are also generated that are used to evaluate the discriminant score of each function to classify into different groups. The classification results based on the above are generated by statistical analysis and are presented in Table 5.8.

Table 5.7 Classification results[a]

		wpclass	Predicted Group Membership			Total
			0	1	2	
Original	Count	0	8	1	1	10
		1	2	12	1	15
		2	1	2	31	34
	%	0	80.0	10.0	10.0	100.0
		1	13.3	80.0	6.7	100.0
		2	2.9	5.9	91.2	100.0

a. 86.4% of original grouped cases correctly classified.

Based on the above analysis, various combinations of the predictor variables were tried out and it was found that a combination of total energy and the energy levels at decomposition levels 8-11 were giving a better classification rate of 89.8% of the original cases. Hence the features vector was reduced to contain only the total energy and the energies at decomposition levels from 8-11. Using these components in the features vector, the coefficients for the discriminant function were generated (Table 5.8).

Table 5.8 Classification function coefficients for weld depth

	Function	
	1	2
energy	-.060	-.695
d11	.491	1.239
d10	.199	.548
d9	.043	.897
d8	.572	.400
(Constant)	-4.424	4.867

Further analysis was carried out to verify the contribution of wavelet analysis to the direct measurements, the classifier model was trained using only peak intensity and FWHM measurements. Using these two parameters, the classification rate of 78% was achieved. This clearly showed that wavelet coefficients provide additional details of the probe signals that is helpful in characterising the electron beam.

Classifier for weld width

For the classification of weld width, the same predictor variables as for penetration depth were used. However, the dependent variable was categorised based on the weld profiles as there is no direct way prescribed in the standards for tolerance limits on this parameter. Though, BSI (2012) specifies the allowable limits for weld width which ranges from 1 to 3.5 mm for a 5 mm weld penetration depth. However, it appeared from the weld profiles that the absolute value of the weld width was not sufficient to characterise it as a good weld or bad weld. As the interest was focused on the welds within the penetration depth tolerance limits, the welds of class 1 in the previous section were examined for their weld profiles and the criterion for weld widths was established after discussion with experts at TWI in weld acceptance qualifications.

Table 5.9 shows the weld images that were within the tolerance limits for penetration depth. Based on these images, though the general impression was ‘pass’ for all the welds, however, there was apprehension regarding weld number 60 and 26 as they appeared to be near the limit at the top that might have led to excessive distortion. Also, weld number 69 appeared on the narrower side.

Table 5.9 Weld images with weld depth within the specified tolerance limits.

Weld No.	Weld Image	Weld No.	Weld Image
20		50	
26	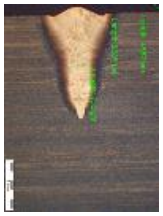	55	
60	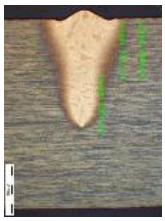	21	
36		74	
30		41	
69		16	
40		49	
44			

Based on the above images and discussions, it was seen that instead of considering the absolute measurements of weld width, the ratio of weld width to weld depth could be a better parameter to be considered to classify the weld categories based on weld width. The tolerance limits were set based on the profiles of the above welds to be between .40 to .55 for acceptable welds and classified as class 1, the welds below the lower limit as class 0 and above the upper limit as class 2.

Similar process as in previous section was followed to develop the classifier model for weld width. Based on the above classification criterion, there were 10 cases to represent class 0, 18 cases for class 1 and 31 for class 2. Hence, the requirements of minimum cases in the smallest group were fulfilled. Due to the difference in sizes of the groups in all classes, the option of prior probabilities based on the relative sizes of the groups was selected.

When all the components in the features vector were used, the classification rate of 89.8% was achieved. In an attempt to reduce the dimensions of the features vector, the results of combinations of various components were compared. When only peak intensity and FWHM were used, the classification rate was 72.9%. Using only the total energy and the energy in different decomposition levels, 88.1% of classification rate was observed. However, including FWHM resulted in addition to the energy levels resulted in a classification rate of 89.8%. When peak intensity was used along with energy distributions, no change was observed in the classification rate of 88.1%. This indicated that in the surface width of the welds, contribution of FWHM was more as compared to peak intensity. Hence, the features vector for weld width constituted FWHM, total energy and the energy levels at decomposition levels d11-d8. The coefficients for the discriminant function generated have been shown in Table 5.10.

Table 5.10 Classification function coefficients for weld width

	Function	
	1	2
energy	-.852	-.576
d11	2.031	.994
d10	1.038	.678
d9	.830	.907
d8	1.529	.852
PI	-4.051	18.965
FWHM	49.058	29.138
(Constant)	-4.985	5.462

Analysis of across direction signals

The above classification of weld depth and weld width was carried out using the in direction signal i.e. the signal ‘b’ in Figure 5.4. In this section, the classification results based on the measurement of signal across the weld direction i.e. signal ‘d’ have been analysed. The peak intensity and FWHM measurements of welds 16-75 have been given in Table A4 in appendix ‘A’.

The wavelet transform was carried out in the similar way as for signal ‘b’. The features vector was generated using the new wavelet coefficients of signal ‘d’. The results appeared to be similar as in case of in direction signal. For weld penetration depth, when all the components of the features vector were used, a classification rate of 89.7% was achieved that was much higher than the 82.8% rate using only peak intensity and FWHM. Hence, verifying the contribution of wavelet energies at different decomposition levels. After using the various combinations, the best classification rate of 93.1% was achieved by using only total energy and the energies at decomposition levels d8-d11. This was again following the pattern as with in direction signal. Weld width classification also followed the pattern of in direction signal. The best classification rate 82.8% though less than the in direction signal was achieved by using FWHM in addition to the energy components.

5.3. Summary

This chapter has shown the effectiveness of wavelet transform technique in characterising the electron beam and to correlate with the weld quality. Melt runs were carried out and the probe signals were acquired for each of the machine settings used for weldments. Wavelet transform was carried out of the acquired probe signals and energies at different decomposition levels were used for the analysis. Welds were examined by radiographs for the defects measurements and were micro-machined to assess their profiles.

Weld defects and the profiles were assessed against the limits suggested by the qualification standards. No cracks were observed. There were no gas pores, however, some welds did have linear porosity that was within tolerance limits. Weld penetration depth and weld width measurements were used for developing the classifier model to which the components of features vectors were used as predictors. Weld profile measurements were categorised in three classes, one within limits, second below limits and third above limits. Wherever the quality measurements were not clearly specified by the standards or were not felt to be adequate, the methods of assessing those parameters were developed. As there were defined categories of the weld outputs, the supervised method of classification was opted. The classifier trains itself based on the predictor values and their corresponding outputs. The accuracy of the classifiers highly depends on the training data. Hence, 59 cases were selected to train the classifier.

The results of the classifier based on features vector for in direction and across direction of welds were analysed for weld penetration depth and surface width. The improvement in classification rates was clearly showing significance of analysing the probe signals at decomposition levels in addition to using peak intensity and full width half maximum. It has also been seen that the effect of adding the decomposition level details to the features vector worked in the similar fashion whether it was in direction or across direction signal in correlating with the weld profiles. The results achieved through this work have shown that the wavelet transforms can be successfully used for characterising the electron beams to map the weld quality parameters.

Chapter 6. Conclusions and Recommendations for Future Work

This chapter concludes the research work carried out and reported in this thesis. The main conclusions derived are presented and possible areas for future research have been identified. Brief descriptions of each of the identified future work are given.

6.1. Conclusions

This research was focused on developing a novel technique to characterise electron beams and to correlate with weld quality parameters aiming at critical quality requirements of the aerospace industry. In such a high value manufacturing process, it is essential to check beam quality before carrying out welds to keep rework or scrap to a minimum possible cost.

A detailed literature review of methods and devices evolved over time to characterise electron beams has been carried out that described the present status of development and possibilities of further research in this area. Some of these devices provide detailed information of the intensity distribution of the beams but are limited to measuring low power beams. The method to effectively use the information for quality assurance of the welds is not very clear. These devices are being used mainly for developmental work or laboratory research. The focus of the present research was to detect the variations in the beam quality that can occur due to changes in any of the parameters in the process including the focus settings and to indicate when these variations will result in welds out of the tolerance limits of quality requirements.

Present research has been carried out using the two-slit probe due to its suitability for a production environment and it's capability for use at higher powers. Material selection and quality assessment of the welds was based on typical aerospace

requirements. As mentioned in chapter-3, two sets of melt runs on titanium plates were carried out. With the first set of melt runs, the range of beam current at sharp focus was identified for the required weld depth. With the second set of melt runs, combination of beam currents and 5 focus settings (two under-focussed, one sharp focus and two over-focused) were used at 10% intervals of sharp focus setting. Welds were assessed for defects and their profile measurements that helped in narrowing down on the required beam current and focus settings. This was done by selecting the ranges of both parameters based on the required and achieved weld quality.

Probe traces acquired for different settings of beam current and focus settings were processed using a wavelet transform method to decompose the signals into different frequency bands. Energy distribution in different frequency bands was analysed as described in Chapter–4. The analysis showed promising results in characterising the electron beams using features generated by wavelet transform. It was established that there was a strong correlation between the beam characteristics and the energy distribution among decomposition levels that can enable beams of different characteristics to be distinguished. This work was limited by the problems of ripple and changes in the gun conditions during the experiments and therefore, correlation between weld quality and extracted features from probe signals could not be established. This led to carrying out further work to correlate weld quality parameters with electron beams using features vector.

Based on the outcomes of Chapter-3 and Chapter-4, an extensive experimental programme was carried out. Melt runs and acquisition of probe traces was carried out with 2 replications of each of the combination of beam current and focus settings to counter variations in the process and hence, in beam characteristics. Probe signals were analysed using wavelet transform to derive the energy distribution among different frequency bands. These parameters were used to form a features vector in addition to previously used parameters of peak intensity and FWHM measurements. To see the effect of wavelet analysis, parameters of features vectors were used as predictors for classification of weld quality parameters. Weld quality parameters were classified into different categories where the criterion for defining categories was based on specifications of qualification standards. For weld width tolerance limits, feedback of experienced

members was also considered along with specifications defined by the standard. Due to simplicity and robustness, linear discriminant analysis was used to model the classifier which was trained on the results obtained from the experiments. Various combinations of the parameters from features vector were assessed for classification performance that resulted in different classification rates. As expected, there was significant improvement in the classification rates of more than 10% when features based on wavelet analysis were used. These were examined for the welds' penetration depths and surface widths for in direction and across direction signals acquired from the two-slit probe.

The results achieved from this research support the use of proposed method of characterisation of electron beams using features vector derived from wavelet transform analysis for quality assurance of welds. It is believed that this work contains the first reported application of wavelet transforms in characterising electron beams for welding quality assurance. As of today, the use of probe devices in this area is uncommon and the present research has developed a methodology to correlate beam measurements with weld quality industry standards.

From the work carried out the following conclusions are drawn:

- A number of devices exist for characterising electron beams with their relative pros and cons. For characterising high power electron beams, the two-slit or inverted two-slit probes provide a simpler solution.
- The electron beam characteristics can be varied by changing a number of parameters. The variations in beam current and focus settings were able to generate electron beams with sufficiently different characteristics and welding performance.
- A two-slit probe is being used in aerospace industry for nearly 4 years and has the feedback of low maintenance requirement. However, the initial alignment of the probe in the chamber and verification of the same on removal or repositioning is a difficult task. The inverted two-slit probe is very helpful in overcoming this problem by providing additional signals to verify the position.
- The analysis of the probe signals using wavelet transform is capable of differentiating between beams of different characteristics. The energy

distribution among various decomposition levels has been used to develop features vector to characterise the beams.

- A pattern based classification method has been applied to the experimental data containing the features vector and the weld quality parameters. The correlation between these has resulted in a classification rate of 89.8%. This has proven that wavelet analysis can be applied to beam measurements to provide the fine differentiation of the beam quality necessary to detect variations before crossing weld defect thresholds.

6.2. Future Work

The work carried out in this thesis identified a number of areas which can be explored further.

A number of applications evidenced use of energy distribution among decomposition levels representing different frequency bands in features vectors for classification purposes. In Chapter-4, the use of same was explored to represent the electron beam characteristics. Based on the results achieved, it was further explored to characterise the electron beam to correlate with the weld quality. Wavelet transforms are very flexible and a variety of features other than energy distribution can be generated using wavelet coefficients in different decomposition levels. A lot of statistical parameters can be generated representing time and frequency localization. The efficacy of these parameters can be examined for better characterization of the electron beams or by using in combination with parameters used in this research. It has also been reported in the literature that different sampling rates used for acquiring the data can give different results. In the present analysis, the signals were captured at 1 GHz sampling rate. Different sampling frequencies can be tried out to evaluate the effect and on selection of optimum sampling rate.

Present research has been carried out on thin sections of welding. It will be interested to see the performance for thick section welding also provides the similar improvement in diagnosis. Also, the present work has examined the correlations of features vector with the weld penetration and weld surface width. Other parameters defining the weld quality should also be examined in the similar

way. The present work essentially defines a one dimensional problem. This work can be further expanded to represent the complete weld profile for example in a 2-d image and correlating fusion zone shape or heat affected zone shapes with the beam measurement features vector.

Though the use of linear methods for classification is recommended for its simplification and robustness, the non-linear classification algorithms can give better results for more complex data relationships. In view of this, non-linear methods can be applied for similar work to evaluate if these work better for this application.

Electron beams are being used in advanced manufacturing practices. Additive manufacturing (EB melting) is one of the state-of-art technologies being explored for aerospace components. This technology has enabled manufacture of complex geometries which are not possible with conventional technologies. In this area also the requirement for monitoring the beam quality is essential to order to manufacture the components according to qualification standards. The process of additive manufacturing is different from the welding process in that it needs a more complex design of probing system and associated signal processing, as the beam is deflected across a powder bed, and must be measured at a sample of positions. However, for this application also, the present research can form the basis of further work to be carried out.

Appendix ‘A’

Table A1. Weld profile measurements for melt runs – 3

Weld No.	Weld penetration depth, W_p (in mm)	Weld surface width, W_{wws} (in mm)	Weld width at 50% of penetration depth, W_{w50} (in mm)
1	4.57	2.17	0.78
2	7.27	1.6	0.78
3	5.764	1.65	0.71
4	5.46	1.9	0.8
5	4.4	2.26	0.87
6	4.6	2.3	0.68
7	6.12	1.78	0.71
8	5.27	1.73	0.68
9	6.14	2.02	0.81
10	4.33	2.42	1.04
11	5.15	2.13	0.83
12	6.8	1.81	0.67
13	6.48	1.97	0.7
14	5.3	2.09	0.8
15	3.92	2.56	0.92
16	5.04	2.3	0.848
17	6.26	1.77	0.8
18	7.16	1.58	0.67
19	6.58	1.77	0.76
20	4.57	2.17	0.78
21	4.92	2.44	0.79
22	5.9	1.97	0.78
23	5.95	1.79	0.8
24	4.04	2.66	1.05
25	4.21	2.4	0.87
26	4.58	2.59	0.73
27	6.01	2.1	0.73
28	6.68	1.72	0.58
29	6.38	2.13	0.65
30	4.75	2.48	0.93
31	5.86	2.58	0.84
32	6.55	1.94	0.74
33	7.03	1.85	0.78
34	5.93	2.32	0.68
35	4.32	2.47	0.88
36	4.68	2.37	0.87

37	7.39	1.8	0.67
38	6.76	1.76	0.64
39	6.3	2.17	0.87
40	5.12	2.52	1
41	4.94	2.58	0.97
42	7.39	1.98	0.64
43	7.42	1.78	0.77
44	5.41	2.04	0.91
45	2.61	3.07	2.22
46	6.07	2.67	0.78
47	7.6	2.02	0.74
48	7.33	2.3	0.7
49	5.23	2.22	0.89
50	4.76	2.64	0.99
51	5.74	2.42	0.78
52	8.02	1.96	0.73
53	7.32	1.86	0.78
54	6.8	2.16	1
55	4.87	2.57	1.1
56	5.6	2.37	0.96
57	7.54	1.94	0.8
58	8.04	1.9	0.74
59	5.93	2.3	1.01
60	4.61	2.59	1.06
61	4.23	2.38	0.86
62	6.22	1.94	0.8
63	5.94	1.67	0.73
64	4.37	1.84	0.83
65	3.71	2.33	0.94
66	4.33	2.3	0.72
67	6	1.78	0.76
68	6.23	1.9	0.59
69	5	1.93	0.65
70	3.7	2.39	0.86
71	4.06	2.54	0.83
72	5.76	1.84	0.73
73	5.83	1.99	0.73
74	4.93	2.04	0.72
75	3.38	2.43	1.2

Table A2. Peak intensity and FWHM measurements of signal ‘b’ for melt runs – 3

Weld No.	Peak intensity (in mV)	FWHM (in µs)
1	-	-
2	-0.47	0.27
3	-0.32	0.47
4	-0.25	0.53
5	-0.18	0.75
6	-0.27	0.43
7	-0.40	0.30
8	-0.42	0.34
9	-0.25	0.60
10	-0.17	0.77
11	-0.29	0.42
12	-0.49	0.28
13	-0.31	0.45
14	-0.23	0.58
15	-0.16	0.83
16	-0.24	0.52
17	-0.42	0.31
18	-0.38	0.35
19	-0.27	0.56
20	-0.16	0.93
21	-0.33	0.40
22	-0.44	0.31
23	-0.40	0.34
24	-0.27	0.53
25	-0.19	0.74
26	-0.24	0.48
27	-0.41	0.29
28	-0.45	0.30
29	-0.27	0.51
30	-0.18	0.77
31	-0.3	0.45
32	-0.53	0.29
33	-0.42	0.36
34	-0.23	0.73
35	-0.12	1.26
36	-0.23	0.55
37	-0.48	0.28
38	-0.34	0.44
39	-0.34	0.46

Weld No.	Peak intensity (in mV)	FWHM (in µs)
40	-0.19	0.82
41	-0.29	0.49
42	-0.46	0.29
43	-0.43	0.36
44	-0.26	0.59
45	-0.19	0.75
46	-0.32	0.45
47	-0.53	0.29
48	-0.36	0.45
49	-0.21	0.76
50	-0.22	0.74
51	-0.29	0.50
52	-0.53	0.29
53	-0.43	0.37
54	-0.32	0.48
55	-0.22	0.74
56	-0.33	0.47
57	-0.51	0.28
58	-0.45	0.35
59	-0.26	0.59
60	-0.22	0.71
61	-0.29	0.37
62	-0.41	0.29
63	-0.35	0.36
64	-0.17	0.82
65	-0.15	0.82
66	-0.27	0.41
67	-0.42	0.28
68	-0.37	0.34
69	-0.24	0.57
70	-0.18	0.75
71	-0.21	0.55
72	-0.41	0.29
73	-0.35	0.35
74	-0.22	0.57
75	-0.12	1.13

Table A3. Porosity measurements of welds

Weld no	Average dia. (in mm)	max dia (in mm)	Accumulated length of pores over 75mm of weld length (in mm)
1	0.096	0.140	0.38
2	0.091	0.210	5.00
3	0.056	0.140	2.69
4	0.070	0.175	1.19
5	0.096	0.140	0.38
6	0.105	0.210	1.05
7	0.081	0.210	2.52
8	0.053	0.140	2.83
9	0.069	0.280	1.92
10	0.000	0.000	0
11	0.233	0.280	2.8
12	0.112	0.175	4.13
13	0.107	0.175	3.11
14	0.132	0.245	1.71
15	0.000	0.000	0
16	0.182	0.280	0.91
17	0.127	0.210	4.97
18	0.131	0.210	3.67
19	0.109	0.210	4.48
20	0.123	0.140	0.49
21	0.088	0.175	1.05
22	0.044	0.105	1.54
23	0.051	0.105	3.67
24	0.000	0.000	0
25	0.070	0.070	0.14
26	0.047	0.070	0.28
27	0.052	0.105	1.82
28	0.041	0.105	1.96
29	0.058	0.175	3.18
30	0.070	0.105	0.35
31	0.097	0.350	1.26
32	0.051	0.210	2.66
33	0.050	0.175	3.71
34	0.068	0.280	2.03
35	0.070	0.070	0.07
36	0.063	0.070	0.31
37	0.050	0.105	4.06

38	0.042	0.105	2.83
39	0.047	0.105	1.96
40	0.040	0.070	0.28
41	0.043	0.105	0.38
42	0.046	0.105	2.24
43	0.042	0.105	2.34
44	0.043	0.070	1.33
45	0.000	0.000	0
46	0.050	0.105	0.7
47	0.043	0.105	2.66
48	0.042	0.175	2.48
49	0.037	0.070	0.59
50	0.050	0.070	0.35
51	0.041	0.070	0.77
52	0.046	0.105	2.87
53	0.042	0.105	3.22
54	0.047	0.105	2.17
55	0.045	0.070	0.31
56	0.040	0.070	0.59
57	0.044	0.105	2.66
58	0.046	0.105	3.15
59	0.049	0.140	2.06
60	0.045	0.070	0.31
61	0.042	0.070	0.21
62	0.040	0.070	1.12
63	0.043	0.105	2.41
64	0.070	0.175	0.35
65	0.000	0.000	0
66	0.035	0.035	0.24
67	0.037	0.070	1.33
68	0.045	0.070	2.06
69	0.047	0.105	1.61
70	0.000	0.000	0
71	0.070	0.140	0.21
72	0.039	0.105	1.68
73	0.039	0.105	2.03
74	0.045	0.105	0.77
75	0.000	0.000	0

Table A4. Peak intensity and FWHM measurements of signal ‘d’ for melt runs – 3

Weld No.	Peak intensity (in mV)	FWHM (in µs)
16	-0.38	0.54
17	-0.62	0.35
18	-0.48	0.48
19	-0.39	0.58
20	-0.23	0.99
21	-0.53	0.41
22	-0.62	0.36
23	-0.55	0.41
24	-0.38	0.59
25	-0.23	1.02
26	-0.39	0.52
27	-0.62	0.35
28	-0.59	0.40
29	-0.36	0.61
30	-0.27	0.86
31	-0.56	0.41
32	-0.68	0.35
33	-0.52	0.47
34	-0.30	0.90
35	-0.16	1.56
36	-0.38	0.55
37	-0.68	0.35
38	-0.53	0.45
39	-0.49	0.52
40	-0.32	0.78
41	-0.41	0.54
42	-0.65	0.36
43	-0.59	0.40
44	-0.35	0.87
45	-0.24	0.96
46	-0.62	0.39
47	-0.69	0.35
48	-0.50	0.53
49	-0.28	0.94
50	-0.28	0.90
51	-0.50	0.48
52	-0.72	0.36

Weld No.	Peak intensity (in mV)	FWHM (in µs)
53	-0.55	0.47
54	-0.50	0.53
55	-0.30	0.84
56	-0.51	0.47
57	-0.73	0.35
58	-0.63	0.41
59	-0.43	0.61
60	-0.31	0.83
61	-0.57	0.35
62	-0.50	0.36
63	-0.45	0.46
64	-0.22	1.04
65	-0.19	1.15
66	-0.42	0.45
67	-0.56	0.35
68	-0.52	0.38
69	-0.34	0.61
70	-0.21	1.02
71	-0.35	0.49
72	-0.58	0.35
73	-0.46	0.43
74	-0.31	0.69
75	-0.16	1.39

Appendix ‘B’

MATLAB Subroutines

```
/************** Example Determining wavelet co-efficients at different decomposition levels and denoising the signal**************/

function ds = proc(signal)

s = signal;
subplot(4,2,1); plot(s);


% perform db3 level5 decomposition
 [C,L] = wavedec(s,5,'db3');

% reconstructing Level4 details
D4 = wrcoef('d', C, L, 'db3', 4);

subplot(4,2,3); plot(D4); title('details level 4');

% denoising the signal

 [thr,sorh,keepapp] = ddencmp('den','wv',s);
 [A,D] = dwt(s,'db3');
noiselev = median(abs(D))/0.6745;
thr = sqrt(2*log(length(s)))*noiselev;


ds = wdencmp('gbl',C,L,'db3',5,thr,sorh,keepapp);



/**************Calculating energy of the signal********/

function y=energy(Sig)

    Signal=double(Sig);

    sumene = 0;

    for i=1:1:length(Signal)

      Sosc = Signal(i)* Signal(i);
      sumene = sumene + Sosc;
```

```
    end
        y = sumene;
end



/**************Calculating percent root difference (PRD), mean square error
(MSE), root mean square difference (RMSD) **************/

function [prd,mse,rmsd]=mwselalgo(de_Sig,Org_Sig)

if nargin == 0,
    error(generatemsgid('Nargchk'),'Not enough input arguments.');
else
    if nargin == 1,
    error(generatemsgid('Nargchk'),'input arguments must be two.');
    end
    Pro_Sig=double(de_Sig);
    Orig_Sig=double(Org_Sig);

    sumse = 0;
    summa = 0;
    for i=1:1:length(Orig_Sig)
      Error = Orig_Sig(i) - Pro_Sig(i);
      se = Error * Error;
      sumse = sumse + se;
      ma = Orig_Sig(i) * Orig_Sig(i);
      summa = summa + ma;
    end
        prd=100*sqrt(sumse/summa)
        mse = sumse/length(Orig_Sig)
        rmsd = sqrt(sumse)

        assignin('base', 'prd', prd);
        assignin('base', 'mse', mse);
        assignin('base', 'rmsd', rmsd);

end
```

References

Ahmed, N. (2005) New developments in advanced welding. Woodhead publishing limited, Cambridge.

American Welding Society (2010) AWS D17.1/D17.1M:2010. Specification for fusion welding for aerospace applications. 2nd edition.

Antonino-Daviu, J., Riera-Guasp, M., Roger-Folch, J., Martínez-Giménez, F. and Peris, A. (2006) Application and optimization of the discrete wavelet transform for the detection of broken rotor bars in induction machines. Applied and Computational Harmonic Analysis, 21(2), 268-279.

Antony, J. (2014) Design of experiments for engineers and scientists. Elsevier.

Arafa, A. A., Saleh, H. I., Ashour, M. and Salem, A. (2009) Investigation of different wavelets for pulse shape discrimination of LSO and LuYAP scintillators in positron emission tomography. In Computer Engineering & Systems, 2009. ICCES 2009. International Conference on (pp. 610-615). IEEE.

AWS (2010) D17.1M.2010: Specification for fusion welding for aerospace applications. American welding society. 2nd edition.

AWS, (2004) Recommended Practices for Electron Beam Welding. American Welding Society.

Berte, M. and Legrand, P. (1981) Device for Quantitative Display of the Current Density within a Charged-Particle Beam. United States Patent 4,290,012 (324/71 EB)

Birnie, J.V. (1976) An Introduction to Electron Beam Welding. Physics in technology.

Bocharov, A. N., Laptenok, V. D. & Murygin, A.V. (2006) Controlling the distribution of the current density of the electron beam in the process of electron-beam welding. Welding International.

Bohm, I. S. (2014) The electron beam as a tool for joining technology. DVS report. Volume 299e.

Boyer, R. R. (1996) An overview on the use of titanium in the aerospace industry. Materials Science and Engineering. A213, 103–114.

British Standards Institution (2001) BS EN ISO 14744-3:2001. Welding Acceptance - inspection of electron beam welding machines. Part 3: Measurement of beam current characteristics.

BSI standards, BS EN 4677-001:2012 (2012) Aerospace series – welded and brazed assemblies for aerospace construction – Joints of metallic materials by electron beam welding. Part 001: Quality of welded assemblies. British standards institution (BSI).

BSI standards, BS EN ISO 13919-1:1997 (1997) Welding. Electron and laser beam welded joints. Guidance on quality levels for imperfections. Steel. British Standards institution (BSI).

BSI standards, BS EN ISO 13919-1:2001 (2001) Welding. Electron and laser beam welded joints. Guidance on quality levels for imperfections. Aluminium and its weldable alloys. British Standards institution (BSI).

Burns, R. P. and Burns, R. (2009) Business research methods and statistics using SPSS. SAGE publications ltd.

Dack, A. J. and Nunn, M. (2013) Laboratory and industrial validation of electron beam probing equipment. TWI industrial member report summary 1045/2013.

Darling, R. B., Seattle, Scheidemann, A. A., Schumacher, F. J. and Jones, P. L. (2005) Charged particle beam detection system. United States Patent 6847036 (250/291)

Dilthey, U. and Weiser, J. (1997) Investigations of EB characteristics and their influences on the weld shape. Weld world 39(2) 89-98.

Dilthey, U., Bohm, S., Dobner, M. and Trager, G. (1997) Comparability and replication of the electron beam welding technology using new tools of the DIABEAM measurement device. International conference on electron beam technologies.

Dilthey, U., Goumeniouk, A., Böhm, S. and Welters, T. (2001) Electron beam diagnostics: a new release of the diabeam system. Vacuum, 62(2–3), pp. 77-85.

Donachie, M. J. (2000) Titanium: a technical guide. ASM International. 2nd edition.

Elmer, J. and Teruya, A. (2001) An enhanced Faraday cup for rapid determination of power density distribution in electron beams. Welding journal - New York, 80(12), pp. 288-s.

Elmer, J. W. (2009) Characterization of defocused electron beams and welds in stainless steel and refractory metals using the enhanced modified Faraday cup diagnostics. Lawrence Livermore National Laboratory report – LLNL-TR-410110.

Elmer, J. W. and Teruya, A. T. (1998) Fast method of measuring power density distribution of non-circular and irregular electron beams. Science and Technology of Welding and Joining.

Elmer, J. W., Palmer, T. A. and Teruya, A. T. (2008) Electron beam diagnostics for profiling high power beams. United States Patent 7348568 (250/397)

Elmer, J. W., Teruya, A. T. and O'Brien, D. W. (1993) Tomographic Imaging of Noncircular and Irregular electron beam current density distributions. Welding Research Supplement.

Elmer, J. W., Teruya, A. T., O'Brien, D. W. (1996) Modified Faraday Cup. United states Patent 5,554,926 (324/71)

Eriksson, L., Johansson, E., Kettaneh-Wold, N., Wikstrom, C. and Wold, S. (2008) Design of experiments: Principles and applications. MKS Umetrics AB. Third edition.

EWF (European Federation for Welding). (2007) Electron Beam Welding. Technical Sheets.

Ganesan, R., Das, T. K. and Venkataraman, V. (2004) Wavelet-based multiscale statistical process monitoring: A literature review. IIE transactions, 36(9), 787-806.

Gao, R. X. and Yan, R. (2010) Wavelets: Theory and applications for manufacturing. Springer Science & Business Media.

Gargoom, A. M., Ertugrul, N. and Soong, W. L. (2004) Comparative study of using different mother wavelets on power quality monitoring. Australasian universities power engineering conference.

Gelles, D. S., Nanstad, R. K., Kumar, A. S. and Little, E. A. (1996) Effects of radiation on materials: 17th international symposium. ASTM publications.

Giedt, W. H. and Campiotti, R. (1996) Method of automatic measurement and focus of an electron beam and apparatus therefor. United States Patent 5,483,036 (219/121)

Giedt, W. H., and Tallerico, L. N. (1988) Prediction of Electron Beam Depth of Penetration. Welding Journal.

Hawkes, P. W. (2011) Advances in imaging and electron physics. Academic press.

Hayafuji, Y. (1986) Faraday Cup. United States Patent 4,608,493 (250/397)

Hicken, G. K., Giedt, W. H. and Bentley, A. E., (1991) Correlation of joint penetration with electron beam current distribution. Welding Research Supplement.

Houldcroft, P. T. (1977) Welding process technology. Cambridge university press.

Huang, J., (2012) The characterisation and modelling of porosity formation in electron beam welded titanium alloys (Doctoral dissertation, University of Birmingham).

IBM Corp. Released (2011). IBM SPSS Statistics for Windows, Version 20.0. Armonk, NY: IBM Corp.

Jeffus, L. (2012) Welding: principles and applications. Delmar, Cengage learning.

Kah, P., Shrestha, M. and Martikainen, J. (2014) Trends in joining dissimilar metals by welding. Applied mechanics and materials. Vol 440 pp 269-276.

Katul, G. G. and Vidakovic, B. (1995) The partitioning of attached and detached eddy motion in the atmospheric surface layer using Lorentz wavelet filtering. Boundary-Layer Meteorology.

Kaur, A., Ribton, C. and Balachandran. W. (2015) Electron beam characterisation methods and devices for welding equipment. Journal of materials processing technology, volume 221, pp. 225-232.

Kaur, A., Ribton, C. and Balachandran, W. (2015a) Characterization of high power electron beams using a two-slit probe and wavelet transforms. IET conference proceedings on Intelligent signal processing. In Press.

Kaur, A., Ribton, C. and Balachandran, W. (2016) Development of a novel device and analysis method for characterising electron beams for welding applications. Submitted to Journal on Electrotechnica & Electronica.

Keast, V. J. and Williams, D. B. (2000) Quantification of boundary segregation in the analytical electron microscope. Journal of microscopy, 199: 45–55.

Kenyon, D.M. (1965) Electron-beam welding. Electronics & Power.

Keswani, R. (2008) Identification of fault in HVDC converters using wavelet based multi-resolution analysis. First International Conference on Emerging Trends in Engineering and Technology, ICETET'08. (pp. 954-959). IEEE.

Khanam, R. and Ahmad, S. N. (2013) Selection of Wavelets for Evaluating SNR, PRD and CR of ECG Signal. International Journal of Engineering Science and Innovative Technology (IJESIT), 2(1), 112-119.

Kobayashi, M. (2001) Wavelets and their applications in industry. Nonlinear analysis 47, 1749-1760.

Koleva, E., Mladenov, G., Kardjiev, M. and Todorov, D. (2014) Electron beam characterization at changes of EBW process parameters. Eleventh International Conference on Electron Beam Technologies at Bulgaria.

Landau, S. and Everitt, B. S. (2004) A handbook of statistical analyses using SPSS. Chapman & Hall, A CRC press company.

Lawrence, G. S. (1975) Filament for electron guns. United States patent, 3869636.

Li, C. J. and Ma, J. (1997) Wavelet decomposition of vibrations for detection of bearing-localized defects. Ndt & E International, 30(3), 143-149.

Liao, Y. (2007) Practical Electron Microscopy and Database. An online book. Second edition. Available at <http://www.globalsino.com/EM/>.

Mathworks. (2012). MATLAB, ver. R2012b. Computer program. The MathWorks Inc., Natick, MA, USA.

Mcnabb, L. A. (1969) Electron beam welding machine. U.S. Patent No. 3,433,923.

Menard, S. (2001) Applied logistic regression analysis. Sage publications.

Merry, R. J. E., and Steinbuch, M. (2005) Wavelet theory and applications. Literature Study, Eindhoven University of Technology, Department of Mechanical Engineering, Control Systems Technology Group.

Metzger, G. and Lison, R. (1976) Electron beam welding of dissimilar metals. Welding research supplement. 230s-240s

Misiti, M., Misiti, Y., Oppenheim, G. and Poggi, J. (2007) Wavelets and their applications. ISTE Ltd.

Misiti, M., Misiti, Y., Oppenheim, G. and Poggi, J. (2009) Wavelet toolbox: For use with Matlab. The mathworks.

Mouritz, A. P. (2012) Introduction to aerospace materials. Woodhead publishing limited.

NASA. (2014) NASA Armstrong Fact Sheet: SR-71 Blackbird. Available online < http://www.nasa.gov/centers/armstrong/news/FactSheets/FS-030-DFRC.html#.VJtkcV4hA> viewed on 25-12-2014.

Nello, O. (2001) Electron beam probing systems – a review. TWI Bulletin

Palmer, T. A. and Elmer, J. W. (2007) Characterisation of electron beams at different focus settings and work distances in multiple welders using the enhanced modified Faraday cup. Science and technology of welding & joining 12(2), 161-174

Palmer, T. A., Elmer, J. W., Nicklas, K.D. and Mustaleski, T. (2007) Transferring electron beam welding parameters using the enhanced modified Faraday cup. Welding research. Vol 86 pp 388s-398s.

Palmer, T. A., Hochanadel, P. W. and Sciaky, K. L. (2011) Quality control of electron beams and welds. Welding fundamentals and processes. Volume 6A.

Palmer, T.A. and Elmer, J.W. (2008) Improving process control in electron beam welding using the enhanced modified Faraday cup. Journal of manufacturing science and engineering, 130(4).

Peng, Y., Wang, K. H., Zhou, Q., Wang, Y.J. and Fu, P. F. (2011) Beam quality test technology and devices of electron beam welding. Vacuum.

Phadke, M. S. (1989) Quality engineering using robust design. PTR Prentice hall, New Jersey.

Pierce, S. W. and Burgardt, P. (2014) Evaluation of two devices for electron beam profiling. Los Alamos national laboratory report LA-UR-14-28680.

Pradeep, T. (2012) A textbook of nanoscience and nanotechnology. Tata McGraw Hill, New Delhi.

Prudnikov, I. A., Toropov, A. S., Chichikalov, Y. F. and Khokhryakov, I. V. (1973) Device for determination of charged particle beam profile and position. Nuclear instruments and methods.

Punshon, C. S. (2013) Deployment of local vacuum mobile systems for power beam welding of thick section structural steel. TWI research report 1041.

Ragheb, M. S. & Zakhary, S. G. (2000) Study of the electron beam diagnostics and beam waist. Radiation Physics and Chemistry.

Reisgen, U., Olschok, S. and Ufer, S. (2014) Accurate diagnostics of electron beam characteristics. Eleventh International Conference on Electron Beam Technologies at Bulgaria.

Rioul, O. and Vetterli, M. (1991) Wavelets and signal processing. IEEE SP magazine.

Roy, R. K. (2001) Design of experiments using the Taguchi approach: 16 steps to product and process improvement. Wiley.

Sanderson, A. (2005) High Power Non-vacuum EB Welding. TWI bulletin.

Sanderson, A. and Adams, M. J. (1970) Electron beam welding. United States patent, 3534387.

Sandstrom, D. J., Buchen, J. F. and Hanks, G. S. (1970) On the measurement and interpretation and application of parameters important to electron beam welding. Welding research supplement.

Saresh, N., Pillai, M. G. and Mathew, J. (2007) Investigations into the effects of electron beam welding on thick Ti-6Al-4V titanium alloy. Journal of materials processing technology. 83-88

Schiller, S., Heisig, U. and Panzer, S. (1982) Electron beam technology. John Wiley and sons.

Schultz, H. (1993) Electron beam welding. Abington publishing.

Seo, J., Ma, H. and Saha, T. K. (2015) Wavelet-based probabilistic partial discharge extraction and interpretation for power transformer. IEEE transactions on dielectrics and electrical insulation. Vol. 22. 1105-1117.

Sifuzzaman, M., Islam, M. R. and Ali, M. Z. (2009) Application of Wavelet transform and its advantages compared to Fourier transform. Journal of physical sciences, volume 13, pp. 121-134

Tabachnick, B. G. and Fidell, L. S. (2013) Using Multivariate Statistics: Pearson New International Edition. [online]. Pearson. Available from:<http://www.myilibrary.com?ID=526967> 29 February 2016

Tinsley, H. E. A. and Brown, S. D. (2000) Handbook of applied multivariate statistics and mathematical modelling. Academic press.

Truchetet, F. and Laligant, O. (2004) Wavelets in industrial applications: a review. International Society for Optics and Photonics. In Optics East (pp. 1-14)

Trushnikov, D. N. (2013) Using the wavelet analysis of secondary current signals for investigating and controlling electron beam welding. Welding International, 27(6), 460-465.

Umamaheswari, R. and Sarathi, R. (2012) Feature extraction of UHF PD signals by wavelet packet based MRSD analysis for defect identification in gas insulated systems. In India Conference (INDICON), (pp. 1218-1222). IEEE.

Williams, D. B. and Carter, C. B. (2009) Transmission electron microscopy: A textbook for materials science. Springer. 2nd edition.

Wojcicki, S. & Mladenov, G. (2000) A new method of experimental investigation of high-power electron beam. Vacuum 58.

Worster, J. (1969) The brightness of electron beams. Brit. J. Appl. Phys.

Yang, Y. Di, L., Yun-Qing, F., Ke, Y., Wei-Dong, C., Jun, X., Zhi-Xian, G., Hutton, R. and Ya-Ming, Z. (2011) Electron beam density study using a portable slit imaging system at the Shanghai electron beam ion trap. Chin. Phys. B.

Yasuda, K., Usuda, S. and Gunji, H. (2001) Simultaneous alpha, beta/gamma, and neutron counting with phoswich detectors by using a dual-parameter technique. IEEE transactions in nuclear science. Volume 48, Issue 1, 1162-1164.

Yoon, C. S. (2003) Electron beam welding diagnosis using wavelet transform. Journal of Welding and Joining. The Korean Welding and Joining Society. Volume 21, pp. 33-39

Zohrevandi, S. and Bashiri, M. (2014) Evaluation of full experimental design method against fractional design method and Taguchi design method in machining operation. Journal of control science and engineering. Vol. 2 43-51.